Monitoring Spatial Distribution of Solvent Extractable Petroleum Hydrocarbons in Pit Lake Fluid Fine Tailings

Monitoring Spatial Distribution of Solvent Extractable Petroleum Hydrocarbons in Pit Lake Fluid Fine Tailings

By: Mikhail Dereviankin, B.Sc.

A Thesis Submitted to the School of Graduate Studies in Partial Fulfillment of the Requirements for the Degree Master of Science

Master of Science (2020)

McMaster University Hamilton, Ontario

TITLE:	Monitoring Spatial Distribution of Solvent Extractable Petroleum Hydrocarbons in Pit Lake Fluid Fine Tailings
AUTHOR:	Mikhail Dereviankin, B.Sc (University of Guelph)
SUPERVISORS:	Prof. Gregory F. Slater
NUMBER OF PAGES:	118

Abstract

The extraction of bitumen from the cretaceous oil sands ore within the Athabasca Oil Sands Region (AOSR) in Northern Alberta has generated over 1.18 trillion liters of by product in the form of Fluid Fine Tailings (FFT) and Oil Sands Process Water (OSPW)[3]. A reclamation strategy being investigated is water capped tailings technology (WCTT), that involves the development of Pit Lakes (PLs) by sequestering FFT below a water cap composed of both OSPW and fresh water to steadily densify these tailings over time[4]. A challenge that may impede this reclamation strategy is that as FFT densifies porewater containing oxygen consuming constituents (OCC) derived from anaerobic microbial degradation of labile petroleum hydrocarbons, such as gases (e.g. H_2S, CH_4), dissolved organic carbon (DOC) and dissolved ions (e.g. NH_4^+, HS^-, and Fe^{2+}), have the potential to be mobilized into to the overlying water cap.

This dissertation is focused on developing an optimized comprehensive two-dimensional gas chromatography time-of-flight mass spectrometry (GC×GC/TOFMS) methodology for analyzing the spatial distribution for a subset of identifiable solvent extractable PHCs species from FFT within Base Mine Lake (BML) the first full-scale demonstration of PL technology. The chemical "fingerprint" constructed from the concentration of each identified PHC isomer at a given depth and cosine theta (cos-Θ) similarity metric suggested the contribution of a singular source of PHCs within BML. Although a similar source fingerprint persisted throughout the study site, the spatial distribution for the isomers identified suggested differences in PHC input contributions across the FFT sampling platforms with the largest variation in concentration being attributed to the labile low molecular weight *n*-alkanes (C11 – C13) and postulated biomarker, drimane. These low molecular weight compounds, with the exception of drimane, are suspected components of residual naphtha, and the large variabilities in concentration are suggestive that these species may be linked with fluctuating inputs and/or sorption of naphtha to the organic phase of the FFT. Equally possible, the pronounced variability in the low molecular weight *n*-alkanes concentrations

may be linked to increased biogeochemical cycling and/or FFT species exchange with the water column as these species are expected to be preferentially biodegraded and have higher water solubilities. The isomer variability in BML FFT was further assessed through a chemometric approach using Principal Component Analysis (PCA) and Hierarchical Cluster Analysis (HCA). These metrics highlighted that the FFT sampling platforms were spatially distinguished due to either a relatively depleted or elevated concentration for a subset of lower molecular weight alkylated poly-cyclic aromatic hydrocarbons (primarily C1 and C2-FL class). While the concentration of these lower molecular weight alkylated poly-cyclic aromatic hydrocarbons was variable between sampling platforms, the concentration for the heavier molecular weight alkylated poly-cyclic aromatic hydrocarbons C3-NAP, C4-NAP and C1-DBT remained consistent. As these lower molecular weight compounds are suspected be preferential biodegraded and have increased water solubilities, FFT depths containing elevated concentration of these lower molecular weight compounds relative to the heavier molecular weight compounds may be indicative of increased potential for biogeochemical cycling and/or FFT species exchange with the water column in BML.

Acknowledgments

I would like to express gratitude to my supervisor, Dr. Greg F. Slater. Thank you for the opportunity to join your research group and reaffirm the way I perceive chemistry. Your patience and teachings during the early days were critical to challenging the black and white scientific approach I built in my career as a quality assurance auditor. The approach you have taken in your scientific career to distill the complexity associated with your research is truly an artform and one I aim to replicate in my consulting practice. The graduate student – supervisor relationship is often a frequently conversed topic among students, and I am grateful that my experience has been positive in all aspects. I am appreciative that in all my conversations with Greg, that he has focused on keeping the objective geared towards challenging my critical thinking. Today, whenever I am thinking of a solution to a problem, one of Greg's patented expression comes up, "how can you explain the importance of this to your client?".

My graduate experience would not have progressed so smoothly if it were not amazing support I have gotten from both Jennie Kirby, the handiest laboratory technician on the planet, and the other students in the Slater group. No matter what sort of problem you will encounter throughout your graduate experience you can trust that Jennie will have some sort of solution neatly tucked away in the laboratory. I'll always remember the immense amounts of joy I had walking into our lab looking for something common like a socket set to find out that Jennie has multiple sets neatly organized (always both metrics and imperial). Whether it be cramming for our mass spec course final projects or figuring out how MetaboAnalyst works, I will always cherish these moments with all the other members of the Slater group. Specifically, I'd like to thank Mohamed for passing down his breadth of knowledge amount GCGC trouble shooting and his infectious positive attitude driven by his love for salsa dancing, Chris for always entertaining me with his undergrad stories and Sian for bonding over our love for making graphs pretty (hopefully one day my PowerPoints become 10% as pretty as yours). Thanks to the rest of the group for putting up with my daily

complaints about how long the walk from the parking lot to the office is or how the pool at McMaster pool just isn't the right temperature. I'd like to take the opportunity to thank our industrial collaborators, Syncrude Canada Ltd., for allowing me to be part of this innovative project. Specifically, thank you for Carla Wytrykush, providing edits to my abstracts, conference presentations and thesis work, which was improved the overall clarify of my research.

Graduate school has offered a unique opportunity to not only expand my ability to critical think but given me a second chance to pursue varsity athletics. To both the Men's Water Polo and Swim Team who have pushed me day in and day out to accomplish things I would never have expect in my, "advanced", age. Thank you to the Fairley brothers for letting the old man get one more chance. If I can impart any lesson to future graduate students, it would be to *focus on mastering what is in the box before you start to think outside of it*.

Table of Content

List of Figures

List of Tables

List of Equations

Chapter One: Introduction

Oil Sands Reclamation Overview

The oil sands are naturally occurring petroleum deposits composed of sand, clay, water and viscous crude oil, which contain 166.3 billion barrels (or 97%) of Canada's 171 billion barrels of proven oil reserves[1]. These deposits cover a combined area more than 142,000 square kilometres (km^2) within Alberta and Saskatchewan, which can be segregated into three distinct regions: Athabasca, Cold Lake and Peace River. Surface mining operations in the Athabasca Region in Northern Alberta, create large open pits to access oil sands deposits where crude oil is present in the form of bitumen[1]. To extract bitumen from the sands, the cretaceous ore is combined with hot water and sodium hydroxide in a process referred to as the 'Clark Hot Water Extraction'[2]. In certain extraction facilities, a hydrocarbon diluent developed from downstream refining of bitumen, referred to as naphtha, is added in the extraction procedure to reduce water-in-bitumen emulsification, decrease bitumen viscosity and density, and enhance oil recovery[44]. Although only 20% of all bitumen reserves are extracted with this protocol[1], over 1.18 trillion liters of by product has been produced in the form of tailings containing solids, dissolved salts and oil sands process-affected water (OSPW) that are stored in tailings ponds[3,5]. Following discharge into tailings ponds, the sand-sized fraction dominated by quartz [SiO_2], with particles >44 μm in diameter, settle rapidly while the particles <44 μm in diameter settle at a significantly slower rate. The fraction that remains suspended is comprised of clay minerals, which form an aqueous matrix referred to as fluid fine tailings (FFT)[5].

The Tailing Management Framework (TMF) issued by the Alberta Energy Regulators in 2015[4] has issued a zero-release policy that has led to research initiatives into management strategies for the reduction of tailings and reclamation of open pit mines. Within the surface mining operations in the Athabasca Region, oil sands operators are primarily investigating three different reclamation technologies for the management of open pit oil sands mining and extraction by-

products: composite tailings (CT), tailings centrifugation and pit lakes (PL)[15]. The longest studied technology is the conversation of FFT into CT. To produce CT, the FFT from the extraction facility are cycloned to produce a densified sand[15]. This densified sand is then combined with controlled amounts of gypsum ($CaSO_4 \bullet 2H_2O$; 1 kg per m^3 of FFT) to form a non-segregating slurry[15]. The CT product is then pipelined and deposited either on the surface or sub-aqueously into an open pit mine[15]. The next type of technology utilizes industrial centrifuges, gypsum and a polymer solution to densify the FFT[15]. The densified FFT product is referred to as cake and is directly deposited into the open pits[15]. The lighter phase in the centrifuges exits as centrate which is collected and then pumped back to the fluid tailings pond[15]. Both CT and cake depositing are considered, “dry”, reclamation strategies as the underlying goal is to fill open pit mines for future land use[15]. The alternative reclamation activities focus on a, “wet”, reclamation strategy in which the open pit mines are converted into boreal lake ecosystem. PL fall under this reclamation category and are the focus in this dissertation. These lakes employ water capped tailings technology (WCTT) by introducing tailings into open pit mines and capping with several meters of water allowing the FFT to steadily densify over time[5]. Freshwater inputs, including precipitation and runoff, and *in-situ* biogeochemical processes are expected to improve the quality of the water cover over time leading to the establishment of a boreal lake ecosystem [6].

First Full-Scale Application of Pit Lakes in the Athabasca Oil Sands Region: Syncrude Ltd. Base Mine Lake

Syncrude Ltd. Canada has launched the first full-scale pilot PL, Base Mine Lake (BML) (**Figure 1**), within the Athabasca Oil Sands Region (AOSR) located north of Fort McMurray, Alberta, Canada. Between 1994 and 2012, 48 m of FFT were deposited across a surface area of approximately 8 km^2 into Syncrude’s decommissioned West In-Pit Area, which would later become BML. Several physical and chemical constructs have been implemented within BML to expediate FFT densification and reclamation comparatively to conventional tailing ponds. Following the final FFT deposition in 2012, Syncrude introduced a deeper water cover with an

average depth of 6.5 m composed of both OSPW and fresh water to promote increased FFT densification and an oxic water column[7]. Field studies beginning in 2015 characterizing the physical chemistry of the BML water cap from the FFT water interface (FWI) to the surface have identified that the water cap thermally stratifies and that oxygen persists, albeit at low levels (i.e. < 5% saturation) to the FWI[38]. The biogeochemical environment within FFT is known to be anoxic due to *in-situ* microbial metabolism, higher temperature, and mass transfer limitation. *In*-vivo experiments with native microcosm from FFT have demonstrated that anaerobic microbial biodegradation persists due to the presence of labile petroleum hydrocarbons (PHCs) derived from inputs of unrecovered bitumen and/or naphtha[5,6]. Anaerobic degradation of hydrocarbons including, but not limited to, *n*-alkanes and monoaromatics (i.e., BTEX compounds) allows for the production of fermentation products H_2 and acetate. These fermentation products may be subsequently utilized by nitrate (NO_3^-)-reducing, iron (Fe^{III})-reducing, sulfate (SO_4^{2-})-reducing, or methanogenic conditions releasing gases (e.g. H_2S, CH_4), dissolved organic carbon (DOC) and dissolved ions (e.g. NH_4^+, HS^-, and Fe^{2+}) into the water column. Generally, hydrogenotrophic and acetoclastic methanogens dominate the anoxic microbe environment within FFT contributing to localised releases of CH_4 and CO_2 (**Equation 1**)[5-7,16,44]. In addition to the COD generated by methane cycling, the associated increase in dissolved CO_2 promotes carbonate-mineral dissolution, which results in increased advection of porewater within the FFT to the overlaying water-cap[5]. A concern in BL is that as FFT settles and densifies porewater containing by products derived from these anaerobic processes can be mobilized into to the overlying water cap[44]. The exchange of these species between the FFT and water column has the potential to hinder the reclamation potential of BML by increasing the chemical oxygen demand (COD) leading to decreased oxygen concentration in the water column[9,38]. Oxygen also plays a critical role as a Terminal Electron Acceptor (TEA) in aerobic respiration pathways of macro-organisms whose presence is required for a stable boreal lake ecosystem to develop[17].

$$(a)\ H_2 + CO_2 \rightarrow CH_4 + CO_2$$

$$(b)\ CH_3COOH \rightarrow CO_2 + CH_4$$

Equation 1 – (a) Hydrogenotrophic (b) Acetoclastic Methanogenesis[5-7,44].

Within BML, densification after initial FFT deposition occurred quickly reaching ~15 wt % solids within a few weeks and ~20% solids after 3–9 months[5]. During this initial stage of densification, species transport between FFT porewater and the water column was driven by advection[5]. Advection is mechanical transport of solutes via the flux of the aqueous phase[18]. Advection can be expressed in terms of solute concentration in an aqueous system (**Equation 2**)[39]. Porewater expression became slower and produced Mature Fine Tailings (MFT) when solids content reached 30 wt % after 5–10 years of deposition[38]. The rate of advection between FFT porewater and the overlaying water column is expected to decrease with time as FFT densifies.

$$J_A = vC_A$$

Equation 2 – Advection as mass transfer represented in molarity (mol/(m^2s)), where v represents linear velocity (m/s), C_A represents concentration of analyte (mol/m^3)[39].

In addition to advection, the transfer of species between FFT porewater and the water column is governed by molecular diffusion. Diffusion between the FFT porewater and water column is a passive transport mechanism governed by Fick's Law (**Equation 3**). Fick's law describes the flux for a solute under random thermal motion to transfer from a region of higher concentration to a region of lower concentration through a permeable layer[40]. Molecular diffusion represents the lengthier process of mass transport and is controlled by the random movement of molecules as a function of distance travelled.

$$J = -D\frac{dC_a}{d_z}$$

Equation 3 – Fick's Law, where J represents the flux, D represents the diffusivity, dC_a represents the change in concentration and d_z represents the change in depth[40].

Gas bubbling associated with *in-situ* biodegradation contributes to an additional mechanism of species exchange between FFT porewater and water cap. While this process does not contribute as significantly to species exchange comparatively to advection, it accounts for faster cycling than molecular diffusion during initial FFT deposits [5-9,19]. Ebullition of these *in*-situ formed gas bubbles is governed by the solubility of the gas bubble and is expressed by Henry's Law of Partial Pressures (**Equation 4**), which expresses the ratio of a compound's partial pressure in air to the concentration of the compound in an aqueous matrix at a given temperature[41].

$$S_{(g)} = K_H P_{(g)}$$

Equation 4 – Henry's Law of Partial Pressures, where $S_{(g)}$ represents the concentration of gas in the aqueous phase, K_H represents the Henry's Law constant for that specific gas, and $P_{(g)}$ represents the partial pressure of the gas in the gaseous phase[41].

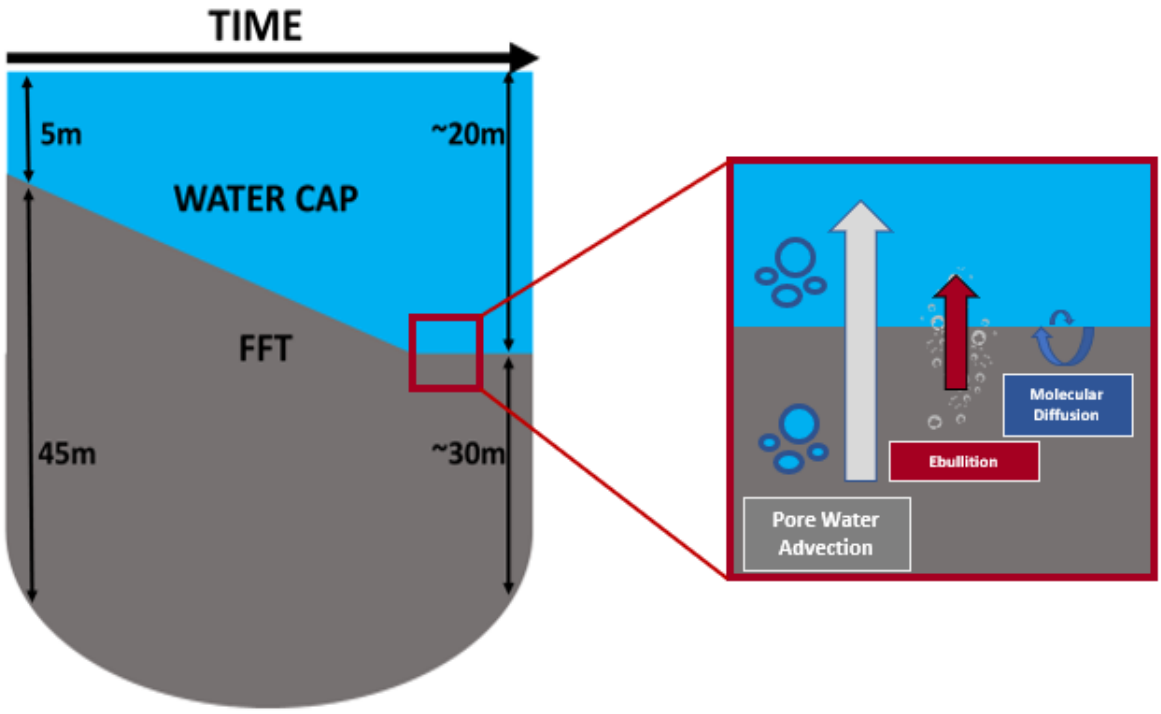

Figure 1 – Schematic diagram highlighting FFT densification as a function of time within Syncrude Ltd. Canada's Base Mine Lake (BML) and associated mechanisms of species transfer from FFT into overlaying water column.

Organic Constituents of Petroleum Hydrocarbons in Fluid Fine Tailings

Understanding the chemical properties of the petroleum hydrocarbons (PHCs) within the FFT capable of undergoing fermentative and/or redox reactions is important, as different organic constituents within these subsets of compounds are known to be anaerobically biodegraded at varying rates. The non-polar PHCs within FFT fall into three classes[20]:

1. Paraffins - saturated hydrocarbons, straight or branched chains but no ring structures
2. Naphthenes – often referred to as, "biomarkers", in petrology, these are saturated hydrocarbons with one or more rings. These hydrocarbons may have one or more paraffinic side chains.

3. Aromatics - hydrocarbons with one or more aromatic nuclei; these hydrocarbons may be connected to naphthenic rings and/or paraffinic side chains.

The source of PHCs within Syncrude Canada Ltd. FFT is a result of residual bitumen and/or residual organic diluent used in oil extraction processes, referred to as 'naphtha'[6]. Although both petroleum products contain the same classes of PHCs, there is a difference in the distribution of chemical constituents that distinguish these two petroleum products. The standard convention in industry is to represent the compositional differences of petroleum hydrocarbons in terms of SARA (saturates, aromatics, resins, and asphaltenes) content. In general, as the molecular weight of the petroleum fraction increases, there is a decrease in the abundance of paraffins and an increase in the naphthenes and aromatics. Bitumen is considered a heavy molecular weight fraction petroleum product and bitumen derived from the Athabasca oil sands has the following SARA composition:

Table 1 – Properties and SARA fractionation results for Athabasca Bitumens[20].

	Athabasca Bitumen ASTM20007
Saturates (wt%)	17.27
Aromatics (wt%)	39.7
Resin (wt%)	25.75
Asphaltene (wt%)	17.28
Carbon (wt%)	83.34
Hydrogen (wt%)	10.26
Sulfur (wt%)	4.64
Oxygen (wt%)	1.08
Nitrogen (wt%)	0.53
Residues (wt%)	0.15

While the bitumen contains high molecular weight species, the naphtha used by Syncrude Ltd. Canada (CAS No. 64742-49-0) is a mixture of aliphatic and aromatic compounds (C_3-C_{14}) in which the majority on the compounds are n-alkanes (heptane (C_7), 1-5% by wt; octane (C_8), 5-10% by wt; nonane (C_9), 1-5% by wt) with the remaining constituents comprised of *iso*-alkanes, benzene, toluene, ethyl-benzene, and xylenes (BTEX) compounds[6]. Due to these different compositional differences, light paraffins PHCs (C_3-C_{14}) and BTEX compounds are considered sourced from naphtha, while the heavier molecular weight PHCs are considered sourced from bitumen.

Introduction to Paraffins

Paraffins have the general formula C_nH_{2n+2}, with methane (CH_4) being the lightest paraffin. The carbon chains in paraffins can be straight or branched. Melting point increases with carbon number and long-chain n-paraffins melt at relatively high temperatures, while their branched-chain isomers melt at lower temperatures.

Introduction to Naphthenes

Naphthenes are molecules that have lost their functional groups but whose basic skeleton has been preserved and are often referred to as, “biomarkers”, in the field of petrology. Due to their resistance to *in-situ* degradation they can act as tracers associated with a specific environment, class of organism, or petroleum source rock[13]. Notable examples utilized in biogeochemistry are pentacyclic triterpenoids and their derivatives, which are attributed to the decay of higher plant resins, and hopanoids, which are biomarkers preserved from bacteria during diagenetic processes. Biomarkers can also provide a geochemical fingerprint to differentiate sources of petroleum products. A notable demonstration of the ability to use these biomarkers to fingerprint petroleum products was studied by Nelson et al. (2019), who used petroleum biomarkers to explore the complexity of two crude oil spills in the Gulf of Mexico, Ixtoc I and Deepwater Horizon (DWH). The most obvious difference between these crudes was the presence or absence of de-A-steranes; de-A-cholestane, de-A-methylcholestane, and de-A-ethylcholestane were present in

Ixtoc I crude and absent in the DWH crude. In addition, another notable difference, useful for discriminating between Ixtoc I and DWH was that the diasterane, DiaC27βα-20S demonstrated a larger abundance than 17α(H),21β(H)-hopane (H) in the DWH crude than in Ixtoc I crude. The relatively high abundance of the diasteranes in DWH crude was an indication that DWH is thermally mature in comparison to Ixtoc I as a high degree of thermally induced rearrangements must have occurred to transform steranes to diasteranes.

Introduction to Polycyclic Aromatic Hydrocarbons

Polycyclic aromatic hydrocarbons (PAHs) are a group of organic compounds consisting of two to six fused aromatic rings. Naphthalene ($C_{10}H_8$) forms the smallest parent PAH ring structure with two aromatic rings, while coronene ($C_{24}H_{12}$) forms the largest measured parent structure with six aromatic rings (**Figure 2**). The common nomenclature of PAHs follows that isomers formed by the addition of a aromatic ring are named with numbers and letters enclosed in brackets [ ]. The nomenclature begins with the substituent group(s) added followed immediately by the parent PAH structure. Appropriate letters are used where a ring is fused to more than one face of the molecule (**Figure 3**).

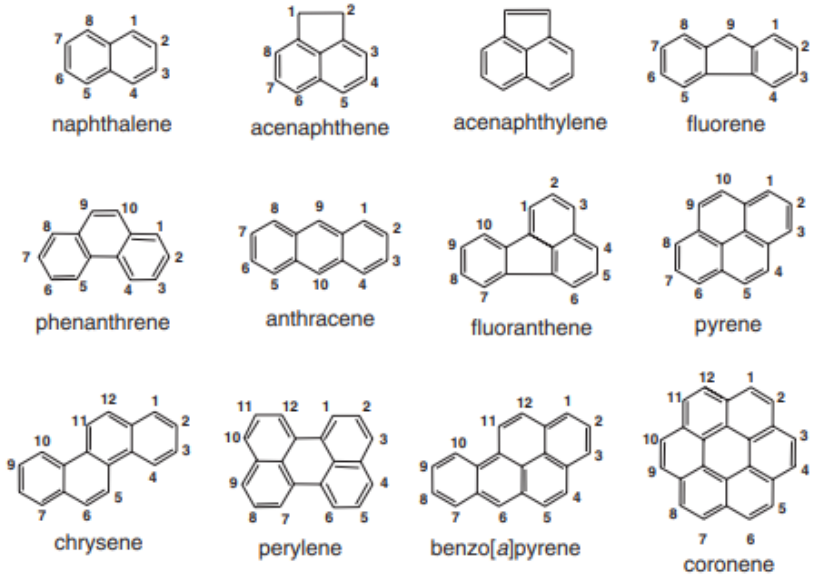

Figure 2 – General structure of parent PAHs[22].

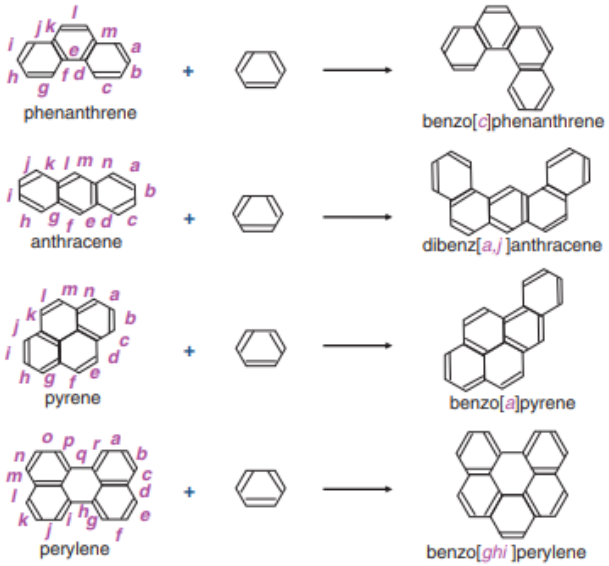

Figure 3– Nomenclature of fused aromatic rings from parent structures[22].

PAHs are neutral, hydrophobic nonpolar molecules with physical and chemical characteristics, such as solubility in water, hydrophobicity, and vapour pressure, varying with molecular weight. As the molecular weight increases, solubility in water (mg/L) decreases[23]. These characteristics cause differences in volatility, solubility and biogeochemical cycling[23].

PAHs in the environment predominantly arise from incomplete combustion processes and/or petrogenic inputs from both natural and anthropogenic sources. PAHs in crude oil, including a wide range of alkylated PAHs, are formed as a result of diagenetic processes through the thermal decomposition of organic molecules and their subsequent recombination. This petrogenic sources begin with recombination reactions from pyrolytic processes above 500°C produce several reactive intermediates and radicals such as ethylene and acetylene[26-28]. The initial formation of the first benzene ring is currently hypothesised to occur through either the self-reaction between 3-carbon C_3H_3 species, the reaction between a 4-carbon species (n-C_4H_5, n-C_4H_3) and 2-carbon species or the reaction of a cyclopentadienyl (C_5H_5) with CH_3[23,26,29].

Alternative pathways in which benzene is not the first aromatic group formed has been proposed. Naphthalene may be formed as the initial aromatic parent group, through the self-reaction between C_5H_5 radicals[23]. After the formation of the initial ring(s), several mechanisms have been proposed for the further growth of PAHs, with the hydrogen abstraction-acetylene addition (HACA) pathway being the most widely accepted[23]. HACA is a process where initial benzene rings and aliphatic hydrocarbon building blocks are converted to larger PAHs through an iterative process of hydrogen abstraction and acetylene (C_2H_2) additions (**Figure 4**). Another proposed mechanism of PAH ring expansion is through the hydrogen abstraction - vinylacetylene addition (HAVA) pathway[25] (**Figure 4**). Generally, PAH formed under these diagenetic processes form products containing full aromaticity, while due to increased reaction temperatures, PAH formed from pyrogenic process form five membered ringed intermediates (fluorene, fluoranthene, perylene etc.). The differentiation between the mechanism of these recombination reactions with temperature form the forensic background for differentiating between pyrogenic and petrogenic PAHs through the use of diagnostic ratios.

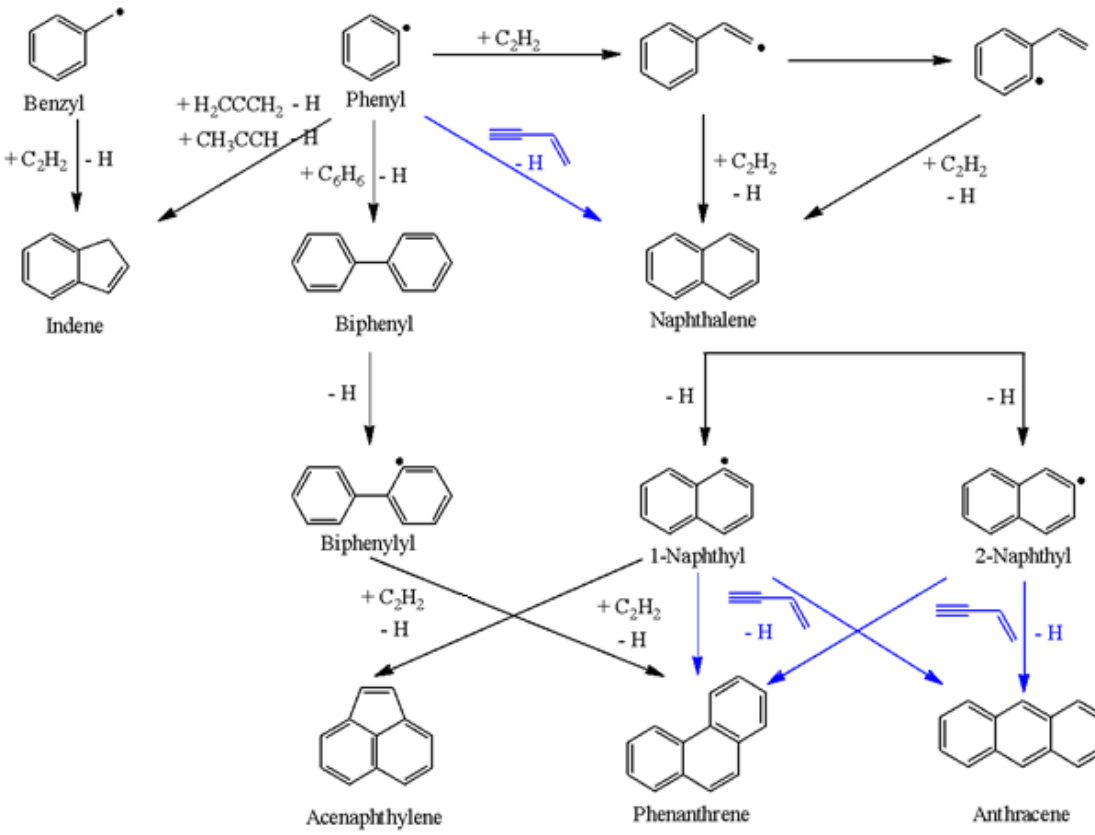

Figure 4 - Complementary pathways to bi- and tricyclic PAHs via the hydrogen abstraction – acetylene addition (HACA) (black) and the barrier-less hydrogen abstraction – vinylacetylene addition (HAVA) pathways (blue)[24,25].

Anaerobic Biogeochemical Cycling of Petroleum Hydrocarbons in Pit Lakes

In terms of a reclamation standpoint, sequestering and hindering the biogeochemical availability of alkylated PAH isomers and paraffins in the FFT would impede the transport of these species and their by-products into the water cap. However, these compounds may exhibit varying degrees of anaerobic degradation within the FFT releasing species that contribute to the reduction of oxygen content of the overlaying water cap. Due to its high molecular weight, it has been demonstrated *in-vivo* that bitumen is unlikely to undergo rapid fermentation and to contribute species susceptible to methanogenesis in the short term[6]. Oil sands tailings are also highly biodegraded in the extent of methanogenesis being already largely expensed prior to deposition

in PLs resulting. To confirm that methanogenic activity is not largely responsible from bitumen deposits, Holowenko *et. al* (2006) amended Mature Fine Tailing (MFT) samples with increasing concentrations of bitumen and incubated for nearly 250 days under methanogenic conditions. After 250 days, they did not detect any enhanced methane production in these bitumen-amended microcosms. As such, the large extent of *in-situ* biodegradation of petroleum hydrocarbons within the FFT is suspected as result of biodegradation of the organic constituents of naphtha and/or residual petroleum hydrocarbons from the oil sands deposition. Tarique *et. al* (2006), have extensively studied the native anaerobic microcosms present in MFT and their ability to biodegrade the PHCs derived from residual naphtha. MFT amended with complex hydrocarbons (diluents), BTEX, long-chain *n*-alkanes (C14–C18), and some iso-alkanes exhibited co-domination of acetoclastic and hydrogenotrophic (members of Methanomicrobiales) methanogens. These native hydrogenotrophic and acetoclastic methanogens present in MFT biodegraded spiked *n*-alkanes in the sequence $C_{10} > C_8 > C_7 > C_6$; degradation of 100% C_{10}, 97% C_8, 74% C_7, and 44% C_6. The resulting trend of preferential microbial degradation is due to acclimatization of microcosms to naphtha components dominated by relatively high molecular weight paraffins ($>C_{10}$). Higher molecular weight *n*-alkanes (C_{14}, C_{16} and C_{18}) are also degraded under methanogenic conditions in oil sands tailings, although they exhibit an increased lag time (~180 d) before the onset of methanogenesis.

Reports on anaerobic biodegradation of PAHs are relatively recent, and only a limited number of preliminary studies have demonstrated the anaerobic degradation of PAHs including naphthalene, anthracene, phenanthrene, fluorene, acenaphthene and fluoranthene[32,33]. However, detailed information on anaerobic degradation of PAHs under fermentative, nitrate (NO_3^-)-reducing, iron (Fe^{III})-reducing, sulfate (SO_4^{2-})-reducing, or methanogenic conditions is scarce and very little is known about their degradation pathways, catabolic genes/enzymes and/or regulatory

mechanisms. With the increased resistance to *in-situ* biodegradation, anaerobic biogeochemical cycling within the FFT is considered limited to the paraffin components of PHCs.

Instrumental Analysis of Fluid Fine Tailings

GC-LRMS

Gas chromatography coupled to low resolution mass spectrometry (GC/LRMS) has been applied to numerous studies examining the constituents within FFT[12,13].The limitation with this analytical method is that the majority of analytes elute in an unresolved complex mixtures (UCM) in the total ion current (TIC) chromatogram. These UCMs correspond to a raised baseline hump with unresolved chromatographic peaks and overlaying mass spectra. Although GC/LRMS remains a workhorse for the analysis of many environmental samples, development of improved methods for identifying and quantifying UCM components will allow improved understanding of biogeochemical processing within the FFT. As a compensation for the insufficient peak capacity associated with GC/LRMS, complex and time-consuming sample preparation methods have been established (example, ASTM D2549)[15].

GC×GC

GC×GC is a powerful tool in oil sands forensics as it offers unparalleled chromatographic separation, peak capacity and has been used in recent years to resolve individual constituents within complex mixtures, including structural isomers[11]. GC×GC has already been notably used in oil sands forensics to investigate the compositional difference between various oil sands process water (OSPW)[16], differentiation in groundwater systems from naturally occurring bitumen deposits[17] and assessment of the temporal and spatial variations of naphthenic acids in tailing ponds[18].

Fundamentals

In comprehensive GC×GC, two capillary GC columns of different stationary phase are connected via a modulation unit that transports eluent from the first column into the second column. In a

properly tuned GC×GC chromatogram, the separation between the long primary column (generally 30 – 120 m) and the relatively short secondary column (generally ~ 1m) is orthogonal, meaning the retention times in the two dimensions are independent of one another. Following the elution from the primary column where separation is dictated by boiling point, the modulator interface traps the effluent for a short period of time by cryogenically freezing the compounds with liquid nitrogen. After a fixed time referred to as the modulation time (M_T), the frozen compounds are rapidly heated and injected into the second-dimension column as a narrow pulse. By utilizing a secondary column with a relatively smaller diameter in comparison to the primary column, GC×GC is able to exploit the Bernoulli principle to vastly increasing the chromatographic sensitivity. As the total among of gas moving through the secondary column remains consistent from the primary, the flow rate and correspondingly the kinetic energy will increase resulting in narrowed peak widths. The rapid elution of effluent in the secondary column allows for separation of analytes to be isothermal, with no boiling point contribution, and controlled by the interaction between the analyte and stationary phase. Following the complete separation in the secondary column, another fraction of the first-dimension column effluent is injected in the second-dimension column. This process is repeated continuously for the duration of the primary retention time. Consequently, the resulting chromatograph is constructed from transforming the modulated segments of primary column into a one-dimensional chromatograph and further reconstructing them into a two-dimensional chromatograph.

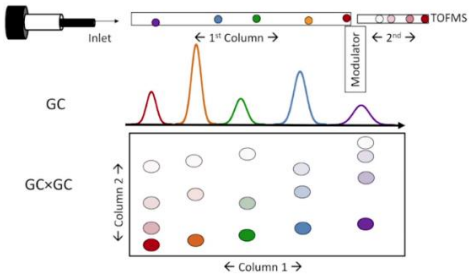

Figure 5 – Schematic of GC×GC/TOFMS set up (Source: LECO® website https://www.leco.com/analytical-science/76-category-all/hidden-pages)

$$P1 + \frac{1}{2}\rho v_1^2 + \rho g h_1 = P2 + \frac{1}{2}\rho v_2^2 + p g h_2$$

Equation 5 - Bernoulli's principle where P represents pressure, $\frac{1}{2}\rho v$ represents kinetic energy per unit volume and ρgh represents potential energy per unit volume[43].

Resolution

Chromatographic resolution assesses the distance separating two adjacent peaks through the use of peak retention times (***t***) and peak widths (***w***) measured from the baseline (**Equation 6a**)[20]. Assuming the chromatographic peaks have a Gaussian distribution allows for the replacement of averaged peak widths with units of standard deviation ($\boldsymbol{\sigma}$) (**Equation 6b**). Complete baseline separation between peaks is considered achieved when the neighbouring peaks only overlap by 0.15 % corresponding to a resolution factor ($\boldsymbol{R_s}$) of 1.5. Satisfactory quantification is achieved when $1.5 > R_s > 1$ (**Figure 6**)[20].

$$R_s = \frac{t_2 - t_1}{\left[\frac{w_1 + w_2}{2}\right]} = \frac{\Delta t}{w_{av}} \ (\mathbf{a})$$

$$R_s = \frac{\Delta t}{4\sigma} (\mathbf{b})$$

Equation 6 – (**a**) Chromatographic resolution in terms of distance and retention time between neighbouring peaks where Δt represents the average time and w_{av} represents the average peak width. (**b**) Chromatographic resolution as a function of standard deviation assuming Gaussian distribution for peaks.

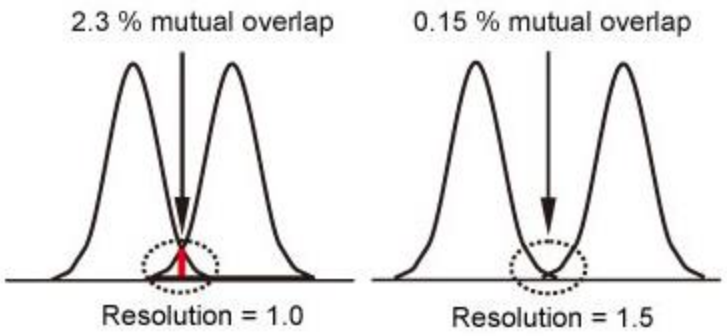

Figure 6 – Satisfactory chromatographic resolution for 1.5 > R_s > 1.0[20].

Retention Indices

With the significant sensitivity GC×GC has for resolving individual peaks, many unknown compounds can be identified. To confirm these unknowns with literature, the relative position in two-dimensional space needs to be cross evaluated. This is accomplished with retention index (**Equation 7**), which standardizes the position of the analyte with a known standard removing any retention time ambiguities between runs.

$$I_x^2 = 100n + \frac{(t_{Rx}^2 - t_{Rn}^2)}{(t_{Rn+1}^2 - t_{Rn}^2)} * 10$$

Equation 7 – Two-dimensional retention indices, where I_x^2 is the second-dimension retention index of the analyte of interest, t_{Rx}^2 is the second-dimension retention time of analyte of interest, t_{Rn}^2 is the second-dimension retention time of a standard with shorter retention time, and t_{Rn+1}^2 is the second dimension retention time of a standard with longer retention time[35].

Modulator

Programmed capillary GC columns utilized within 1-DGC can produce primary peaks with widths at half-maximum of approximately 2 s. Based on the Bernoulli's principle, the modulation-focused approach of the GC×GC results in the production of primary peaks with widths at half-maximum between 50 and 500 ms. The modulator units used within GC×GC systems are either dual stage

quad-jet thermal modulator commercialized by the LECO corporation, which is the most widely used and the two-stage loop modulator commercialized by the ZEOX corporation. Although both systems vary mechanistically, the resulting increase in peak resolution is equivalent[42]. The thermal modulator consists of two heating jets in-line with a liquid nitrogen cooling jet (**Figure 7a**). Briefly, the cooling jets freeze the effluent exiting the primary column and it becomes thermally desorbed with by the heating jet. This process is completed within the span of the modulation time (M_T). While the thermal modulator follows a linear path, the loop-type modulator consists of a secondary column that is looped twice within the modulation unit allowing the effluent to trapped and desorbed continuously **(Figure 7b)**.

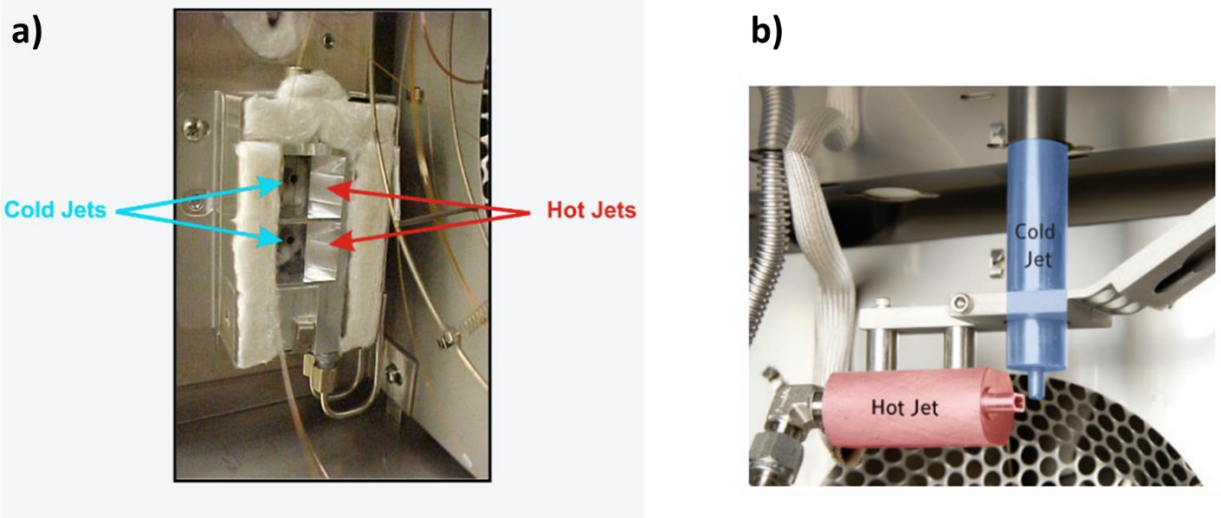

Figure 7 – (a) LECO QUADJET™ Thermal Modulator (b) Loop-type modulator[42].

Tools for Quantitation

Coupling GC×GC with a quantitative detector produces a third-dimension, intensity. Using appropriate software, a surface plot can be constructed with the x-axis representing retention in the first-dimension column, y-axis representing the retention in the second-dimension column, and z-axis representing the intensity of the diverged peak.

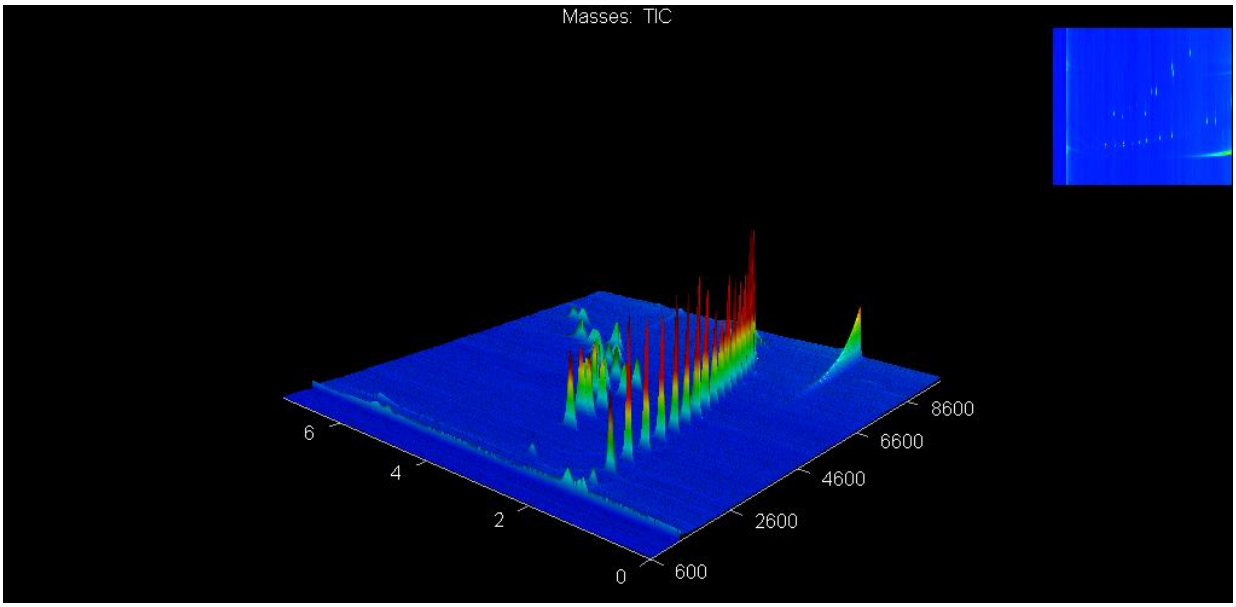

Figure 8 – GC×GC/QTOF surface plot of authentic standards of alkylated PAH isomers, d^{12}-dibenzoantharacene (ISTD) and C7-C40 alkanes run on the NP/P column orientation.

The limitation of the increase in chromatographic peak capacity is that detectors with lower acquisition rates cannot be utilized. As a result, these instruments are often coupled with time-of-flight mass spectrometers (TOFMS), flame-ionizing detectors (FIDs) and high-resolution mass spectrometers (HRMS), which have relatively high acquisition rates that allow for increased resolving power. Resolving power is defined as the ability to separate two peaks with similar masses (**Equation 8; Figure 9**). In practice, high resolution designates a mass analyzer with resolving power > 10 000, thereby excluding quadrupole mass filter, triple quadrupole, and quadrupole ion trap mass analyzers.

$$Resolving\ Power = \frac{m}{\Delta m}$$

Equation 8 – Where m is the smaller value of m/z. The denominator is the separation of the two peaks when the overlap at full width half maximum (FWHM)[37].

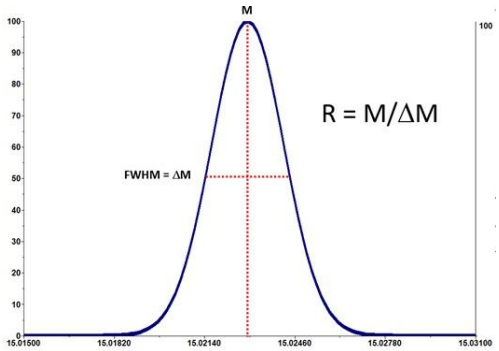

Figure 9 – Graphical representation of the calculated Mass Resolving Power using FWHM[37].

With a linear range proportional to solute mass over seven orders of magnitude and increased limits of detection, the FID detector is the preferred detector for petroleum hydrocarbon analysis[41]. As the chromatographic effluent travels into the FID detector, it is burned in a mixture of H_2 and air producing CH radicals, which are subsequently oxidized in the air to produce CHO^+ ions and electrons (**Equation 9**). Eluted analytes produce a current of 10^{12} A, which is converted to a digital signal. Thus, the ion production and associated voltage has a linear association with the number of susceptible carbon atoms entering the flame. Although the FID detector is the optimal set up for hydrocarbon quantification due to its large linear range it does not provide any identification information as no mass spectrum is produced; compounds can only be confirmed with authentic standards.

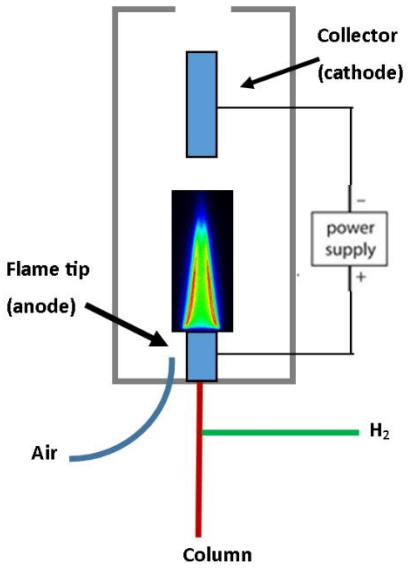

Figure 10 – Schematic diagram of FID detector.

$$CH + O \rightarrow CHO^{+} + e^{-}$$

Equation 9 - Labile carbon radical and electron formation within FID detector[37].

The TOFMS mechanism (**Figure 11**) involves the acceleration of positive ions out of the source by a backplate (repeller), which applies a voltage of 5000 V three thousand to twenty thousand times per second[45]. The accelerated ions are released into field free drift path (drift region), which contains no electric or magnetic field to further accelerate the ion. After exiting the repeller and entering the drift region, the former potential energy of the charged ions are converted to translation motion in the form of kinetic energy ($E_{\text{kin}} = ezU = \frac{1}{2}mv^2$) where m is the mass of the ion and v is its velocity, z is the number of electrons of charges e, and U is the voltage. Assuming the ion is initially at rest, the equation for kinetic energy can be arranged in terms of velocity (**Equation 10a**). The time required for the charged ion to travel through the field-free environment can be solved from substituting **Equation 10a** into the relationship between time (t), distance (s) and velocity ($t = s/v$) (**Equation 10b**). In practicality, ions exiting the source have different kinetic

energies based on their proximity to the backplate; ions closer to the backplate will have increased kinetic energies when entering the drift region. To account for this deviation, prior to entering the drift region ions are exposed to deflector plates, which restrict all ions of identical mass to reach the space focus plane at the same time. After the space focus plane, ions diverge again with faster ions overtaking slower ones. The accelerated ions are stopped and directed to the detector once they enter the reflectron (electrostatic mirror). This region consists of positively charged ring electrodes whose potential is more positive than that off the backplate. The flight path within the reflectron vary depending on the difference in kinetic energy with ions carrying greater kinetic energy, corresponding to decreases in mass, travelling further into the decelerating field. The ions are directed in the opposite direction and expelled from the reflectron when their kinetic energy reaches zero. The elongation of the flight path through the reflectron provides an improvement in the TOF analyzers resolving power. Increases in resolving power through using longer flight tubes can also be achieved with the caveat that these instruments may decrease the overall performance of the analyzer due to loss of ions based on increased reflection angles and/or scattering of ions after collisions with residual gas.

$$v = \sqrt{\frac{2ezU}{m_i}} \ (\boldsymbol{a})$$

$$t = \frac{s}{\sqrt{\frac{2ezU}{m_i}}} \ (\boldsymbol{b})$$

Equation 10 – (**a**) re-arrangement of velocity for based on the kinetic energy for a charged ion within the field-free drift region[45]. (**b**) time required for a charged ion to travel through a field-free environment[45].

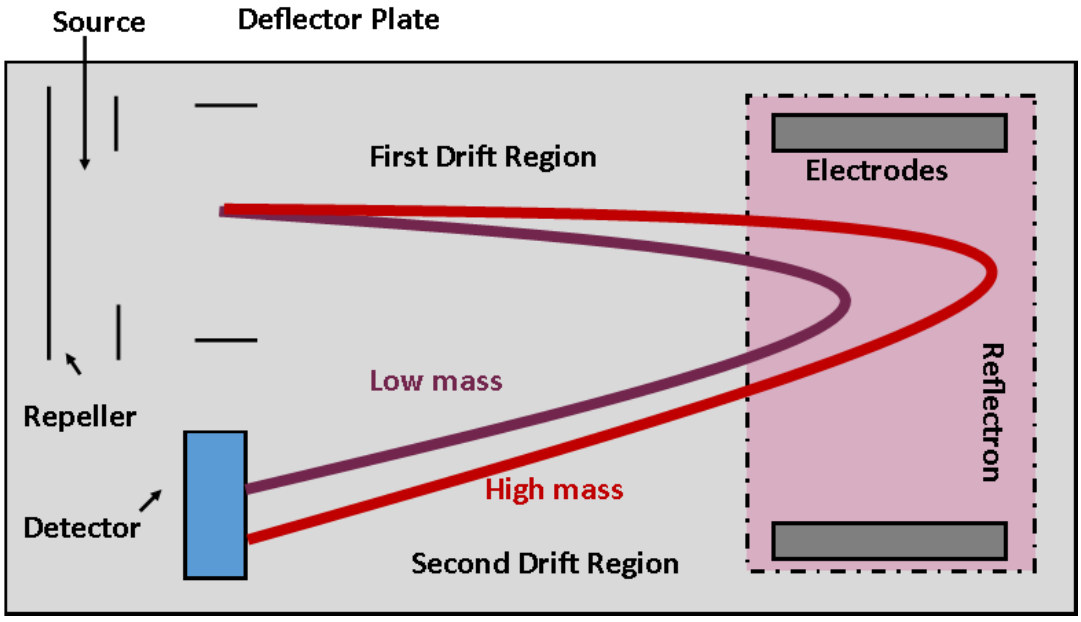

Figure 11 – TOFMS Schematic. Positive voltage (+V) applied through the backplate (repeller) accelerate ions into the space focus plane where ions of identical mass are diverged into the drift region. Ions of identical mass are re-directed to the detector by positive electrodes within the reflectron (electrostatic mirror)[37].

Comprehensive Two-Dimensional Chromatography Mass Spectrometry Challenges for Users

Although GC×GC/MS offers advantages over single dimension chromatography, users may encounter the following challenges:

(1) Baseline changes in modulation often cause issues with sample reproducibility and retention time consistency. Retention shifts can be caused by stationary phase decomposition, column change during usage, or different modulation temperatures over the experiment. Thus, there is a need to accurately record retention indices.

(2) Every GC×GC/MS run produces extremely large and information-rich three-way arrays of data in the range of 500 – 4000 megabytes (MB) per sample. Often data processing of these large data sets is limited to the processing capabilities of the computer.

(3) Wrapping Effect. The wrapping effect occurs when the modulation period is shorter than the time for the previous modulation phase to elute from the second column. If compounds remain on the second column, there will be an overlap in retention times. For example, this would occur if a first sample has a modulation time of 10 seconds, but the compounds in your sample have a maximum retention time of 15 seconds. Not all the compounds in the sample will elute during the modulation period but will elute during the next modulation period after 5 seconds. These heavier compounds will appear to have a retention time of 5 seconds. When constructing a method, it is therefore crucial to ensure that the modulation time is greater than the maximum secondary retention time of any compound in the sample.

Thesis Objectives and Overview

The underlying objective is to monitor a subset of organic constituents in BML FFT to ascertain the extent PHC inputs, biogeochemical cycling and/or species exchange with the water column occurring. The transpiration of OCC in the water column primarily in the form of dissolved methane have been sourced to anaerobic biogeochemically cycling in the FFT layer of BML[38]. Although the temporal and spatial geochemistry of OCC mobilization within the water cap of BML have been extensively monitored, research initiatives towards ascertaining the spatial variation of *in-situ* anaerobic biogeochemical processing on residual PHCs in FFT potentially releasing OCC have not been pursued. These objectives will be achieved through the accurate identification a subset of identifiable solvent extractable organics comprised of alkylated poly-cyclic aromatic hydrocarbon species, petroleum biomarkers and low molecular weight paraffins within BML FFT collected in 2017. GC×GC/TOFMS is advantageous for this approach as it provides increased peak capacity, analytical sensitivity, and the ability to specifically identify isomers unlike GC/LRMS. Historically, monitoring of these group of compounds groups has been achieved. However, little is known about the variation in specific isomers abundances.

The second chapter of this thesis introduces an analytical methodology utilizing GC×GC/TOFMS (with nominal mass resolution) for the improved separation between the subset of solvent extractable organics representative of residual inputs from bitumen and/or naphtha in 2017 BML FFT. In this study, GC×GC/TOFMS was used as a discovery tool to identify which individual species can be resolved within the 2017 BML FFT.

The third chapter of this dissertation applies the increased peak capacity of GC×GC/TOFMS to assess the spatial variability of species representative of residual inputs of naphtha and/or bitumen within the near surface (range = 0.2 – 1.9 m from Fluid Water Interface(FWI)) and a reference sample below these depths (range = 3.8 – 5.0 m from FWI) in 2017 BML FFT. The objective was to monitor the concentrations for a subset of PHC species and characterize their chemical species “fingerprint” at each site. Additionally, the correlation between the concentrations for labile PHC species and considerable less biogeochemically active species are expected to ascertain whether there is evidence of *in-situ* anaerobic biogeochemical processing on residual inputs of naphtha and/or bitumen that potentially mobilize OCCs into the overlaying water cap.

References

1. Natural Resources Canada (**2016**). Oil Sands Extraction Processing. https://www.nrcan.gc.ca/energy/energy-sources-distribution/crude-oil/oil-sands-extraction-and-processing/18094.
2. Masliyah, J., Zhou, Z., Xu, Z., Czarnecki, J., Hamza, H. (**2004**). Understanding water-based bitumen extraction from Athabasca oil sands. *Can. J. Chem. Eng*. 82, 628–654
3. Government of Alberta (**2015**). Lower Athabasca Region: Tailings Management Framework for the Mineable Athabasca Oil Sands. https://open.alberta.ca/dataset/962bc8f4-3924-46ce-baf8 d6b7a26467ae/resource/7c49eb63-751b-49fd-b746-87d5edee3131/download/2015-larp-tailingsmgtathabascaoilsands.pdf.
4. Allen, E.W. (**2008**). Process Water Treatment in Canada's Oil Sands Industry I. Target Pollutants and Treatment Objectives. *J. Environ. Eng. Sci*. 7, 123-138.

5. Dompierre, K. A., Lindsay, M. B. J., Cruz-Hernández, P., & Halferdahl, G. M. (**2016**). Initial geochemical characteristics of fluid fine tailings in an oil sands end pit lake. *Science of the Total Environment*, 556, 196–206.
6. Siddique, T., Fedorak, P.M., Foght, J.M. (**2006**). Biodegradation of short-chain n-alkanes in oil sands tailings under methanogenic conditions. *Environ. Sci. Technol*. 40, 5459–5464.
7. Siddique, T., Fedorak, P.M., MacKinnon, M.D., Foght, J.M. (**2007**). Metabolism of BTEX and naphtha compounds to methane in oil sands tailings. *Environ. Sci. Technol*. 41, 2350–2356.
8. Caughill, D.L., Morgenstern, N.R., Scott, J.D. (**1993**). Geotechnics of nonsegregating oil sand tailings. *Can. Geotech. J*. 30, 801–811.
9. Marriott, P.; Shellie. R. (**2002**). Principles and Applications of Comprehensive Two-Dimensional Gas Chromatography. *Trends Anal. Chem.* 21 (9−10), 573−583.
10. Rowland, S. J., West, C. E., Scarlett, A. G., Ho, C., Jones, D. (**2012**). Differentiation of two industrial oil sands process-affected waters by two-dimensional gas chromatography/mass spectrometry of diamondoid acid profiles. *Rapid Commun. Mass Spectrom*. 26 (5), 572– 576.
11. Frank, R. A., Roy, J. W., Bickerton, G., Rowland, S. J., Headley, J. V., Scarlett, A. G., West, C. E., Peru, K. M., Parrott, J. L., Conly, F. M., et al. (**2014**). Profiling oil sands mixtures from industrial developments and natural groundwaters for source identification. *Environ. Sci. Technol.* 48 (5), 2660–2670.
12. Bowman, D. (**2017**). Chemical fingerprinting of naphthenic acids by GC×GC/MS. Thesis.
13. White, W.M. (**2013**). Geochemistry. Wiley-Blackwell. 608-609.
14. Kavanagh, R.J., Frank, R.A., Oakes, K.D., Servos, M.R., Young, R.F., Fedorak, P.M., MacKinnon, M.D., Solomon, K.R., Dixon, D.G., Van Der Kraak, G. (**2011**). Fathead minnow (Pimephales promelas) reproduction is impaired in aged oil sands process-affected waters. *Aquat. Toxicol*. 101, 214–220.
15. Young, R. (**2019**). 2018 Mildred Lake Tailings Management Report Oil Sands Conservation Act Commercial Scheme Approval No. 8573.
16. Faidz, M., Shahimin, M., & Siddique, T. (**2017**). Sequential biodegradation of complex naphtha hydrocarbons under methanogenic conditions in two different oil sands tailings. *Environmental Pollution*, 221, 398–406.

17. Hutchins, S. R. (**1991**). Biodegradation of Monoaromatic Hydrocarbons by Aquifer Microorganisms Using Oxygen, Nitrate, or Nitrous-Oxide as the Terminal Electron-Acceptor. *Applied and Environmental Microbiology*, 57(8), 2403–2407.
18. Albarède, F. (**1995**). Transport, advection, and diffusion. In Introduction to Geochemical Modeling (pp. 401-476). Cambridge: Cambridge University Press.
19. Hurley, D. L. (**2017**). Wind waves and internal waves in Base Mine Lake. *Thesis*.
20. Rahimi, P.M., Gentzis, T. (**2006**) The Chemistry of Bitumen and Heavy Oil Processing. In: Hsu C.S., Robinson P.R. (eds) Practical Advances in Petroleum Processing. Springer, New York, NY.
21. Nelson, R. K., Gosselin, K. M., Hollander, D. J., Murawski, S. A., Gracia, A., Reddy, C. M., & Radovic, J. R. (**2019**). Exploring the Complexity of Two Iconic Crude Oil Spills in the Gulf of Mexico (Ixtoc I and Deepwater Horizon) Using Comprehensive Two-Dimensional Gas Chromatography (GC × GC). *Energy Fuels*. 33, 3925−3933.
22. Hayakawa, N. (**2018**) Polycyclic Aromatic Hydrocarbons. Springer Nature Singapore Pte Ltd.
23. Mackay, D. Y., Wan, S., Kuo, C. M. (**1992**) Illustrated handbook of physical-chemical properties and environmental fate for organic chemicals. CRC Press (Lewis Publishers), Boca Raton.
24. Yang, T., Kaiser, R.I., Troy, T.P., Xu, B., Kostko, O., Ahmed, M., Mebel A.M., Zagidullin, M.V., Azyazov, V.N. (**2017**). HACA's Heritage: A Free-Radical Pathway to Phenanthrene in Circumstellar Envelopes of Asymptotic Giant Branch Stars. *Angew. Chem. Int. Ed*., 56, 4515-4519.
25. Yang, T., Muzangwa, L., Kaiser, R.I., Jamal, A., Morokuma, K. (**2015**). A Combined Crossed Molecular Beam and Theoretical Investigation of the Reaction of the Meta-tolyl Radical with Vinylacetylene- toward the Formation of Methylnaphthalenes. *Phys. Chem*. 34, 461-514.
26. Llamas, A., Al-Lal, A.M., García-Martínez, M.J., Ortega, M.F., Llamas, J.F., Lapuerta, M., Canoira, L. (**2017**). Polycyclic Aromatic Hydrocarbons (PAHs) produced in the combustion of fatty acid alkyl esters from different feedstocks: quantification, statistical analysis and mechanisms of formation. *Sci. Tot. Environ.* 586, 446–456.
27. Ravindra, K., Sokhi, R., Van Grieken, R. (**2008**). Atmospheric polycyclic aromatic hydrocarbons: source attribution, emission factors and regulation. *Atmos Environ*. 42, 2895–2921.

28. Shukla, B.M., Koshi, M. (**2012**). Importance of fundamental sp, sp^2, sp^3 hydrocarbon radicals in the growth of polycyclic aromatic hydrocarbons. *Anal Chem*. 84, 5007–5016.
29. Frenklach, M. (**2002**). Reaction mechanism of soot formation in flames. *Phys Chem*. 4, 2028–203.
30. Holowenko, F. M., MacKinnon, M. D., Fedorak, P. M. (**2000**). Methanogens and sulfate-reducing bacteria in oil sands fine tailings waste. *Can. J. Microbiol*. 46, 927-937.
31. Haritash, A. K., Kaushik, C. P. (**2009**). Biodegradation aspects of Polycyclic Aromatic Hydrocarbons (PAHs): A review. *J Hazard Mater*. 169, 1–15.
32. Van Herwijnen, R., Wattiau, P., Bastiaens, L., Daal, L., Jonker, L., Springael, D., … Parsons, J. R. (**2003**). Elucidation of the metabolic pathway of fluorene and cometabolic pathways of phenanthrene, fluoranthene, anthracene and dibenzothiophene by Sphingomonas sp. LB126. *Research in Microbiology*, 154(3).
33. Beens, J.; Blomberg, J.; Schoenmakers, P. J. (**2000**). Proper tuning of comprehensive two-dimensional gas chromatography (GC× GC) to optimize the separation of complex oil fractions *High. Resolut. Chromatogr*. 23, 182-188.
34. Lui, Z.; Phillips, J.B. (**1991**) Comprehensive two-dimensional gas chromatography using an on-column thermal modulator interface. *J. Chrom. Sci*. 20 (6), 227-231
35. Mazur, D.M.; Zenkevich, I.G.; Artaev, V.B.; Polyakova, O.V.; Lebedev, A.T. (**2018**). Regression algorithm for calculating second-dimension retention indices in comprehensive two-dimensional gas chromatography. *J. Chrom. Anal*. 1569, 178-185.
36. Tran, T.C.; Logan, G.A.; Grosjean, E.; Ryan, D.; Marriott, P.J. (**2010**). Use of comprehensive two-dimensional gas chromatography/time-of-flight mass spectrometry for the characterization of biodegradation and unresolved complex mixtures in petroleum. *Geochim. Cosmichim. Acta*. 74 (22), 6468-6484.
37. Harris, Daniel C. (**2011**). Harris' Quantitative Chemical Analysis, Eighth Edition. W.H. Freeman and Co.
38. Arriaga, D., Colenbrander, T., Risacher, F. F., Morris, P. K., Goad, C., Slater, G. F., & Warren, L. A. (**2019**). Applied Geochemistry The co-importance of physical mixing and biogeochemical consumption in controlling water cap oxygen levels in Base Mine Lake. *Applied Geochemistry*, 111, 104442.

39. Postigo, C., Martinez, D.E., Grondona, S., Miglioranza, K.S.B. (**2018**). Groundwater Pollution: Sources, Mechanisms, and Prevention. Encyclopedia of the Anthropocene, Elsevier. 5, 87-96.
40. Payne, T.E., Edis, R. (**2012**). Mobility of Radionuclides in Tropical Soils and Groundwater - Radioactivity in the Environment, Elsevier. 18, 93-120.
41. Katyal, A., Morrison, R.D. (**2007**). Forensic Applications of Contaminant Transport Models in the Subsurface – Introduction to Environmental Forensics, Academic Press. 513 – 575.
42. Tranchida, P.Q., Purcaro, G., Dugo, P., Mondello, L. (**2011**). Modulators for comprehensive two-dimensional gas chromatography. *TrAC Trends in Analytical Chemistry*. 30 (9), 1437-1461.
43. Kayode Coker, A. (**1995**). Fortran Programs for Chemical Process Design, Analysis, and Simulation. Gulf Professional Publishing. 150-255.
44. Siddique, T., Stasik, S., Mohamad Shahimin, M. F., & Wendt-Potthoff, K. (**2018**). Microbial Communities in Oil Sands Tailings: Their Implications in Biogeochemical Processes and Tailings Management. *In Microbial Communities Utilizing Hydrocarbons and Lipids: Members, Metagenomics and Ecophysiology.* Handbook of Hydrocarbon and Lipid Microbiology. 1-33.
45. Gross, J.H. (**2011**). *Mass Spectrometry*, Second Edition. Springer-Verlag Berlin Heidelberg. 155 – 176.

Chapter Two – Identification of Solvent Extract Petroleum Hydrocarbon Isomers from Base Mine Lake Fluid Fine Tailings using Comprehensive Two-dimensional Gas Chromatography Time of Flight Mass Spectrometry

Mikhail Dereviankin[1], Gregory F. Slater[1]

Author Affiliation:

[1]School of Geography and Earth Sciences, McMaster University, Hamilton, Ontario, Canada

Author Contribution:

MD and GFS conceived and designed the study. MD performed the sample extraction, GC×GC/TOFMS instrumental analysis, data analysis, interpretation, and wrote the manuscript. GFS edited the manuscript.

Abstract

A systematic workflow was undertaken to optimize an analytical method for the identification of a subset of chemical species from the solvent extraction of total petroleum hydrocarbons (PHCs) in oil sands tailing matrices. Adaptations were applied to the conventional methodology of total PHCs solvent extraction (ASTM D5765) for the specifications required for analysis of fluid fine tailings (FFT) from Syncrude Ltd. Canada's Base Mine Lake (BML) located in Fort McMurray, Alberta, Canada. The analytical resolution of a subset of chemical species from BML FFT was accomplished employing comprehensive two-dimensional gas chromatography time-of-flight mass spectrometry (GC×GC/TOFMS). The enhanced peak capacity of GC×GC/TOFMS offers the ability to accurately identify individual isomers dissimilar to the standardized methodology (ASTM D7363), where species can only be resolved as a summation of their class and require samples to be fractionated into aromatic and aliphatic regions prior to analysis. Firstly, the systematic workflow for method optimization compared different capillary columns for the best resolution of the solvent extractable PHC species. Through direct comparison of the isomers within their respective compound class and molecular weight resolution, it was determined that the non-polar/polar (NP/P) combination of capillary columns provides the greatest representation of the total solvent extractable PHCs. In addition to the resolution of alkylated poly-cyclic aromatic hydrocarbon species representative of PHC inputs, the NP/P combination of capillary column was able to resolve low molecular weight (C7 – C12) paraffins associated with potential labile organic carbon inputs. In total 69 individual alkylated poly-cyclic aromatic hydrocarbon species were semi-quantified: two species of C1-naphthalene, nine species of C2-naphthalene, eight species of C3-naphthalene, fourteen species of C4-naphthalene, four species of C1-fluorene, five species of C2-fluorene, four species of C1-phenanthrene, eight species of C2-phenanthrene, four species of C1-benzothiopehene, 3 species of dibenzothiophenes and six species of C2-dibenzothiophene. One petroleum biomarker was identified, drimane, and semi-quantified with the closest available standard. In total 3 *n*-alkanes (C11-C13) were quantified with authentic

standards. The remaining low molecular weight paraffins present in the unresolved complex matrix (UCM) of BML FFT TLE were not quantified based on limitations of authenticated standards.

Introduction

The conventional methodology of monitoring the total petroleum hydrocarbons (PHCs) species in oil sands tailings uses one-dimensional gas chromatography (1D-GC)[2,21]. The primary criterion for evaluating analytical methods utilizing gas chromatography is peak capacity. In gas chromatography, peak capacity refers to both the peak separation (distance between the peaks) and resolution (width of peak)[28]. Insufficient peak capacity attributed to an overlaying unresolved complex matrix (UCM) associated with these 1D-GC chromatograms requires that total solvent extracted PHCs species are fractionated into aliphatic and aromatic regions prior to analysis[2]. Additionally, isomeric species can only be resolved as the summation of their compound class due to the co-elution of these peaks in 1D-GC. Isomerism finds its importance in the field of organic biogeochemistry and oil sands forensics, as isomers differ in their intrinsic chemical properties, which can act as predictors to assessing fate and transport[22]. It has been shown that individual alkylated poly-cyclic aromatic hydrocarbon isomers, which are markers of petroleum deposition, may exhibit deferential biodegradation rates as the position of alkyl groups influences solubility and conversely bioavailability[22]. A viable methodology to overcome the peak capacity challenges of 1D-GC is the use of comprehensive two-dimensional gas chromatography (GC×GC) to resolve individual isomers of aromatic and aliphatic PHCs. GC×GC is a powerful tool in petroleum forensics as it offers unparalleled chromatographic peak capacity and has been used in recent years to resolve individual constituents within complex mixtures, including structural isomers[9].

In a properly tuned GC×GC chromatogram, the separation is orthogonal, meaning the retention times in the two dimensions are independent of one another. The principal instrumental parameter in GC×GC influencing the orthogonal species separation is the choice in column orientation. In GC×GC, column orientation is the combination of two capillary GC columns connected between the modulation unit[10]. The column orientation used between the first dimension and second

dimension column is not static and can be modified to fit the experimental design. Column orientation can encompass any combination of different GC capillary columns however, to achieve proper orthogonal separation the columns must be of different stationary phase. The use of varying stationary phase in the secondary column, provides a mechanism to separate species that cannot be separated by the stationary phase of the primary column. The conventional orientations for GC×GC are generally categorized into two different orientations: non-polar/polar (NP/P) and polar/non-polar (P/NP), alternatively referred to as “reverse phase”. With the modification of the polarity of columns, the chromatographic separation in the second dimension will be inversed. In the non-polar/polar (NP/P) orientation, which is the conventional orientation for petroleum analysis, the paraffin components elute earlier in the second-dimension result in their lower chromatographic placement comparatively to the aromatic analytes. In the polar/non-polar (P/NP) orientation, the paraffin components exhibit increased retention to the secondary stationary phase and will elute later in the second dimension resulting in higher chromatographic placement as appose to aromatic analytes. It is important to consider that the column orientations are not limited to these conventional set ups and enhanced peak capacity has been achieved using combinations with chiral[10, 24] and ionic liquid columns[23]. Another important consideration is that GC×GC is not limited to only two capillary columns with adequate peak capacity being achieved using three columns (GC×2GC) or four columns (2GC×2GC)[25-27].

In order for GC×GC to be a viable improved chromatographic methodology in comparison to 1-D GC, the instrumental parameters are required to be optimized for the resolution of individual isomers within their respective class. One chromatographic artifact of GC×GC is the “smearing” of compounds resulting in the elongation of a peak in the second dimension. This effect occurs when analytes have increased partitioning coefficients for the second-dimension stationary phase and elute broadly in the second-dimension axis. Another limitation that can occur with non-optimized GC×GC methods is the, “wrapping effect”. The wrapping effect occurs when the

modulation period is shorter than the time for the previous modulation phase to elute from the second column. If compounds remain on the second column, there will be an overlap in retention times. This would occur if a first sample has a modulation time of 10 seconds, but the compounds in your sample have a maximum retention time of 15 seconds. Not all the compounds in the sample will elute during the modulation period but will elute during the next modulation period after 5 seconds. These heavier compounds will appear to have a retention time of 5 seconds. When constructing a method, it is therefore crucial to ensure that the modulation time is greater than the maximum secondary retention time of any compound in the sample.

The objective of the study is aimed to affirm that the NP/P column orientation is the optimal instrumental set up for resolution of PHC isomers in oil sands tailings matrices. The default column orientation used for the resolution of PHC isomers is the NP/P set up. However, no direct assessment has been made between the conventional column orientations for identifying PHC isomers from highly biogeochemically degraded oil sands tailings known to contain an overlaying UCM. Tran *et al.* (2010) have investigated NP/P and P/NP column orientations by comparing the chromatographs of Gippsland crude oil (Wirrah 1, GA#857). The NP/P orientation for the analysis of Gippsland crude oil efficiently separated the aliphatic components from the aromatics (**Figure 12a**). A limitation with this orientation was that the aliphatic components were poorly resolved on the second dimension (polar) column. The inverse polarity set up, P/NP, resulted in an inverted chromatogram where the aliphatic components occupied the upper segment of the 2-dimensional space, while the aromatics occupied the lower segment (**Figure 12b**). Significantly greater resolution of the aliphatic components was achieved with this set up, but the peak capacity for the aromatic components had severely decreased demonstrating that this orientation was ideal for the characterization of isoprenoids. Although this study provides a robust comparison between the two column orientations, the crude oil analyzed by Tran *et al.* (2010) achieved separation of individual alkylated poly-cyclic aromatic hydrocarbons isomers in the 1-D GC chromatograph and

is not representative of biogeochemically degraded oil sands that have an overlaying UCM that does not allow resolution of these isomers in 1D-GC.

Evaluation of species peak capacity and dynamic range of the chromatographic molecular weights facilitates a robust method of determining the appropriate column orientations for analysis of highly biogeochemically degraded oil sands tailings by GC×GC. The dynamic range of the chromatographic molecular weights is represented by the range of linear carbon atoms that the chromatograph can resolve. This metric is calculated from overlaying an authenticated *n*-alkane standard over the chromatograph utilising the same instrumental parameters. Although the most robust method of setting up a comprehensive GC×GC experiment is to choose the ideal column orientation, practical limitations such as resource can limit a researcher's options. As such after a column orientation has been chosen, a systematic approach based on mechanistic arguments needs to be taken to optimize the method to the experimental objectives. Within this chapter, a direct comparison between the NP/P and P/NP orientation for the analysis of oil sands tailings and a systematic approach to optimizing column orientation is assessed. In addition to the methodological study, the structure of individual species of alkylated poly-cyclic aromatic hydrocarbons, petroleum biomarkers and *n*-alkanes from oil sands tailings were elucidated through the interpretation of EI mass spectra, comparison to EI mass spectral database and, if available, confirmed with reference spectra from authenticated standards.

Experimental

Sample Matrix: 2017 Base Mine Lake Fluid Fine Tailing

The oil sands tailings utilized for identification of solvent extractable PHCs were collected from Base Mine Lake (BML) a Pit Lake (PL) that Syncrude commissioned in 2012 and is the first application of this reclamation strategy in the Athabasca Oil Sands Region (AOSR). The FFT sample utilized for column comparison and method optimization was collected at BML Platform 1

(57.010437, -111.6213021) on 23-July-2017 at a depth of 0.2 m from the FFT – Water Cap Interface.

Chemicals & Reagents

Dichloromethane, methanol, hexane (distilled in glass) was purchased from EMO Millipore Corporation. The following compounds were purchased and used as recovery/internal standards in this study: m-terphenyl (96%, Sigma-Aldrich) and benzo[a]anthracene-d12 (98%, Sigma-Aldrich). The following standards were purchased for semi-quantification of target compounds: 1-methylnaphthalene (95%, Sigma-Aldrich), 2-ethylnaphthalene (98%, Sigma-Aldrich), 2,3,5-trimethylnaphthalene (98%, Sigma-Aldrich), 1,4,6,7-tetramethylnaphthalene (98%, Sigma-Aldrich), 1-methylfluorene (98%, Sigma-Aldrich), 1,8-dimethyl-9H-fluorene (98%, Sigma-Aldrich), 9-methylanthracene (98%, Sigma-Aldrich), 9,10-dimethylanthracene (98%, Sigma-Aldrich), 3-methylbenzothiophene (96%, Sigma-Aldrich), 4-methyldibenzothiophene (96%, Sigma-Aldrich), 4,6-dimethyldibenzothiophene (97%, Sigma-Aldrich), Supelco SS TCL Polynuclear Aromatic Hydrocarbon Mix in methylene chloride : benzene (Sigma-Aldrich), SUPELCO C7-C40 Saturated Alkane Mixture in hexane (Sigma-Aldrich).

Extraction Procedure

The method for total lipid extraction (TLE) of the organic constituents from FFT was modified from the method developed by Lopez-Avlla *et. al* (1994). Briefly, 500 mL Nalgene bottles containing FFT were thawed overnight and freeze dried for 72 hours to remove residual moisture. The freeze dried FFT sample was spiked with recovery standard, *m* – terphenyl. A 1:1 hexane: acetone solution was introduced into the sample matrix to extract the organic constituents from the FFT. The mixture underwent microwave extraction with a MARS Microwave Extractor (Serial # MD7382) with the following parameters: Power 100%, Ramp to 115^{o}C hold for 10 mins. The microwaved extract was decanted and passed through a 1.5 μm VWR glass microfiber filter (product number: 691, 28333-125) and washed with hexane. Samples were diluted to their final

volume with hexane and the extract was transferred into GCMS vials using a 0.45 µm PTEE filter syringe. Prior to analysis, all vials were spiked with benzo[a]anthracene-d12 as the internal standard.

Instrumental Analysis: Comprehensive Two-Dimensional Gas Chromatography Time-Of-Flight Mass Spectrometry (GC×GC/TOFMS)

The FFT TLEs were analyzed using a Pegasus 4D system (LECO Corp., St Joseph, MI, USA). The polar/non-polar (P/NP) column orientation utilized a Rtx-17sil ms (30 m x 0.25 mm x 0.15 µm) as the primary column and a DB-5 ms (1.5 m x 0.10 mm x 0.10 µm) as the secondary column. The non-polar/polar (NP/P) Column Orientation utilized a DB1-MS column (60 m x 0.25mm x 0.25 µm film thickness) as the primary column and a DB-17ms column (1.25 m x 0.10mm x 0.10 µm film thickness) as the secondary column. The following comprehensive two-dimensional gas chromatography methods were compared during method optimization of the NP/P column orientation: *2DGC Method A*: The primary oven was programmed to hold at 80 °C for fifteen minutes, ramp to 335 °C at a rate of 1.66 °C/min. The secondary oven offset was set to +5 °C relative to the primary oven. A dual stage quad-jet thermal modulator with modulation period of 7.5 s was used. The modulator temperature offset was +3°C relative to the secondary oven. *2DGC Method B*: The primary oven was programmed to hold at 80 °C for fifteen minutes, ramp to 335°C at 1.66°C/min. The secondary oven offset was set to +5°C relative to the primary oven. A dual stage quad-jet thermal modulator with modulation period of 12 seconds was used. The modulator offset was +3°C relative to the secondary oven.*2DGC Method C*: The primary oven was programmed to hold at 80 °C for fifteen minutes, ramp to 335°C at 1.66°C/min. The secondary oven offset was set to +5°C relative to the primary oven. A dual stage quad-jet thermal modulator with modulation period of 7.5 seconds was used. The modulator offset was +15°C relative to the secondary oven. The ion source and transfer line temperatures were set to 240 °C and 280 °C, respectively. Helium was used as the carrier gas at a flow rate of 1 mL/min. The time-of-flight mass spectrometer was scanned over a mass range of m/z 40 to 600 at a sample

acquisition rate of 100 scans/s with a solvent delay set to 1300s. The detector voltage was offset by 100V with an acquisition voltage of 1678. Data processing of GC×GC/TOFMS data was performed by ChromaTOF version 4.50.8.0 (LECO Corp), which included automatic peak finding with mass spectral deconvolution. Library searches were conducted with the NIST/EPA/NIH Mass Spectral Library 2008 (NIST 08, Gaithersburg, MC, USA) and a user library containing alkylated polyaromatic hydrocarbon reference standards.

Results and Discussion

Column Orientation Comparison for the Analysis of Solvent Extractable Petroleum Hydrocarbon Isomers in Base Mine Lake Fluid Fine Tailings

To facilitate a comparison between the molecular weight range for the P/NP and NP/P column orientation, a SUPELCO C7-40 *n*-alkane standard was overlaid on the total ion chromatograph (TIC) generated from the GC×GC/TOF analysis of the 2017 BML FFT. The TIC of the solvent extractable PHCs analyzed with the P/NP orientation was only able to resolve compounds between the C13 to C22 *n*-alkane range (**Figure 13a**). After the C22 *n*-alkane standard, the higher molecular weight species were not resolved as these compounds exhibited elongated second dimension retention times resulting from their increased partitioning into the secondary column. C7 – C12 *n*-alkanes are not visible or detected in the P/NP TIC due to low partitioning coefficient with the primary column stationary phase resulting in elution of these species within the solvent delay. The retention time range was modified in the P/NP TIC as the solvent persisted to elute from the primary column after the solvent delay set at 600 seconds. The P/NP column orientation successfully separated the aromatic and aliphatic region into two distinct unresolved complex matrices (UCMs) with the caveat that individual species were not resolved in the TIC. In the second dimension, these two UCMs primarily occupied the space between 2 seconds and 3 seconds with equal distribution between the aromatic and aliphatic regions. The column orientation was able to resolve a subset of alkylated poly-cyclic aromatic hydrocarbon isomers by filtering through their nominal mass-to-charge (m/z) ratios.

The TIC of the solvent extractable species in 2017 BML FFT analyzed with the NP/P orientation demonstrated an increased molecular weight range resolution in comparison to the P/NP orientation, with compounds eluting in the C7 to C33 *n*-alkane range (**Figure 13b**). Comparably, the UCM consisted of species larger than C13 *n*-alkane and was primarily composed of aliphatic compounds. The most impactful comparison between the P/NP orientation, was the orientation's ability to utilize the second dimension to separate individual alkylated aromatic species from the majority of UCM components. The second dimension UCM resolution range is also comparable increased to 1.5 seconds – 6 seconds compared to the P/NP orientation. In addition to resolution of aromatic isomers in the TIC, the NP/P orientation was able to resolve low molecular weight (below C13 *n*-alkane) aliphatic components that co-eluted with the solvent using the P/NP orientation. Most notably the NP/P orientation was able to resolve individual lower molecular weight *n*-alkanes (C11-C13 *n*-alkane) that were not components of the UCM aliphatic range (>C14 *n*-alkane).

The second parameter comparing the practicality of the two column orientations was the peak capacity for a subset of alkylated poly-cyclic aromatic hydrocarbon species associated with residual bitumen and/or labile organic carbon inputs in the FFT at BML. In order for GC×GC to be an improved methodology over conventional 1-D GC analysis, the subset of isomers need to be resolved within their respective compound classes. Between the two column orientations the peak capacity for a subset of alkylated poly-cyclic aromatic hydrocarbon species generally remained consistent (74 - 81%). Although both orientations were able to resolve individual isomers of alkylated poly-cyclic aromatic hydrocarbons, the NP/P orientation demonstrated increased peak capacity for isolating these compounds in the TIC while the P/NP orientation required the chromatograph to be mass extracted for the individual class of compound. The ability to resolve individual isomers in the TIC allows the column orientation to be adapted to different detectors, for example Flame Ionization Detectors (FID), that do not have mass spectroscopy functionality. Through direct comparison of the molecular weight range and peak capacity for a subset of

species it was determined that the NP/P is the ideal column orientation for understanding the complexity of the sample matrix in BML FFT as it can not only resolve alkylated poly-cyclic aromatic species in the TIC, but can resolve low molecular weight (C7 – C12) paraffins associated with labile organic carbon inputs.

Optimization of the Non-Polar/Polar Column Orientation for Base Mine Lake Fluid Fine Tailings

From the results of the column comparison study, it was determined that the NP/P set up was ideal for the analysis of BML FFT TLEs as this orientation can not only resolve aromatic species, but can resolve low molecular weight (C7 – C12) organic constituents. These lower molecular weight compounds are considered biogeochemically more labile and monitoring of these compounds provides further contextual information for future studies in BML FFT. However, the caveat in utilizing this column orientation is that higher molecular weight aromatic species were, "smeared", in the second dimension due to increased retention in the secondary column (**Figure 14**). Methyl dibenzothiophene (C1-DBT) was utilized to visualize the second-dimension smearing and as a reference for methodological optimization. In the case for C1-DBT species, wrapping was also occurred resulting from effluent remaining on the secondary column due to high partitioning with the column and eluting after the 7.5 seconds modulation time. In order to prevent any wrapping, the modulation time was increased to 12 seconds (**2DGC Method B**). Through the comparison of the chromatographs for mass filtered C1-DBT (m/z = 198), the increased the modulation time removed the wrapping effect, however the species peaks continued to exhibit poor resolution and "smearing" in the second-dimension axis (**Figure 15**).

The second optimization step involved exploiting the temperature offset between the primary oven and secondary oven containing the modulation unit. The temperature offset between the primary oven and secondary oven influences the rate of desorption of the effluent trapped within the quad-jet modulation unit entering the relatively short second dimension column. Increasing the

temperature offset may increase the rate at which the eluent desorbed from the modulation unit and sharpens the peak within the second dimension. In this study, the temperature offset between the primary oven and modulation unit was increased to +15°C relative to the secondary oven (**2DGC Method C**) to promote the desorption of heavy molecular weight compounds into the secondary column. Through the comparison of the chromatographs for mass filtered C1-DBT, it was apparent that the increase in temperature offset between the primary oven and the modulation unit had no effect on increasing peak resolution (**Figure 16**).

The limitation in peak resolution was determined to be associated with poor alignment of the secondary column between the dual stage quad-jet thermal modulator (**Figure 17**). With poor alignment of the secondary column, heavier molecular weight compounds trapped as effluent from the first dimension are insufficiently desorbed and thus not transferred into the second dimension as a sharp volatile peak segment. After this modification, the chromatographs for mass filtered C1-DBT (**Figure 18**) was able to resolve all species with no wrapping or smearing.

Identification of Petroleum Hydrocarbon Isomers from Pit Lake Fluid Fine Tailings

In GC×GC, isomeric species are typically oriented by angled bands, known as 'roof-tiles', which contribute to confirming peak assignment (**Figure 19**). The roof-tile effect results from the arrangement of isomers in the two-dimensional retention plane by their relative boiling point and isothermal separation in the secondary capillary column[29]. Isomer roof-tiles were identified by mass filtering by the species class nominal mass and isomers were designated a letter based on their relative position in the roof tile. The structure of individual solvent extractable organic isomers derived from residual inputs of bitumen and/or naphtha within the FFT TLE were elucidated through the interpretation of EI mass spectra, comparison to EI mass spectral database and, if available, confirmed with reference spectra from authenticated standards.

Identification of Solvent Extracted Alkylated Poly-Cyclic Aromatic Hydrocarbons

In total 69 individual alkylated poly-aromatic hydrocarbon species were semi-quantified: two species of C1-naphthalene, nine species of C2-naphthalene, eight species of C3-naphthalene, fourteen species of C4-naphthalene, four species of C1-fluorene, five species of C2-fluorene, four species of C1-phenanthrene, eight species of C2-phenanthrene, four species of C1-benzothiopehene, 3 species of C1-dibenzothiophenes and six species of C2-dibenzothiophene (**Table 2**).

C1-NAP isomers were identified in the extracted ion chromatograph (EIC) by mass filtering by their species nominal mass-to-charge ratio (*m/z* = 142). The peak assignment of C1-NAP isomers was confirmed by comparison of the mass spectrum for the authentic 1-methylnaphthalene standard (**Figure 20**) between the clustering of isobaric compounds in the GC×GC roof-tile. All EI mass spectra for the C1-NAP isomers shared a commonality with the base peak at *m/z* = 142 and the fragmentation at *m/z* = 115 resulting from the ethyl cleavage ($-C_2H_3^{\bullet}$) of the molecular ion. C2-NAP isomers were identified in the EIC by mass filtering by their species nominal mass-to-charge ratio (*m/z* = 156). The peak assignment of C2-NAP isomers was confirmed by comparison of the mass spectrum for the authentic 2-ethyl naphthalene standard (**Figure 22**) between the clustering of isobaric compounds in the GC×GC roof-tile. All EI mass spectra for the C2-NAP isomers shared a commonality with the fragmentation at *m/z* = 141 resulting from the methyl cleavage ($-CH_3^{\bullet}$) of the molecular ion. C3-NAP isomers were identified in the EIC by mass filtering by their species nominal mass-to-charge ratio (*m/z* = 170). The peak assignment of C3-NAP isomers was confirmed by comparison of the mass spectrum for the authentic 2,3,5-trimethylnaphthalene standard (**Figure 24**) between the clustering of isobaric compounds in the GC×GC roof-tile. All EI mass spectra for the C3-NAP isomers shared a commonality with the fragmentation occurring at *m/z* = 155 resulting from the methyl cleavage ($-CH_3^{\bullet}$) of the molecular ion. C4-NAP isomers were identified in the EIC by mass filtering by their species nominal mass-

to-charge ratio (*m/z* = 184). The peak assignment of C4-NAP isomers was confirmed by comparison of the mass spectrum for the authentic 1,4,6,7-tetramethylnaphthalene standard (**Figure 26**) between the clustering of isobaric compounds in the GC×GC roof-tile. All EI mass spectra for the C4-NAP isomers shared a commonality with fragmentation occurring at *m/z* = 169 resulting from the methyl cleavage ($-CH_3^{\bullet}$) of the molecular ion. C1-FL isomers were identified in the EIC by mass filtering by their species nominal mass-to-charge ratio (*m/z* = 180). The peak assignment of C1-FL isomers was confirmed by comparison of the mass spectrum for the authentic 1-methylfluorene standard (**Figure 28**) between the clustering of isobaric compounds in the GC×GC roof-tile. All EI mass spectra for the C1-FL isomers shared a commonality with the fragmentation occurring at *m/z* = 165 resulting from the methyl cleavage ($-CH_3^{\bullet}$) of the molecular ion. C2-FL isomers were identified in the EIC by mass filtering by their species nominal mass-to-charge ratio (*m/z* = 194). The peak assignment of C2-FL isomers was confirmed by comparison of the mass spectrum for the authentic 1,8-dimethyl-9H-fluorene standard (**Figure 30**) between the clustering of isobaric compounds in the GC×GC roof-tile. All EI mass spectra for C2-FL isomers shared a commonality with the fragmentation occurring at *m/z* = 179 resulting from the methyl cleavage ($-CH_3^{\bullet}$) of the molecular ion. C1-PH isomers were identified in the EIC by mass filtering by their species nominal mass-to-charge ratio (*m/z* = 192). The peak assignment of C1-PH isomers was confirmed by comparison of the mass spectrum for the authentic 9-methylanthracene standard (**Figure 32**) between the clustering of isobaric compounds in the GC×GC roof-tile. An alkylated isomer of anthracene was used as the authenticated standard instead of phenanthrene due to availability and complementary molecular properties. All EI mass spectra for C1-PH isomers shared a commonality with the fragmentation occurring at *m/z* = 165 resulting from the cleavage of ethyl ($-C_2H_3^{\bullet}$) of the molecular ion. C2-PH isomers were identified in the EIC by mass filtering by their species nominal mass-to-charge ratio (*m/z* = 206). The peak assignment of C2-PH isomers was confirmed by comparison of the mass spectrum for the

authentic 9,10-dimethylanthracene standard (**Figure 34**) between the clustering of isobaric compounds in the GC×GC roof-tile. All EI mass spectra for C2-PH isomers shared a commonality with the fragmentation occurring at *m/z* = 191 resulting from the methyl cleavage (-$CH_3^{\bullet}$) of the molecular ion. C1-BT isomers were identified in the EIC by mass filtering by their species nominal mass-to-charge ratio (*m/z* = 148). The peak assignment of C1-BT isomers was confirmed by comparison of the mass spectrum for the authentic 3-methylbenzothiophene standard (**Figure 36**) between the clustering of isobaric compounds in the GC×GC roof-tile. C1-DBT isomers were identified in the EIC by mass filtering by their species nominal mass-to-charge ratio (*m/z* = 198). The peak assignment of C1-DBT isomers was confirmed by comparison of the mass spectrum for the authentic 4-methyldibenzothiophene standard (**Figure 38**) between the clustering of isobaric compounds in the GC×GC roof-tile. All EI mass spectra for C1-DBT isomers shared a commonality with the molecular ion being the base peak at *m/z* = 198 and with the expected [M+2] ^{34}S isotope peak. C2-DBT and C2-NBT isomers were identified in the EIC by mass filtering by their species nominal mass-to-charge ratio (*m/z* = 212). The peak assignment of C2-DBT and C2-NBT isomers was confirmed by comparison of the mass spectrum for the authentic 4,6-dimethyldibenzothiophene standard (**Figure 40** and **42**) between the clustering of isobaric compounds in the GC×GC roof-tile. All EI mass spectra for C2-DBT and C2-NBT isomers shared a commonality with the fragmentation occurring at *m/z* = 197 resulting from the methyl cleavage (-$CH_3^{\bullet}$) of the molecular ion and with the expected [M+2] ^{34}S isotope peak.

Identification of Petroleum Biomarkers

A biomarker was identified within all samples containing a mass spectrum with a unique fragmentation (*m/z* = 123). This biomarker was identified to belong to the sesquiterpene biomarker (bicyclic terpene) class based on EI mass spectral comparison between literature spectra[30] (**Figure 44**). The sesquiterpene biomarker, herein the biomarker is referred to as drimane, was semi-quantified with the closest available *n*-alkane standard (C14).

Identification of Low Molecular Weight Paraffins

In total 3 *n*-alkanes (C11-C13) were quantified with authentic standards based on relative retention time and EI mass spectral comparison (**Figure 45**).

Conclusion

Through direct comparison of the molecular weight range and peak capacity between the aromatic and aliphatic components of the UCM, it was determined that the default column set up, NP/P, for GC×GC was the ideal column orientation for understanding the complexity of the sample matrix in BML FFT compared to the P/NP. The advantage of this column orientation was that it could not only resolve alkylated poly-cyclic aromatic species in the TIC but could also resolve low molecular weight (C7 – C12) paraffins associated with labile organic carbon inputs. The current methodology provides future applications for comprehensive target analysis of solvent extractable species in BML FFT samples. The distribution in 2017 BML FFT of poly-cyclic aromatic hydrocarbon species and low molecular weight paraffins elucidated in this chapter will be investigation in Chapter 3.

References

1. Natural Resources Canada (**2016**). Oil Sands Extraction Processing. https://www.nrcan.gc.ca/energy/energy-sources-distribution/crude-oil/oil-sands-extraction-and-processing/18094.
2. ASTM D7363-13a, Standard Test Method for Determination of Parent and Alkyl Polycyclic Aromatics in Sediment Pore Water Using Solid-Phase Microextraction and Gas Chromatography/Mass Spectrometry in Selected Ion Monitoring Mode, ASTM International, West Conshohocken, PA, **2013**.
3. Masliyah, J., Zhou, Z., Xu, Z., Czarnecki, J., Hamza, H. (**2004**). Understanding water-based bitumen extraction from Athabasca oil sands. *Can. J. Chem. Eng*. 82, 628–654
4. Government of Alberta (**2015**). Lower Athabasca Region: Tailings Management Framework for the Mineable Athabasca Oil Sands. https://open.alberta.ca/dataset/962bc8f4-3924-46ce-baf8

d6b7a26467ae/resource/7c49eb63-751b-49fd-b746-87d5edee3131/download/2015-larp-tailingsmgtathabascaoilsands.pdf.

5. Allen, E.W. (**2008**). Process Water Treatment in Canada's Oil Sands Industry I. Target Pollutants and Treatment Objectives. *J. Environ. Eng. Sci*. 7, 123-138.
6. Dompierre, K. A., Lindsay, M. B. J., Cruz-Hernández, P., & Halferdahl, G. M. (**2016**). Initial geochemical characteristics of fluid fine tailings in an oil sands end pit lake. *Science of the Total Environment*, 556, 196–206.
7. Siddique, T., Fedorak, P.M., Foght, J.M. (**2006**). Biodegradation of short-chain n-alkanes in oil sands tailings under methanogenic conditions. *Environ. Sci. Technol*. 40, 5459–5464.
8. Siddique, T., Fedorak, P.M., MacKinnon, M.D., Foght, J.M. (**2007**). Metabolism of BTEX and naphtha compounds to methane in oil sands tailings. *Environ. Sci. Technol*. 41, 2350–2356.
9. Caughill, D.L., Morgenstern, N.R., Scott, J.D. (**1993**). Geotechnics of nonsegregating oil sand tailings. *Can. Geotech. J*. 30, 801–811.
10. Marriott, P.; Shellie. R. (**2002**). Principles and Applications of Comprehensive Two-Dimensional Gas Chromatography. *Trends Anal. Chem.* 21 (9−10), 573−583.
11. Rowland, S. J., West, C. E., Scarlett, A. G., Ho, C., Jones, D. (**2012**). Differentiation of two industrial oil sands process-affected waters by two-dimensional gas chromatography/mass spectrometry of diamondoid acid profiles. *Rapid Commun. Mass Spectrom*. 26 (5), 572– 576.
12. Frank, R. A., Roy, J. W., Bickerton, G., Rowland, S. J., Headley, J. V., Scarlett, A. G., West, C. E., Peru, K. M., Parrott, J. L., Conly, F. M., et al. (**2014**). Profiling oil sands mixtures from industrial developments and natural groundwaters for source identification. *Environ. Sci. Technol.* 48 (5), 2660–2670.
13. Bowman, D. (**2017**). Chemical fingerprinting of naphthenic acids by GC×GC/MS. Thesis.
14. White, W.M. (**2013**). Geochemistry. Wiley-Blackwell. 608-609.
15. Young, R. (**2019**). 2018 Mildred Lake Tailings Management Report Oil Sands Conservation Act Commercial Scheme Approval No. 8573.
16. Faidz, M., Shahimin, M., & Siddique, T. (**2017**). Sequential biodegradation of complex naphtha hydrocarbons under methanogenic conditions in two different oil sands tailings. *Environmental Pollution*, 221, 398–406.

17. Tran, T.C.; Logan, G.A.; Grosjean, E.; Ryan, D.; Marriott, P.J. (**2010**). Use of comprehensive two-dimensional gas chromatography/time-of-flight mass spectrometry for the characterization of biodegradation and unresolved complex mixtures in petroleum. *Geochim. Cosmichim. Acta*. 74 (22), 6468-6484.
18. Lopez-Avlla, V., Young, R., Becked, W. (**1994**). Microwave-Assisted Extraction of Organic Compounds from Standard Reference Soils and Sediments. *Anal. Chem.* 66, 1097 – 1106.
19. Ona-Ruales, J.O., Wilson, W.B., Nalin, F., Sander, L.C., Schubert-Ullrich, P., Wise, S. A. (**2016**). The Influence of the Aromatic Character in the Gas Chromatography Elution Order: The Case of Polycyclic Aromatic Hydrocarbons. *Mol Phys.* 114(23), 3533–3545.
20. Harris, Daniel C. (**2011**). Harris' Quantitative Chemical Analysis, Eighth Edition. W.H. Freeman and Co.
21. ASTM D5765-16, Standard Practice for Solvent Extraction of Total Petroleum Hydrocarbons from Soils and Sediments Using Closed Vessel Microwave Heating, ASTM International, West Conshohocken, PA, **2016**.
22. Wammer, K.H.; Peters, C.A. (**2005**). Polycyclic Aromatic Hydrocarbon Biodegradation Rates: A Structure-Based Study. *Environ. Sci. Technol*. 39, 2571-257
23. Adahchour, M.; Taso, A.; Beens, J.; Vreuls, J.J.; Batenburg, A.M.; Brinkman, U.A. (**2003**). Fast comprehensive two-dimensional gas chromatography (GC×GC) using 50-µm ID second-dimension columns. *J. Sep. Sci.* 26, 753-760.
24. Shellie, R.; Marriott, P.; Cornwell, C.J. (**2001**). Application of comprehensive two-dimensional gas chromatography (GC×GC) to the enantioselective analysis of essential oils. *J. Sep. Sci.* 24, 823-830.
25. Seely, J.V.; Kramp, F.J.; Sharpe, K.S. (**2001**). A dual-secondary column comprehensive two-dimensional gas chromatograph for the analysis of volatile organic compound mixtures *J. Sep. Sci.* 24, 444-450.
26. Seely, J.V.; Kramp, F.J.; Sharpe, K.S.; Seely, S.K. (**2002**). Characterization of gaseous mixtures of organic compounds with dual-secondary column comprehensive two-dimensional gas chromatography (GC× 2 GC). *J. Sep. Sci.* 25, 53-59.
27. Adahchour, M.; Jover, E.; Beens, J.; Vreuls, R.J.J.; Brinkman, U.A. (**2005**). Twin comprehensive two-dimensional gas chromatographic system: concept and applications. *J. Chromatogr. A.* 1086, 128-14.

28. Rood, D. (**1997**). Gas Chromatography Problem Solving and Troubleshooting. *J. Chromatogr. Sci.* 35, 458.

29. Vendeurve, C.; Ruiz-Guerrero, R.; Bertoncini, F.; Duval, L.; Thiebaut, D. (**2007**). Comprehensive Two-Dimensional Gas Chromatography for Detailed Characterisation of Petroleum Products. *Oil & Gas Science and Technology*. 62 (1), 43-55.

30. Wang, Z., Stout, S. A., & Fingas, M. (**2006**). Forensic fingerprinting of biomarkers for oil spill characterization and source identification. *Environmental Forensics*, 7(2), 105–146.

Figures and Tables

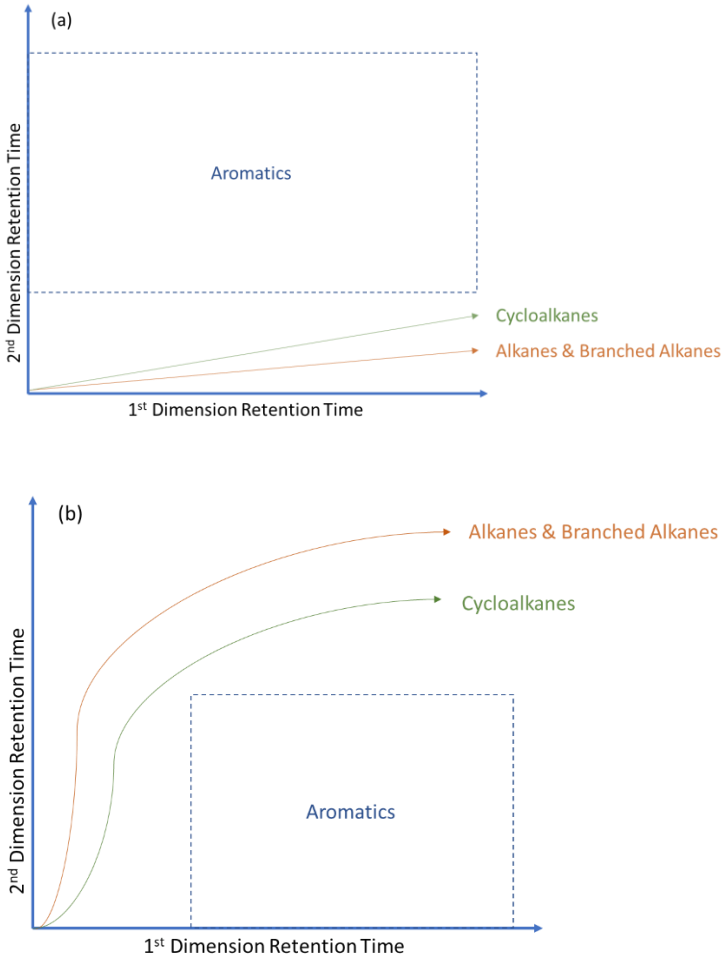

Figure 12 – (a) Schematic GC×GC species separation with non-polar/polar column orientation.[22] (b) Schematic GC×GC species separation with polar/non-polar column orientation[36].

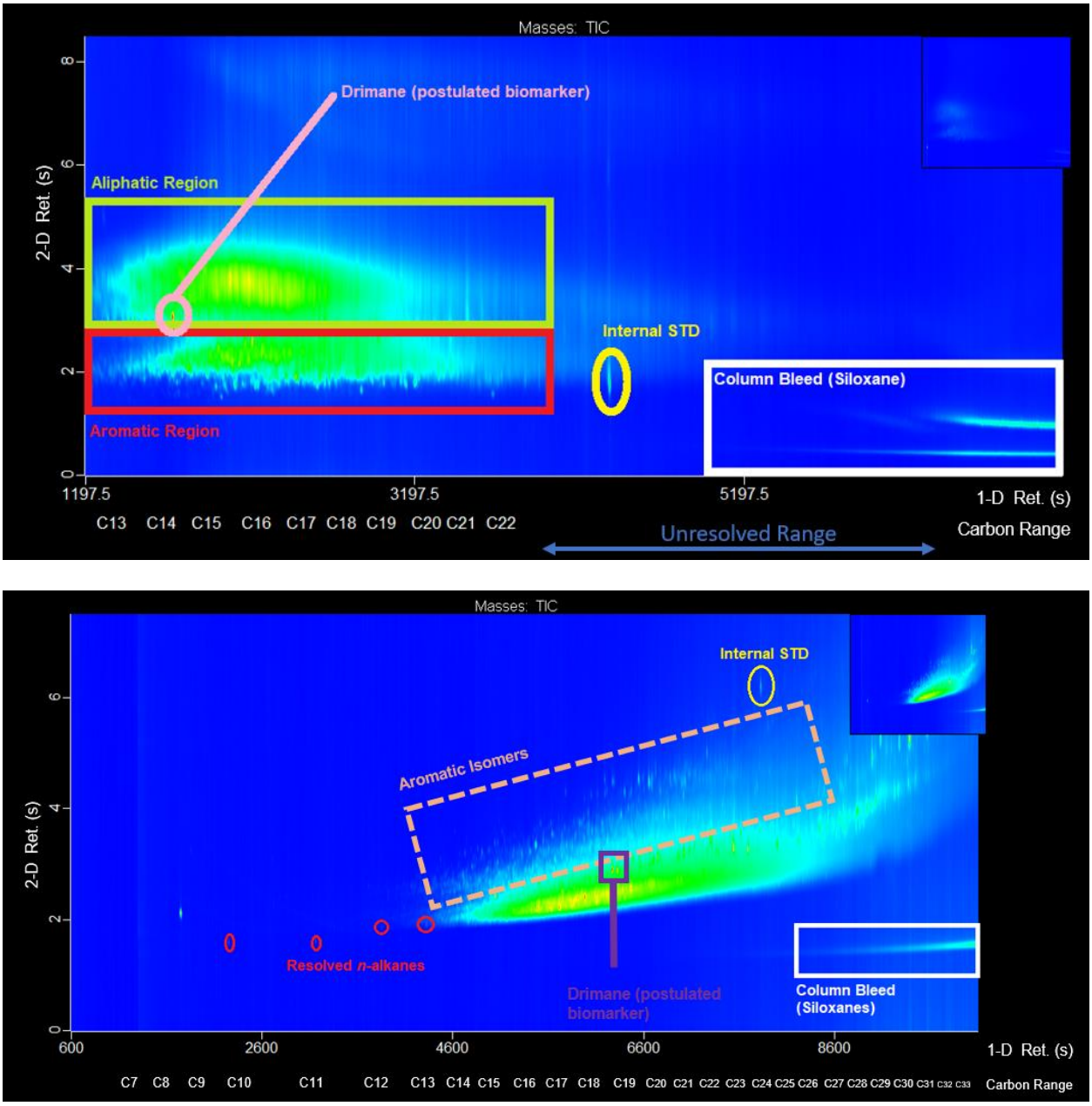

Figure 13 – (a) TIC generated from the GC×GC/TOF analysis of BML FFT TLE collected on 23-July-2017 at a depth of 0.2 m from the FFT – Water Cap Interface with the Polar/Non-Polar (P/NP) column orientation. (a) TIC generated from the GC×GC/TOF analysis of BML FFT TLE collected on 23-July-2017 at a depth of 0.2 m from the FFT – Water Cap Interface with the Non-polar/Polar (NP/P) column orientation.

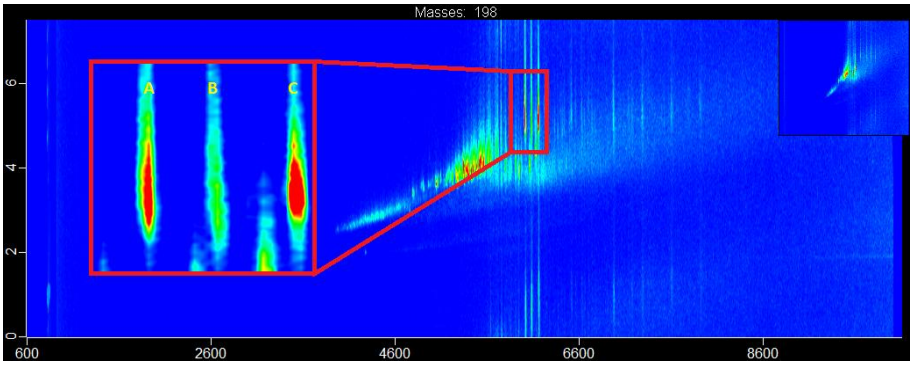

Figure 14 – “Smearing” & Wrapping Effect associated with running 2017 BML FFT TLE illustrated through methyl dibenzothiophene species (m/z = 198).

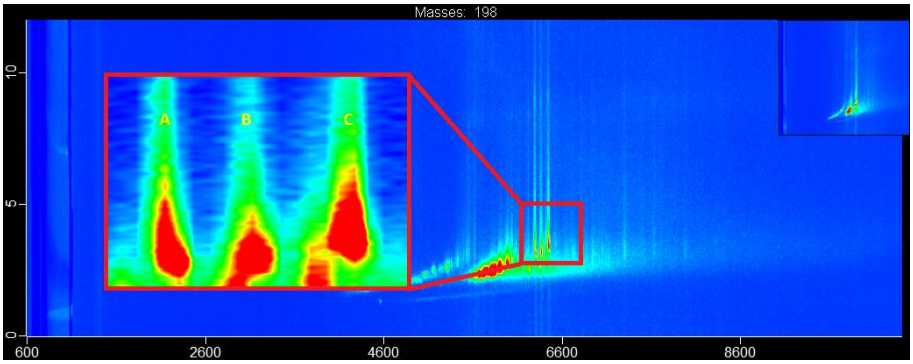

Figure 15 – Reduction of Wrapping Effect using 2DGC Method B associated with 2017 BML FFT TLE illustrated through methyl dibenzothiophene species (m/z = 198).

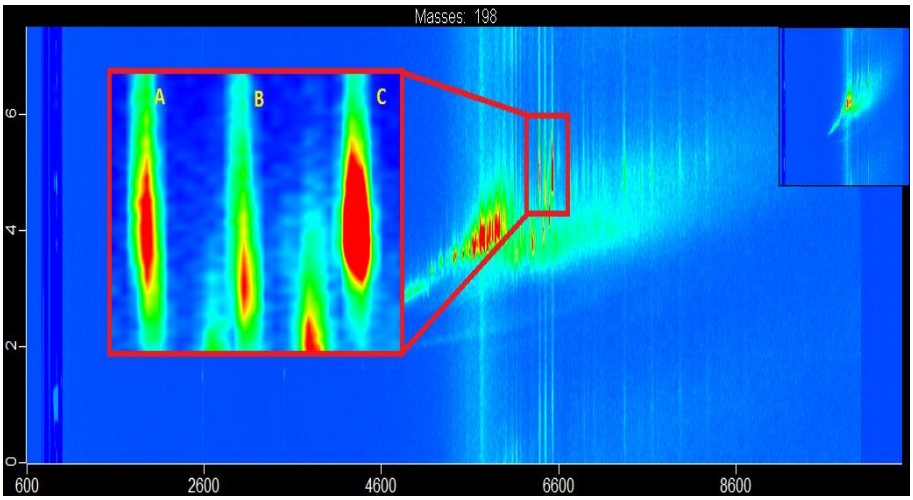

Figure 16 – Ineffective Reduction of Wrapping & “Smearing” using 2DGC Method C associated with 2017 BML FFT TLE illustrated through methyl dibenzothiophene species (m/z = 198).

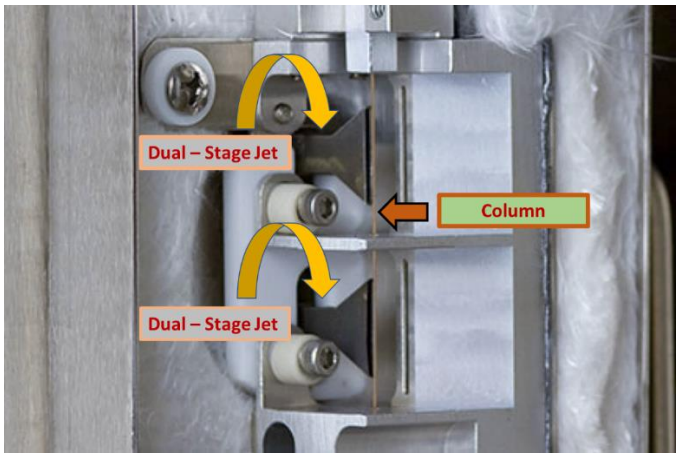

Figure 17 – Proper Alignment of Secondary Column within dual stage quad-jet thermal modulator unit.

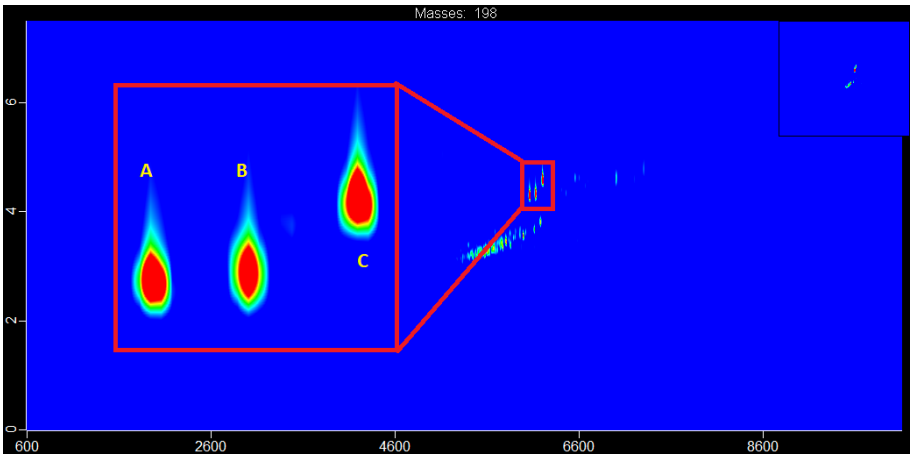

Figure 18 – Optimization of Peak Resolution through Proper Alignment of Column within dual stage quad-jet thermal modulator using 2DGC Method A associated with 2017 BML FFT TLE illustrated through methyl dibenzothiophene species (m/z = 198).

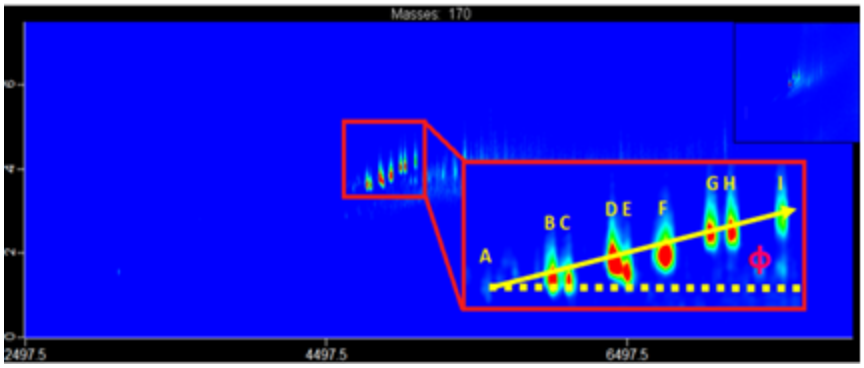

Figure 19 – Roof tile effect (Φ) for trimethyl naphthalene (m/z = 170) for 2017 BML FFT TLE analysed with the NP/P column orientation and Method A.

Table 2 – Semi-quantified Poly-Cyclic Aromatic Hydrocarbon Summary for 2017 BML FFT TLE with NP/P Column Orientation.

Semi-Quantified Standard	Isomer Abbreviations	Quantification Nominal Mass
1-methylnaphthalene	C1-NAP-A to C1-NAP-B	142
2-ethylnaphthalene	C2-NAP-A to C2-NAP-I	156
2,3,5-trimethylnaphthalene	C3-NAP-A to C3-NAP-H	170
1,4,6,7-tetramethylnaphthalene	C4-NAP-A to C4-NAP-O	184
1-methylfluorene	C1-FL-A to C1-FL-D	180
1,8-dimethyl-9H-fluorene	C2-FL-A to C2-FL-G	194
9-methylphenanthrene	C1-PH-A to C1-PH-D	192
9,10-dimethylphenanthrene	C2-PH-A to C2-PH-H	206
3-methylbenzothiophene	C1-BT-A to C1-BT-D	148
4-methyldibenzothiophene	C1-DBT-A to C1-DBT-C	198
4,6-dimethyldibenzothiophene	C2-DBT-A to C2-DBT-C	212
4,6-dimethyldibenzothiophene	C2-NBT-A to C2-NBT-C	212

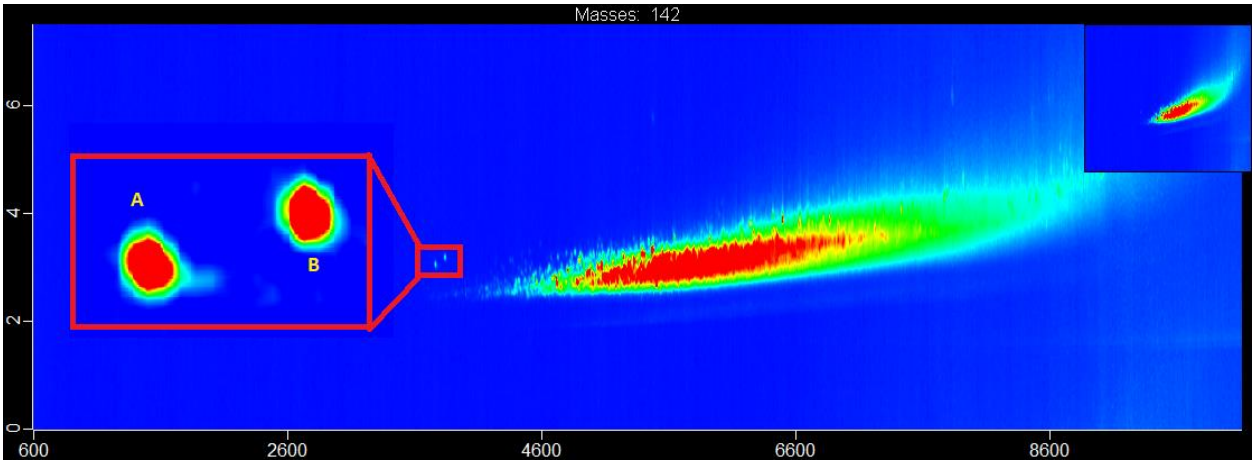

Figure 20 – C1-NAP-A & C1-NAP-B GCxGC/QTOF Chromatographic Separation in P1 2017 BML FFT TLE.

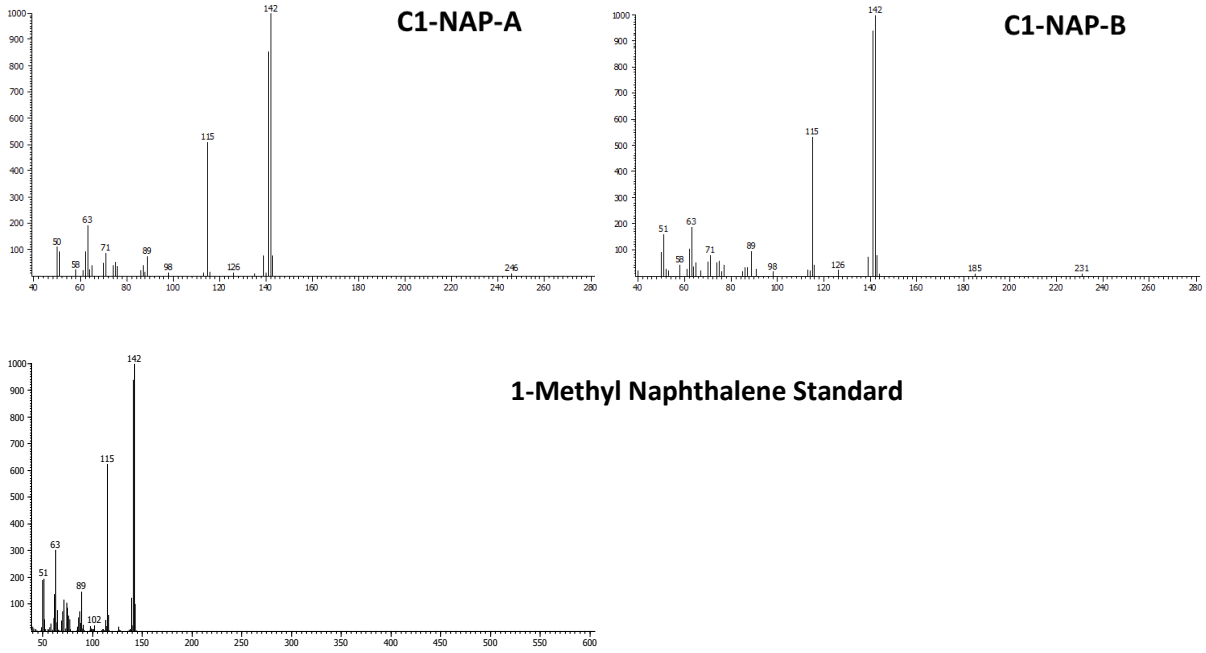

Figure 21 – 70 eV EI Mass Spectrum of C1-NAP-A & C1-NAP-B and 1-methyl naphthalene authenticate standard (m/z = 142).

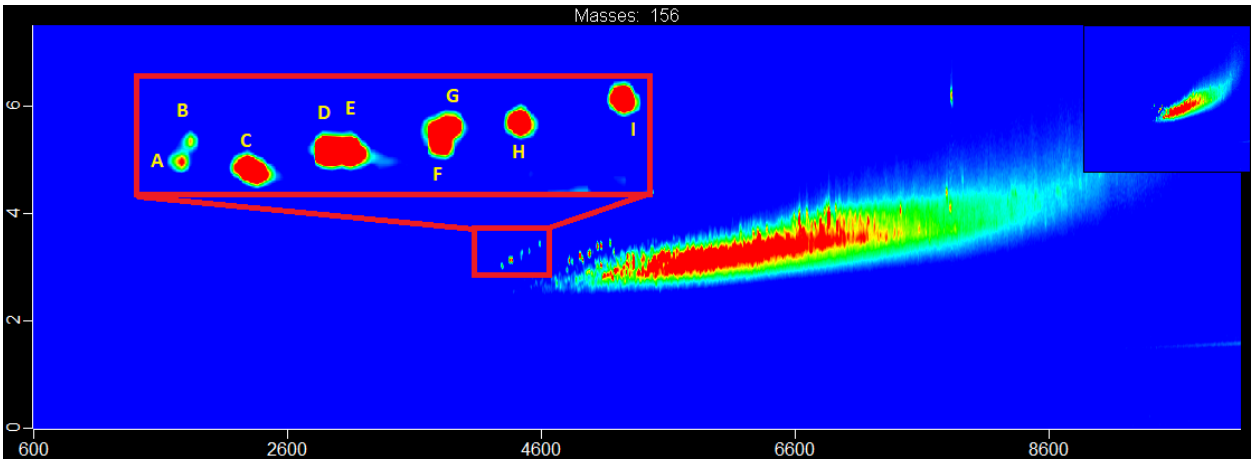

Figure 22 – C2-NAP-A to C2-NAP-I GCxGC/QTOF Chromatographic Separation in P1 2017 BML FFT TLE.

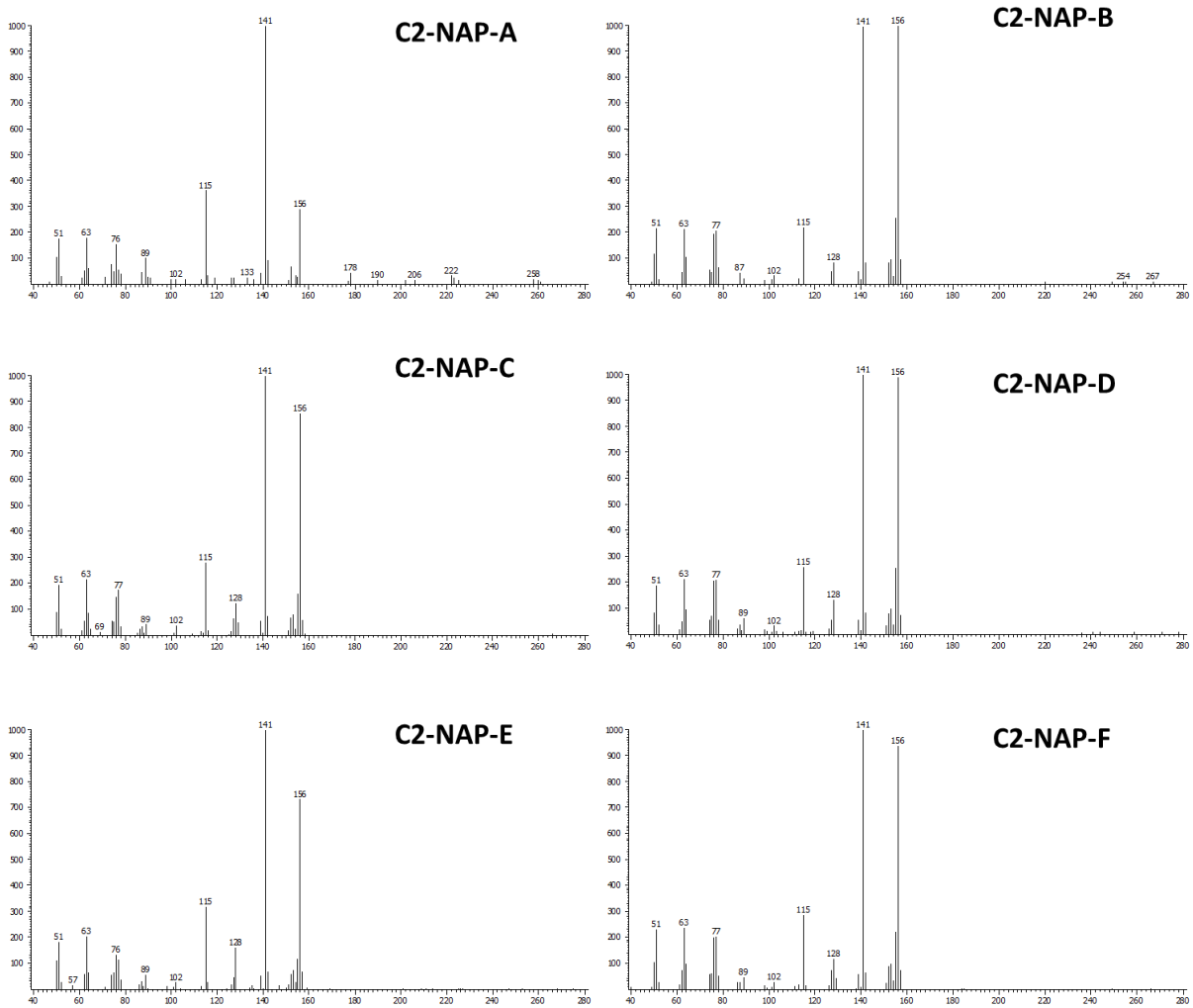

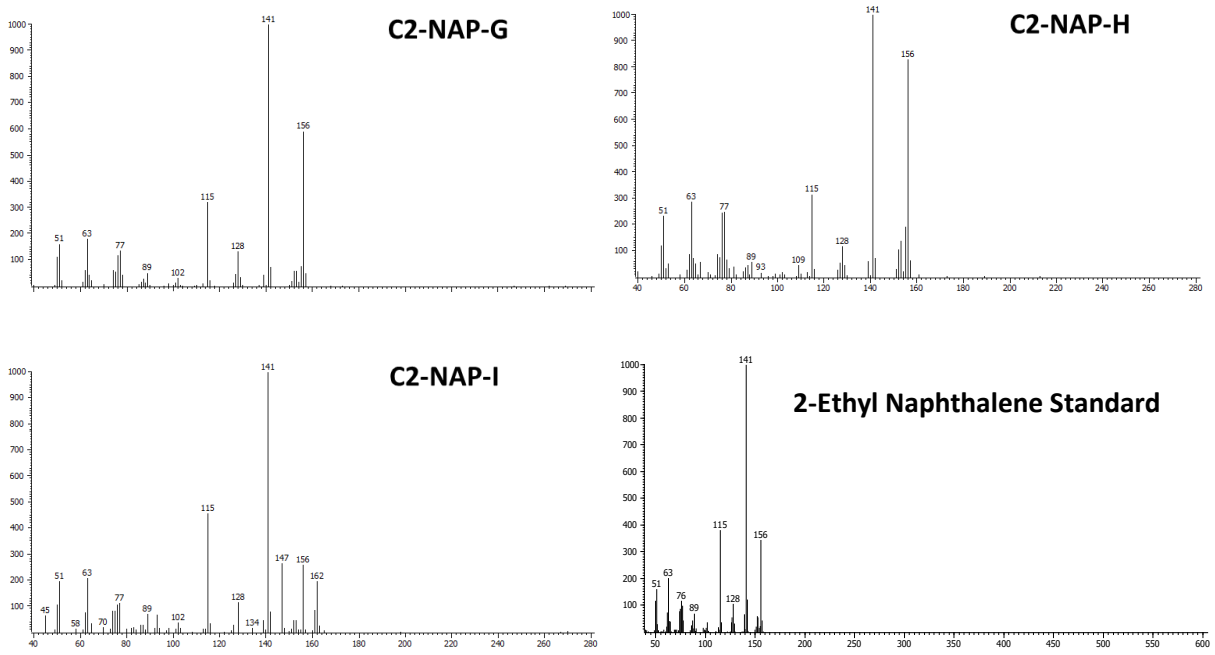

Figure 23 - 70 eV EI Mass Spectrum of C2-NAP-A & C2-NAP-I and 2-ethyl naphthalene authentic standard (m/z = 156).

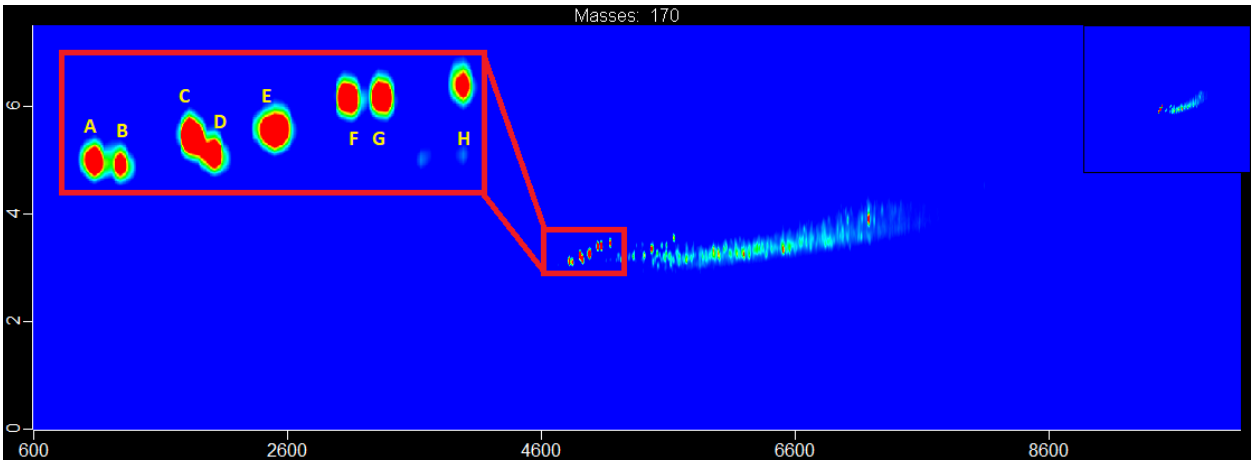

Figure 24 – C3-NAP-A to C3-NAP-H GCxGC/QTOF Chromatographic Separation in P1 2017 BML FFT TLE.

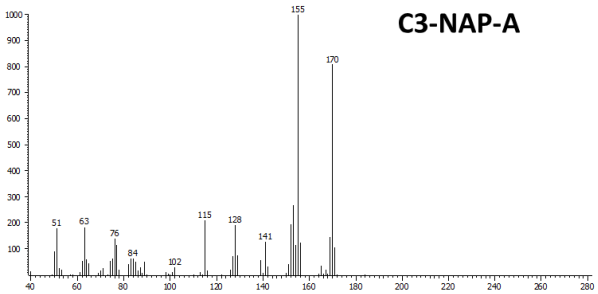

C3-NAP-A

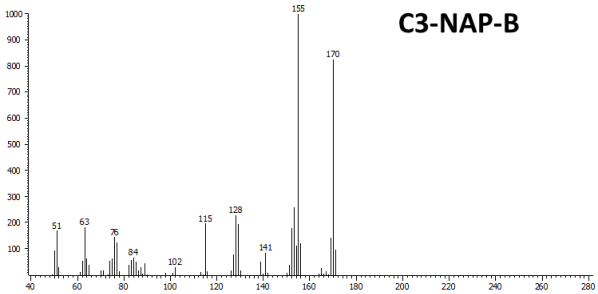

C3-NAP-B

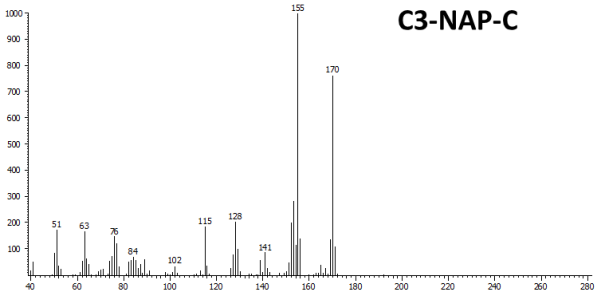

C3-NAP-C

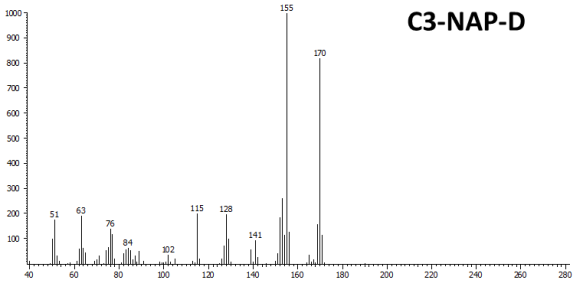

C3-NAP-D

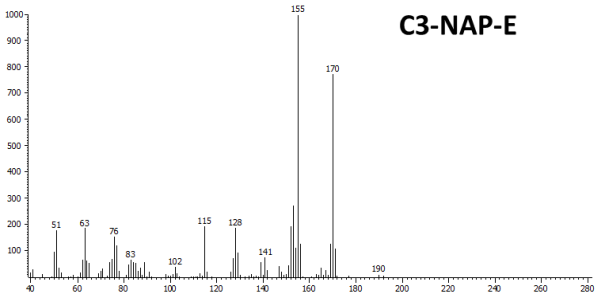

C3-NAP-E

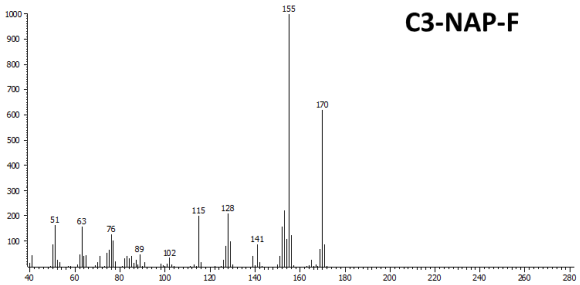

C3-NAP-F

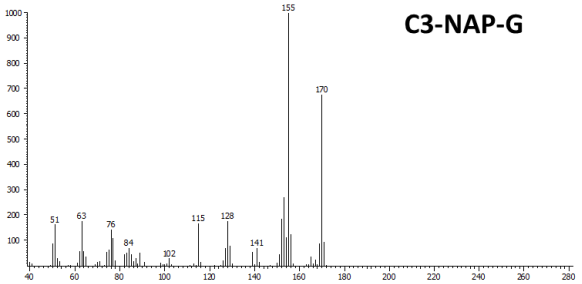

C3-NAP-G

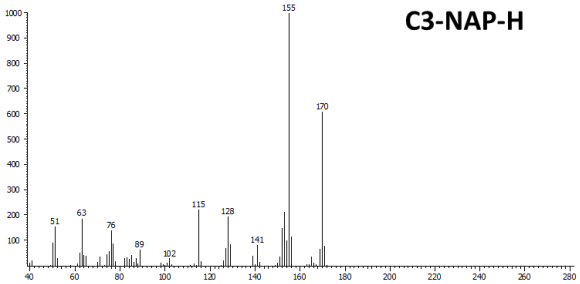

C3-NAP-H

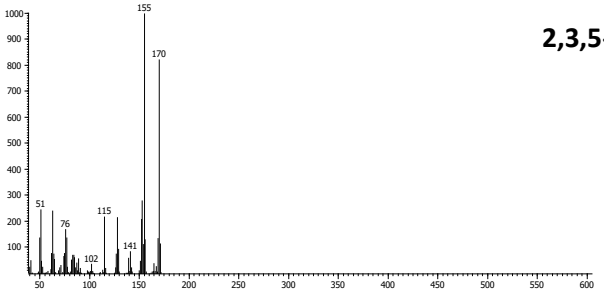

2,3,5-Trimethyl Naphthalene Standard

Figure 25 - 70 eV EI Mass Spectrum of C3-NAP-A & C3-NAP-H and 2,3,5-trimethylnaphthalene authentic standard (m/z = 170).

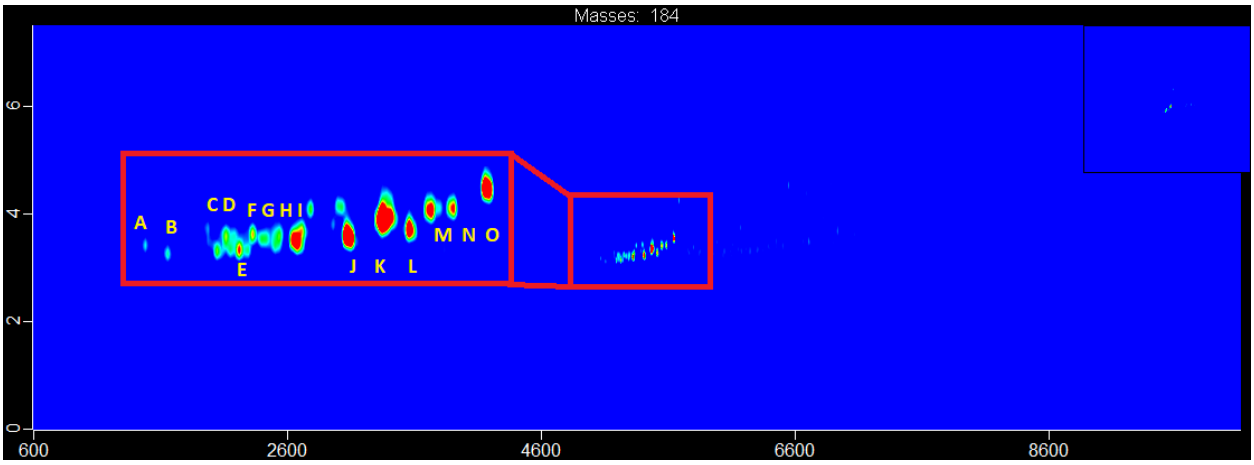

Figure 26 – C4-NAP-A to C4-NAP-O GCxGC/QTOF Chromatographic Separation in P1 2017 BML FFT TLE.

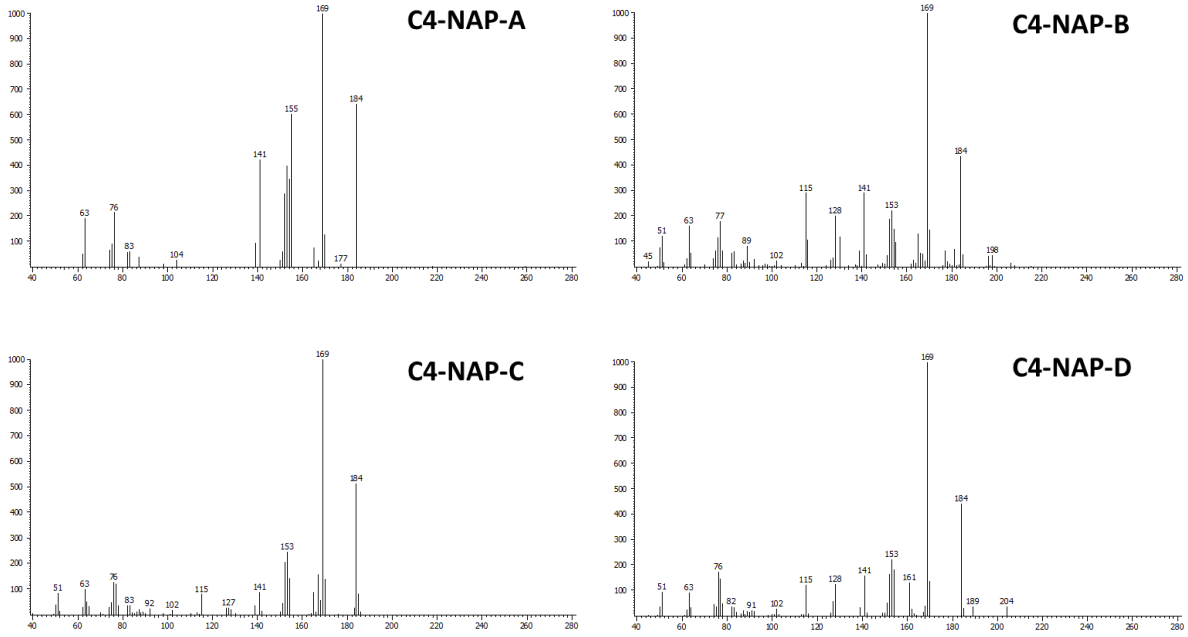

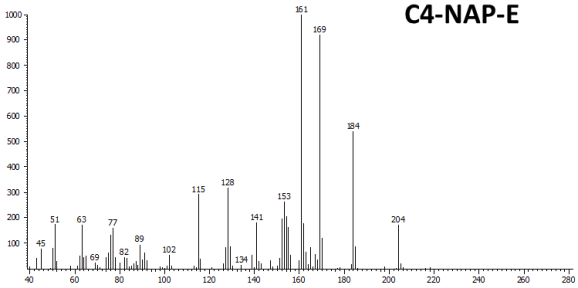
C4-NAP-E
161
169
184
115
128
153
204
51
63
77
89
141
45
69
82
102
134

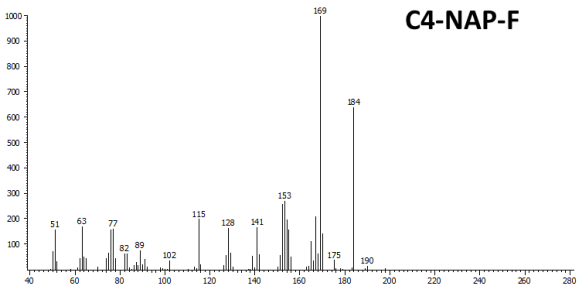
C4-NAP-F
169
184
153
115
128
141
51
63
77
82
89
102
175
190

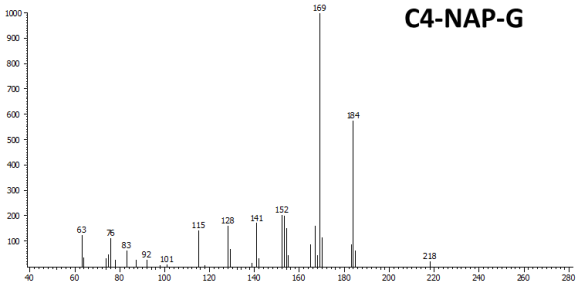
C4-NAP-G
169
184
63
76
115
128
141
152
83
92
101
218

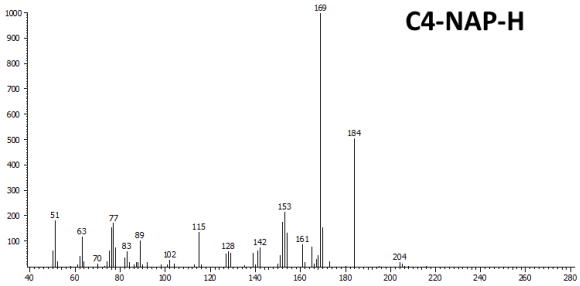
C4-NAP-H
169
184
51
63
77
89
115
153
83
102
128
142
161
70
204

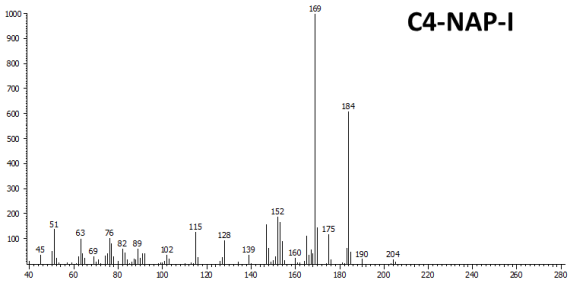
C4-NAP-I
169
184
152
51
63
76
115
175
45
69
82
89
102
128
139
160
190
204

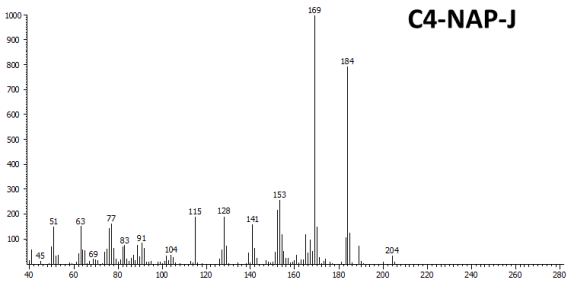
C4-NAP-J
169
184
153
115
128
141
51
63
77
83
91
45
69
104
204

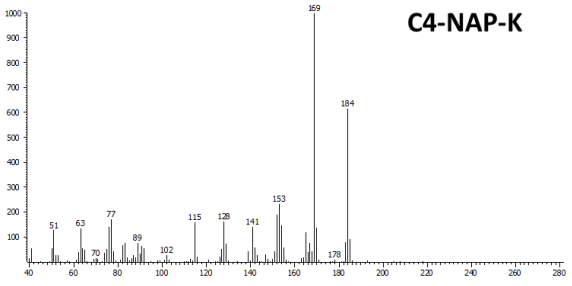
C4-NAP-K
169
184
153
51
63
77
115
128
141
89
70
102
178

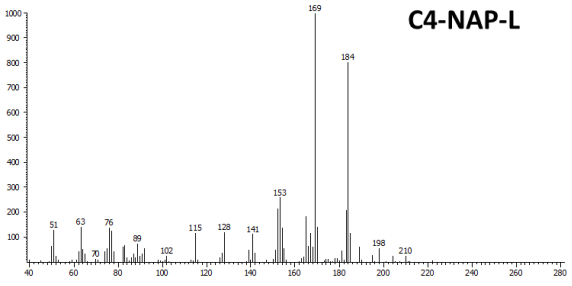
C4-NAP-L
169
184
153
51
63
76
89
115
128
141
70
102
198
210

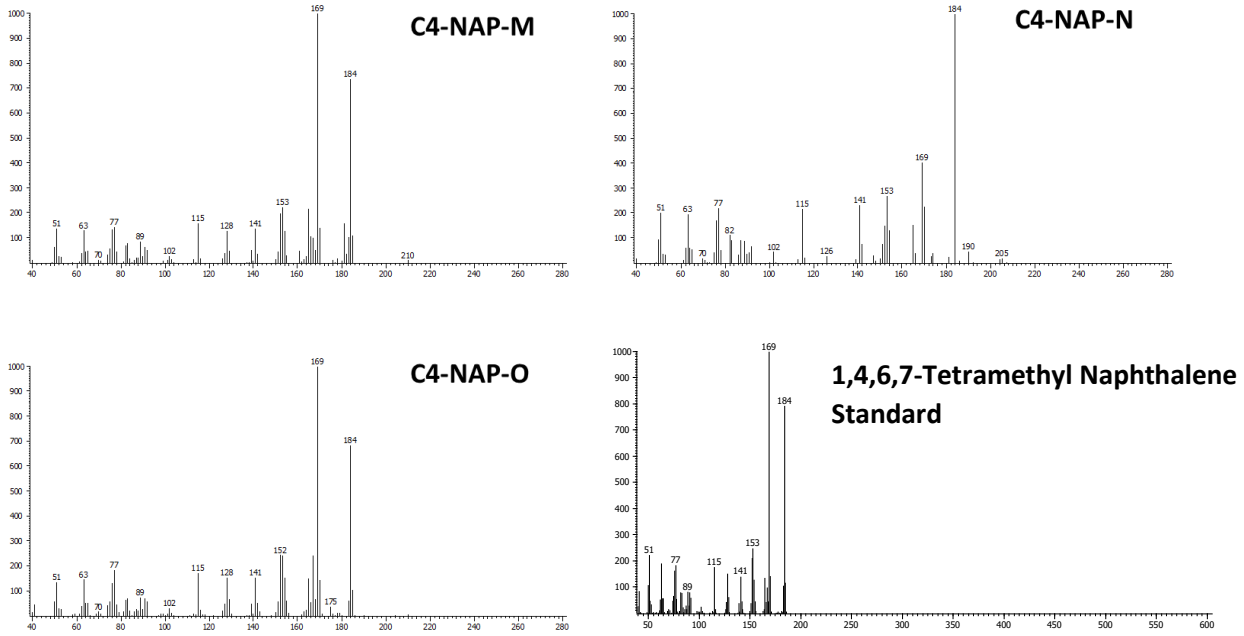

Figure 27 - 70 eV EI Mass Spectrum of C4-NAP-A & C4-NAP-O and 1,4,6,7-tetramethylnaphthalene authentic standard (m/z = 184).

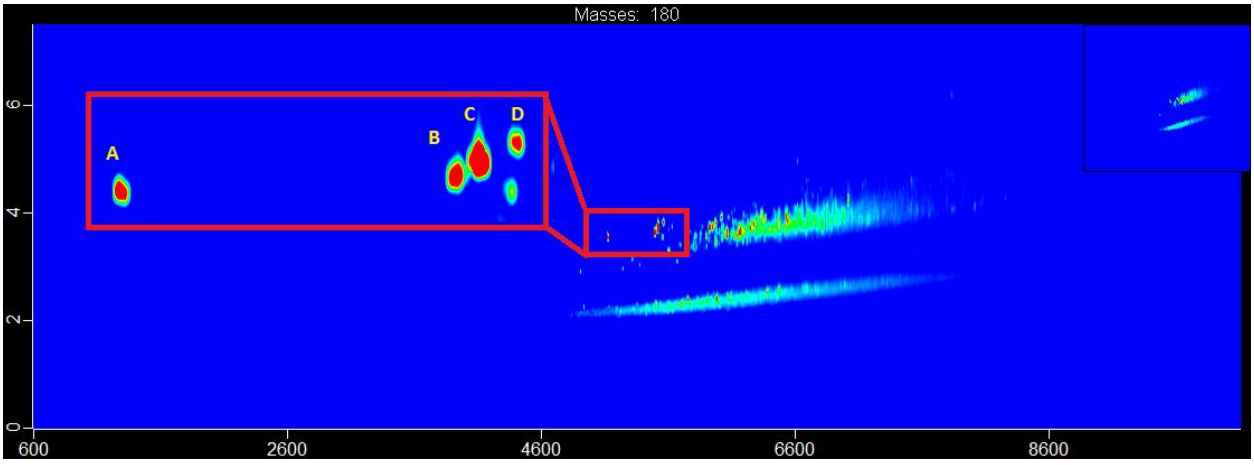

Figure 28 – C1-FL-A to C1-FL-D GCxGC/QTOF Chromatographic Separation in P1 2017 BML FFT TLE.

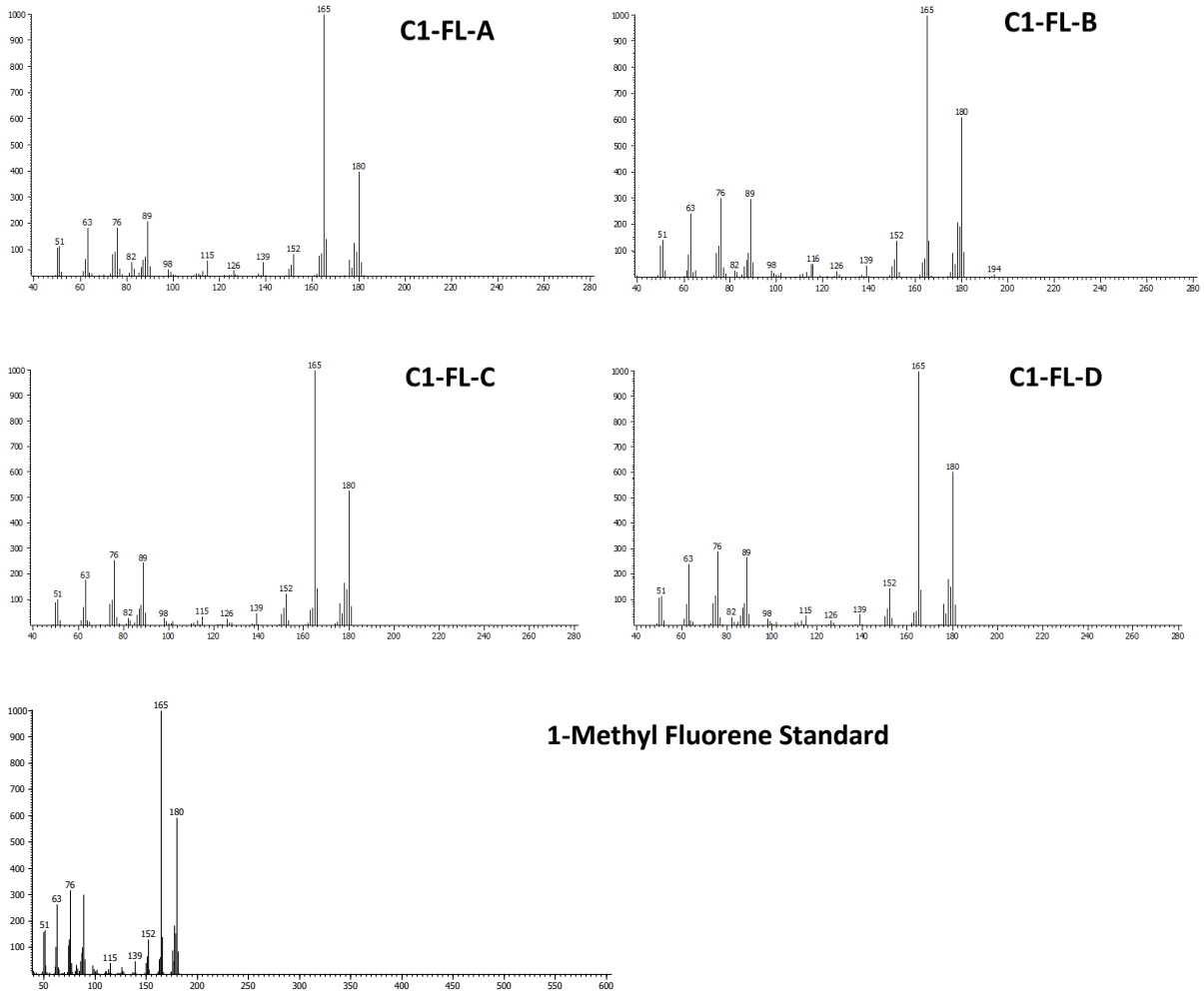

Figure 29 - 70 eV EI Mass Spectrum of C1-FL-A to C1-FL-D and 1-methylfluorene authentic standard (m/z = 180).

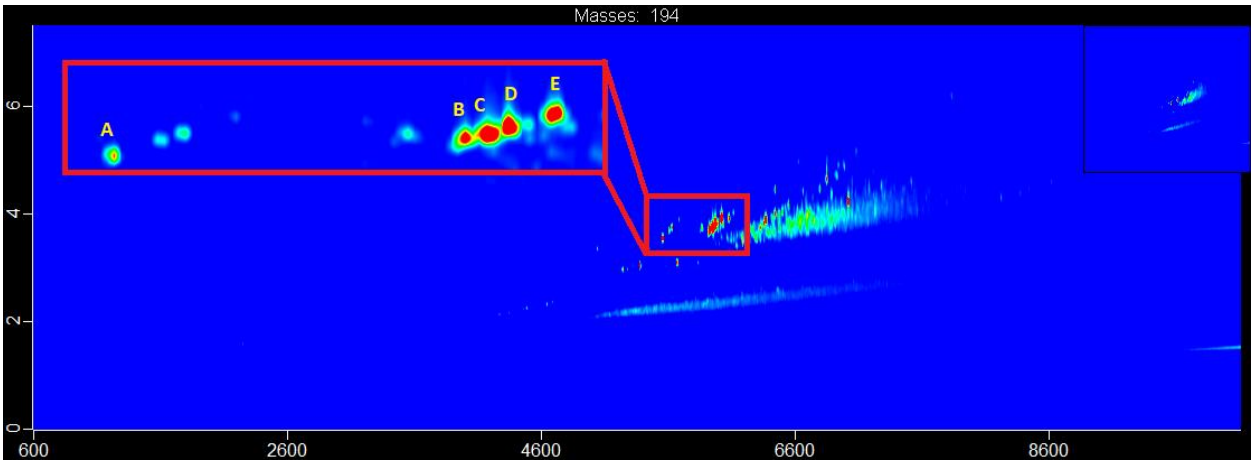

Figure 30 – C2-FL-A to C2-FL-E GCxGC/QTOF Chromatographic Separation in P1 2017 BML FFT TLE.

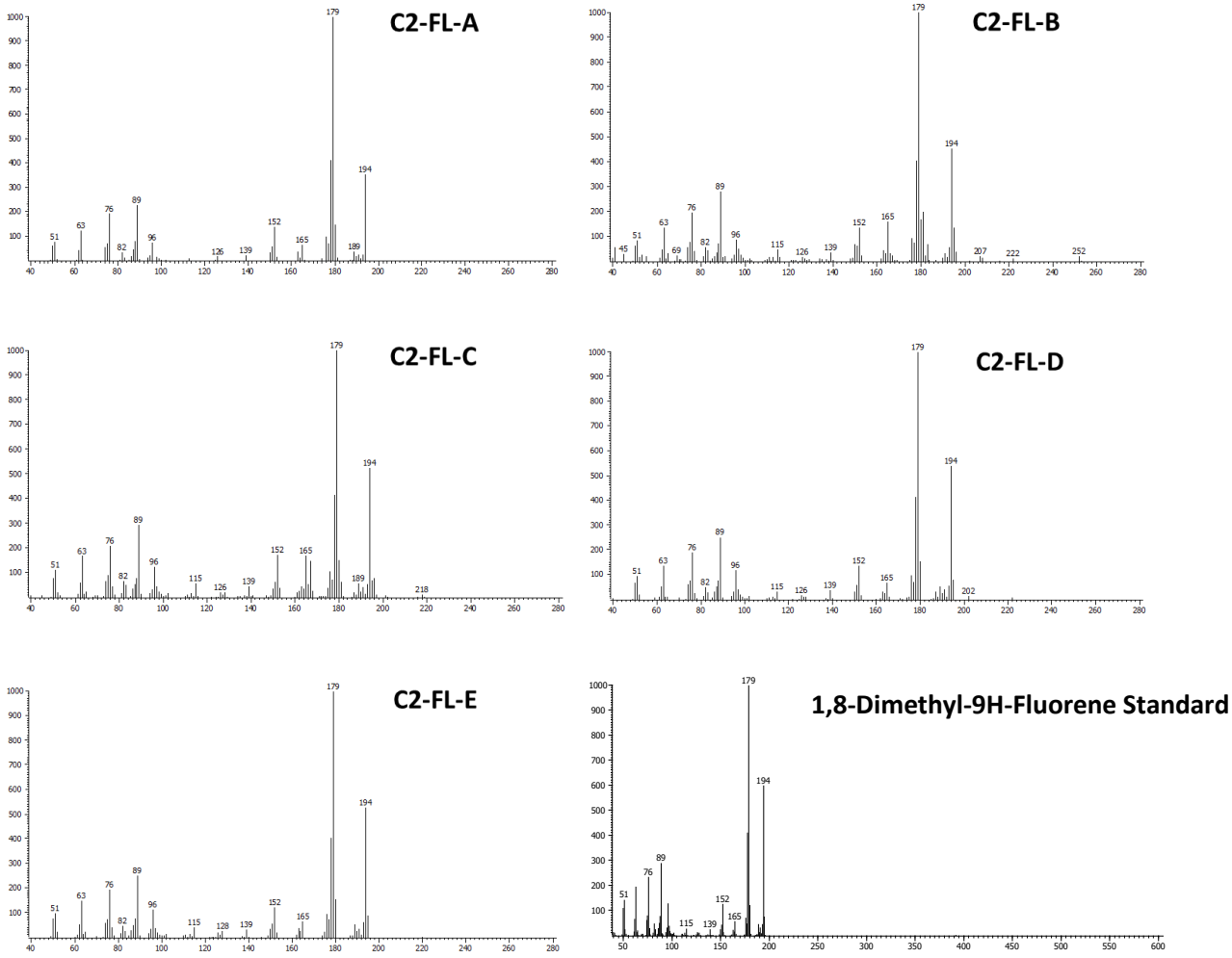

Figure 31 - 70 eV EI Mass Spectrum of C2-FL-A to C2-FL-E and 1,8-dimethyl-9H-fluorene authentic standard (m/z = 194).

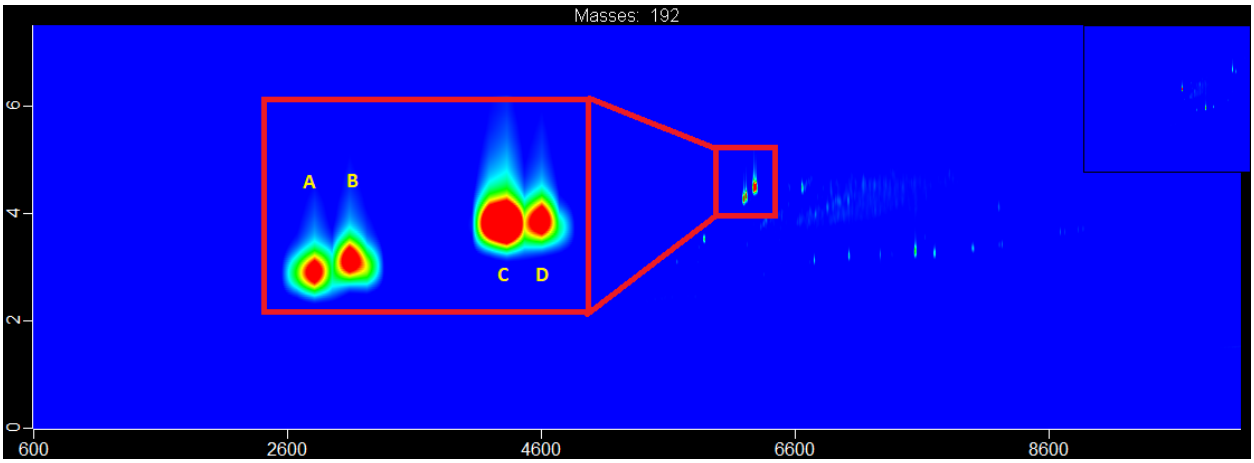

Figure 32 – C1-PH-A to C1-PH-D GCxGC/QTOF Chromatographic Separation in P1 2017 BML FFT TLE.

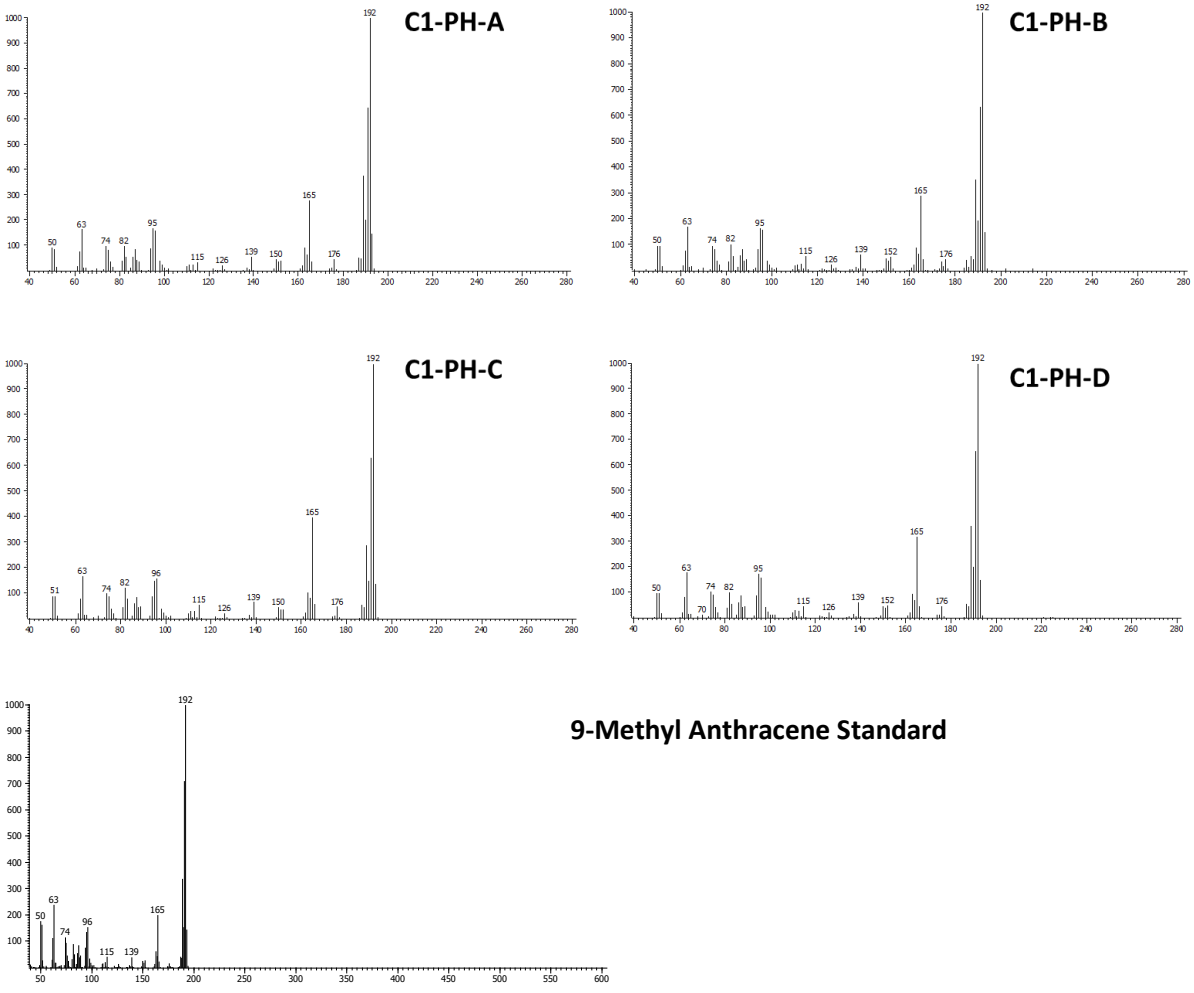

Figure 33 - 70 eV EI Mass Spectrum of C1-PH-A to C1-PH-D and 9-methylanthracene authentic standard (m/z = 192).

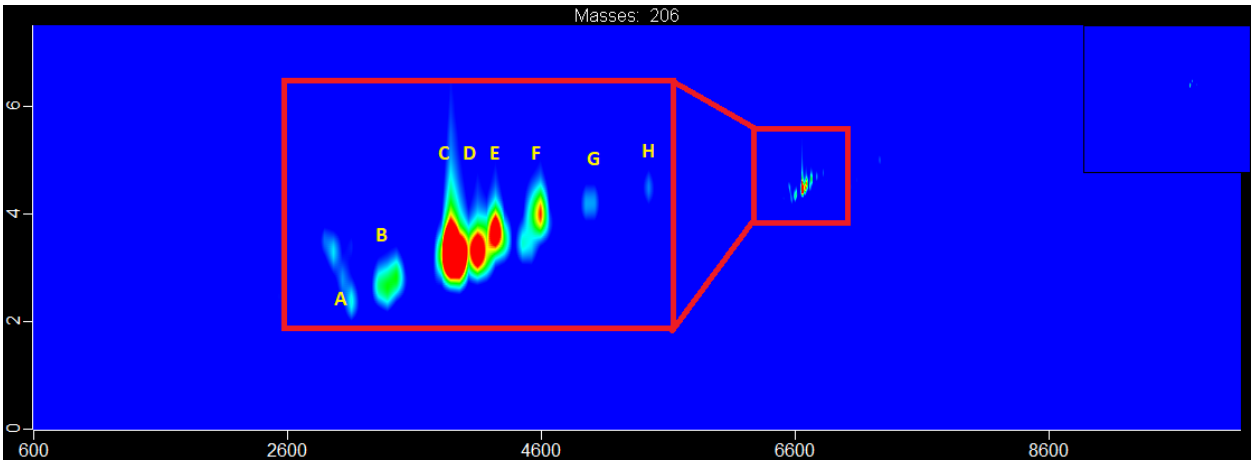

Figure 34 – C2-PH-A to C2-PH-H GCxGC/QTOF Chromatographic Separation in P1 2017 BML FFT TLE.

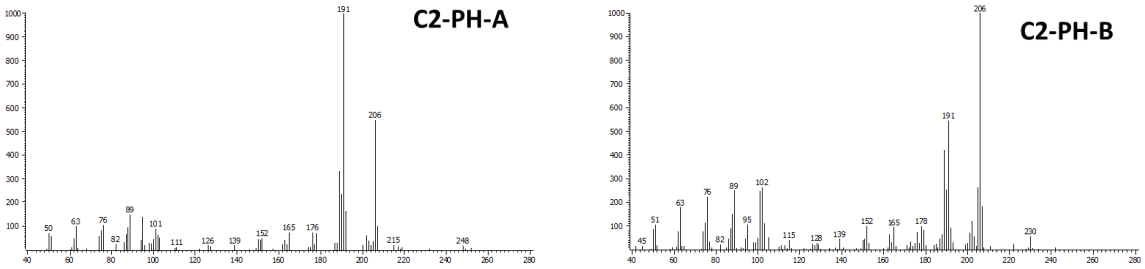

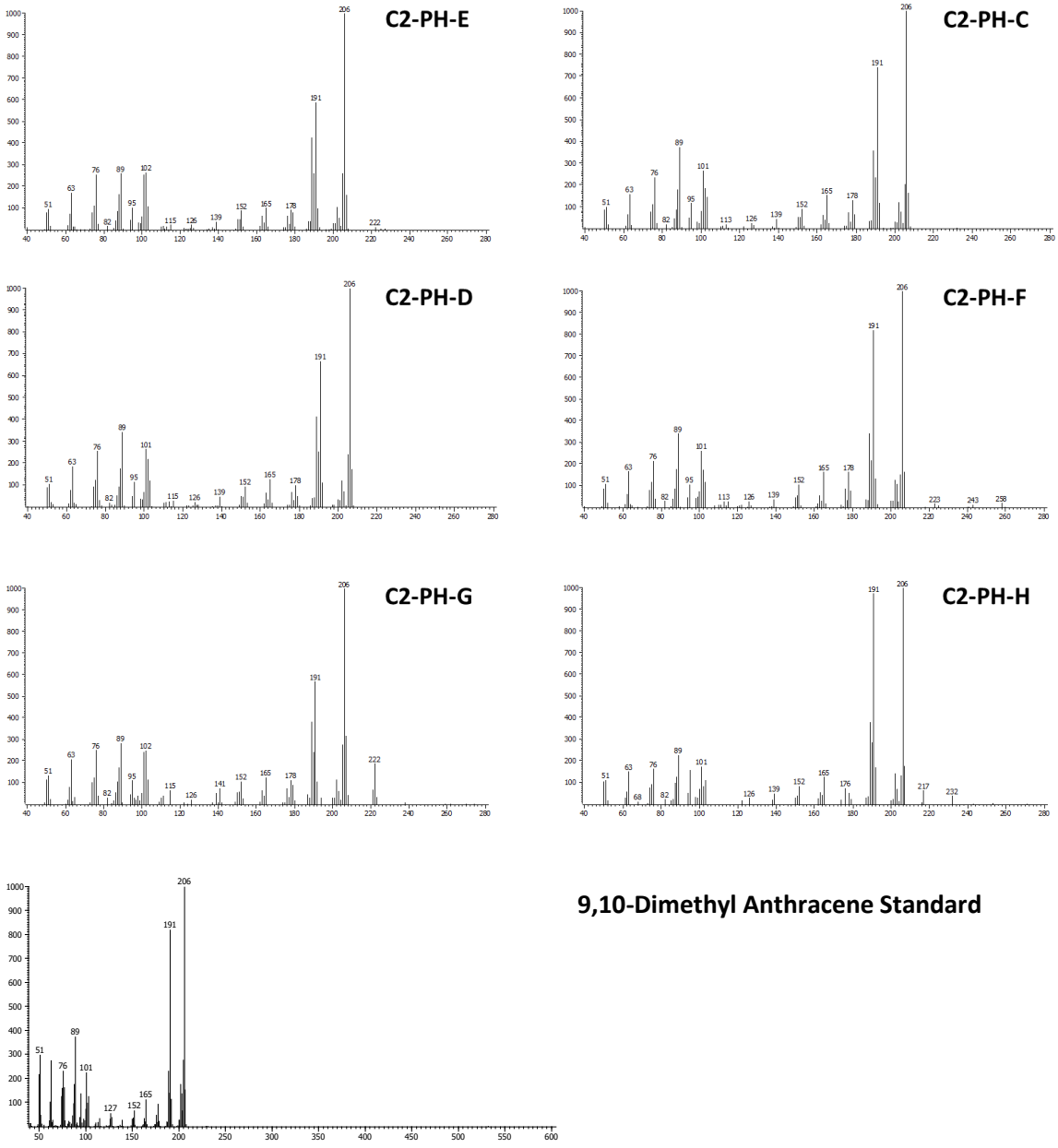

Figure 35 - 70 eV EI Mass Spectrum of C2-PH-A to C2-PH-H and 9,10-dimethylanthracene authentic standard (m/z = 206).

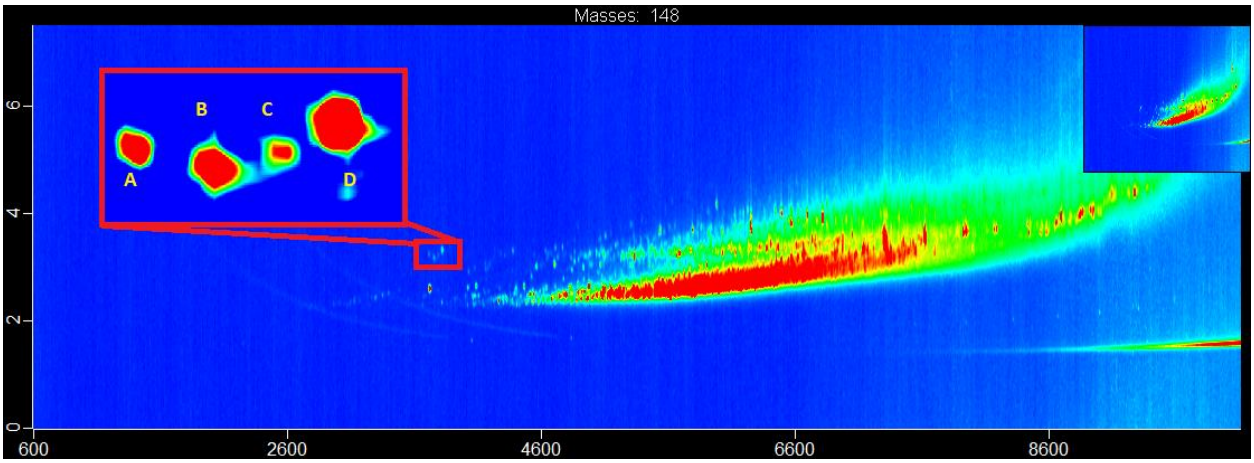

Figure 36 – C1-BT-A to C1-BT-D GCxGC/QTOF Chromatographic Separation in P1 2017 BML FFT TLE.

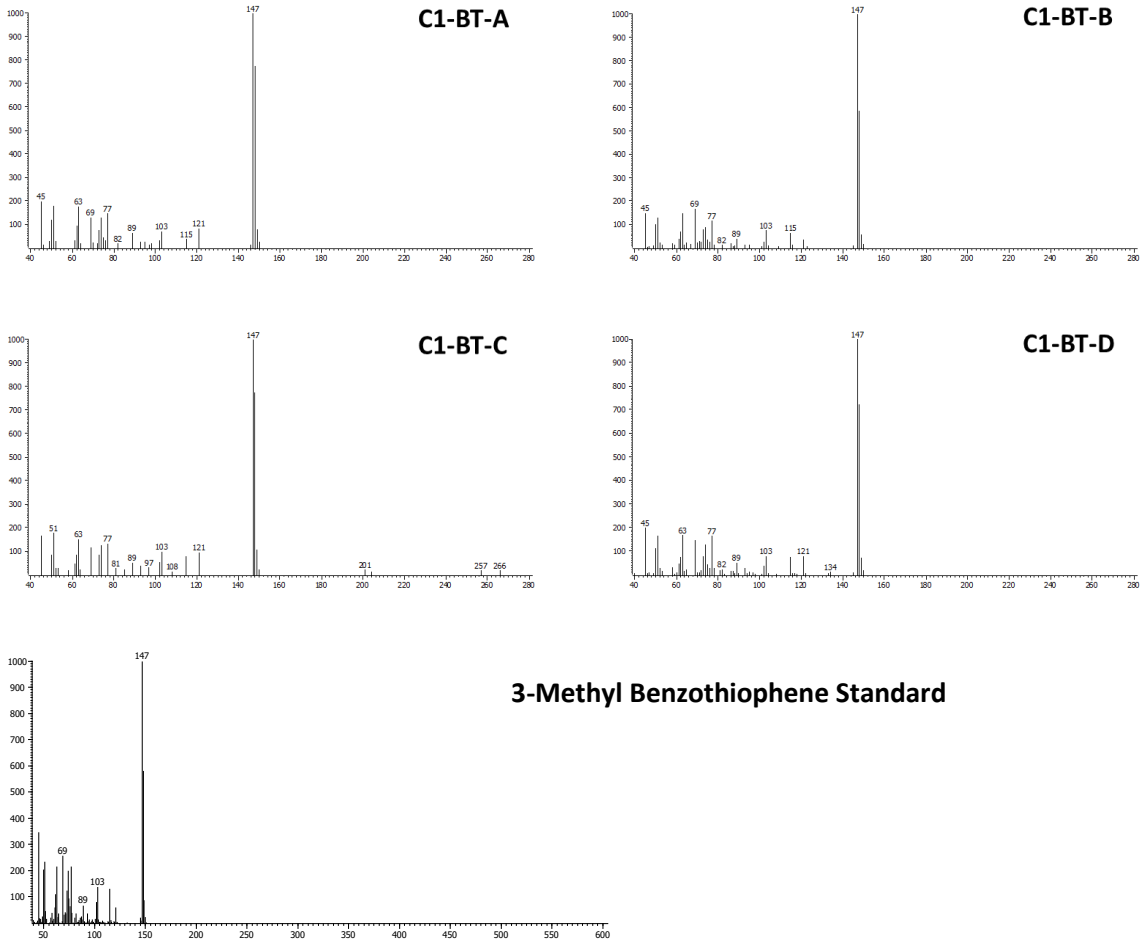

Figure 37 - 70 eV EI Mass Spectrum of C1-BT-A to C1-BT-D and 3-methylbenzothiophene authentic standard (m/z = 148).

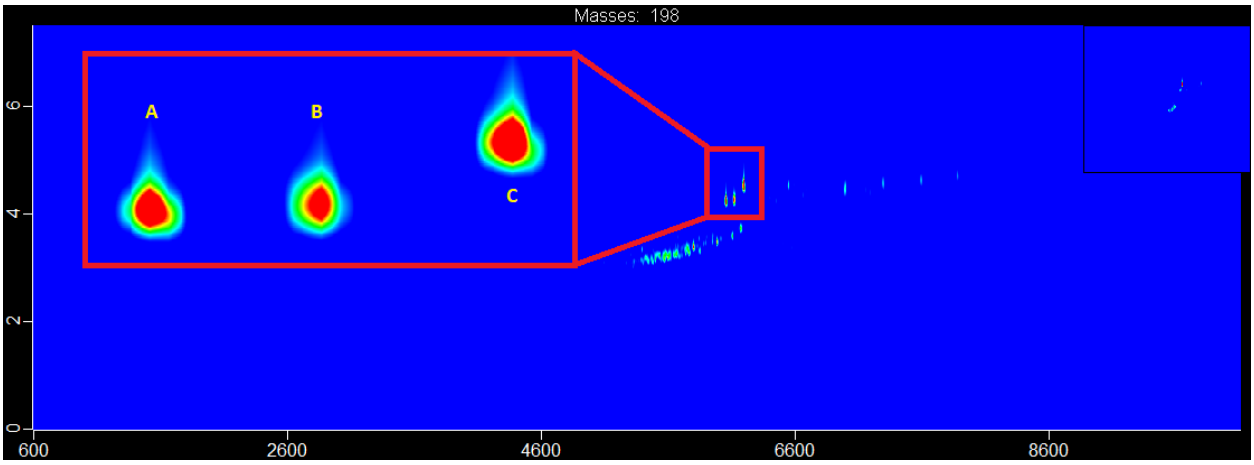

Figure 38 – C1-DBT-A to C1-DBT-C GCxGC/QTOF Chromatographic Separation in P1 2017 BML FFT TLE.

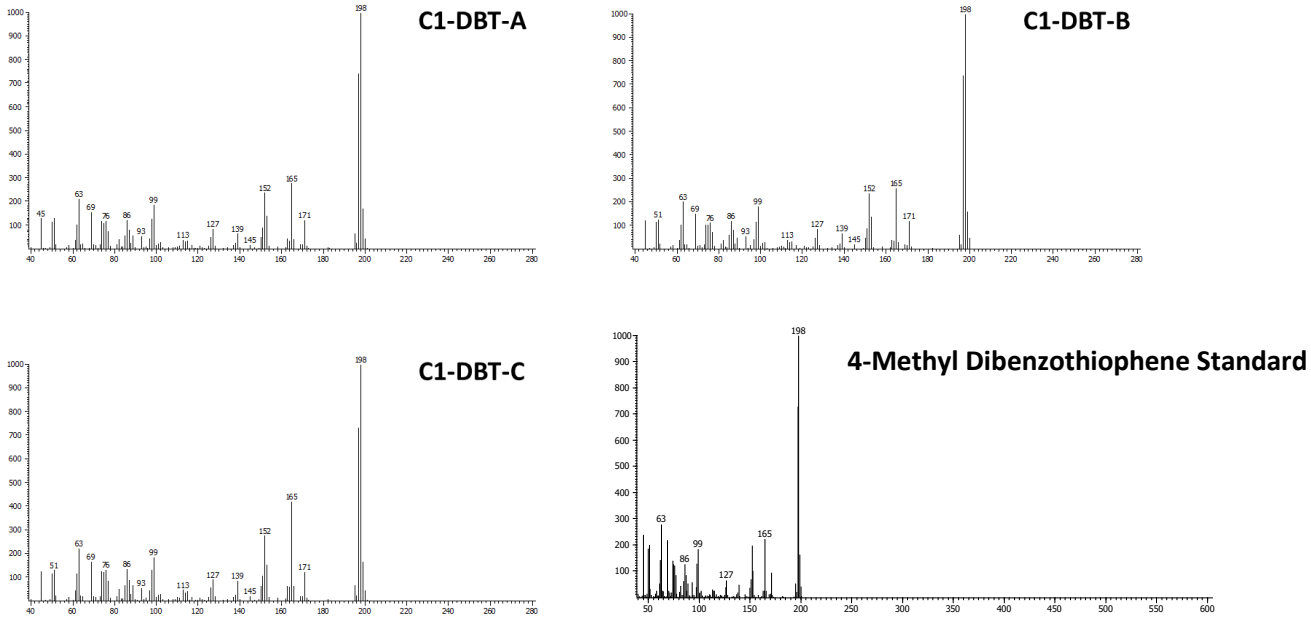

Figure 39 - 70 eV EI Mass Spectrum of C1-DBT-A to C1-DBT-C and 4-methyldibenzothiophene authentic standard (m/z = 198).

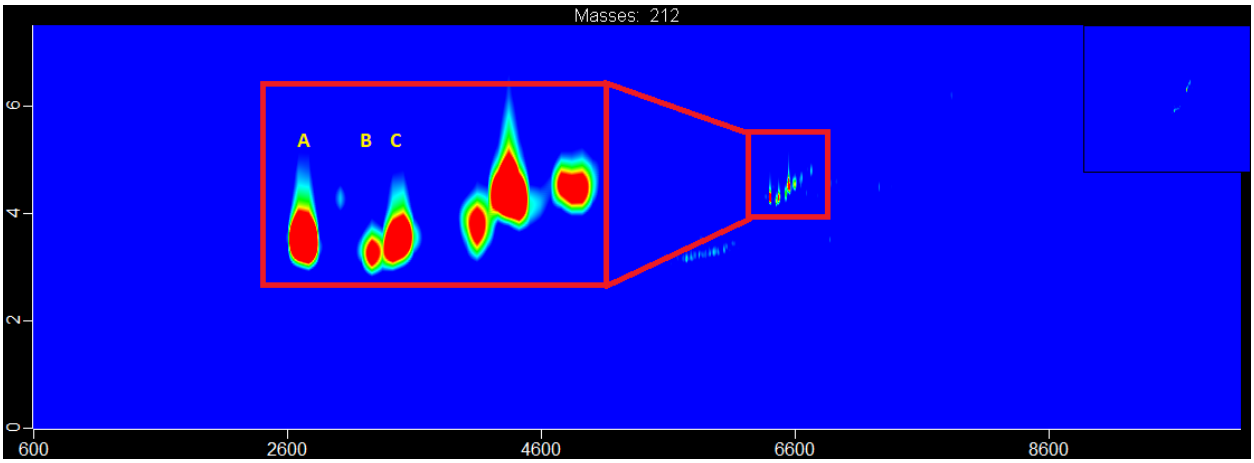

Figure 40 – C2-DBT-A to C1-DBT-C GCxGC/QTOF Chromatographic Separation in P1 2017 BML FFT TLE.

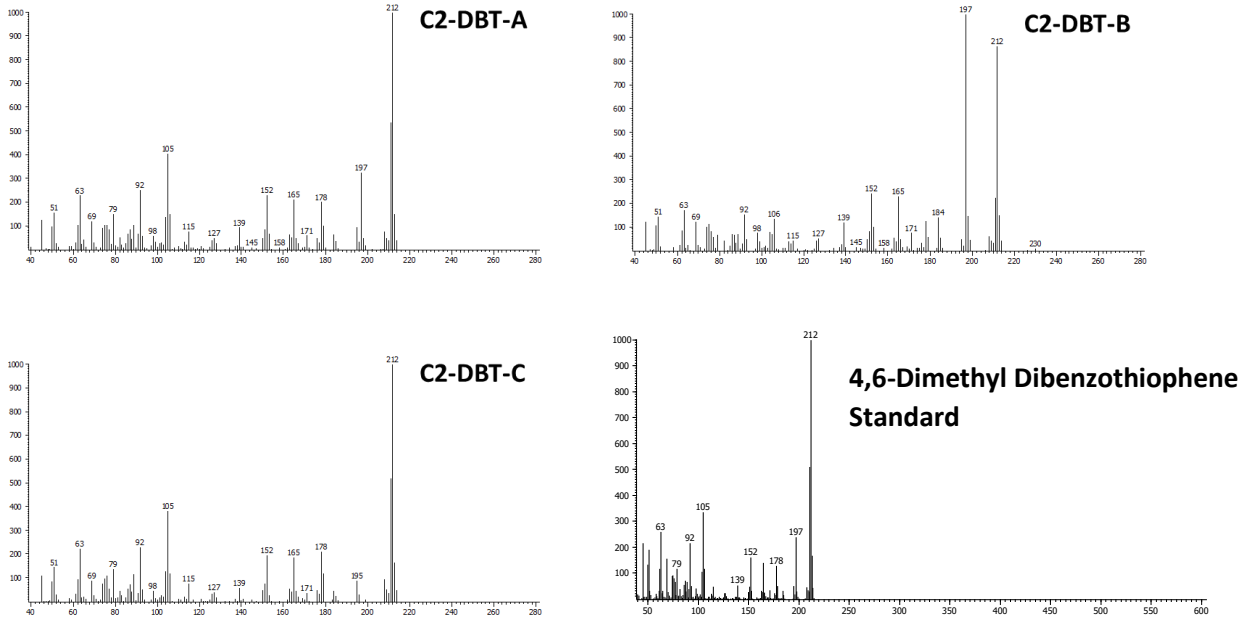

Figure 41 - 70 eV EI Mass Spectrum of C2-DBT-A to C2-DBT-C (m/z = 212).

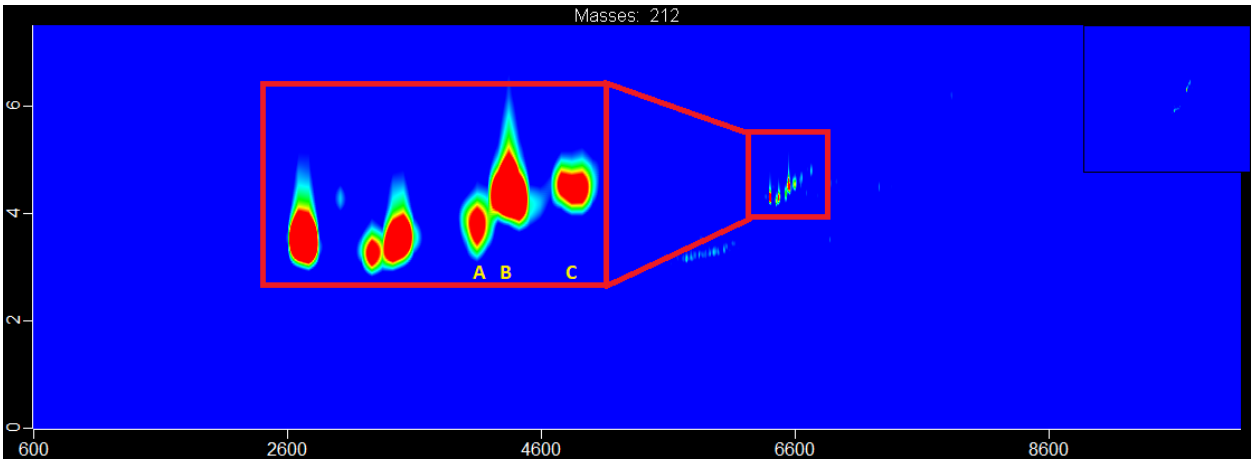

Figure 42 – C2-NBT-A to C1-NBT-C GCxGC/QTOF Chromatographic Separation in P1 2017 BML FFT TLE.

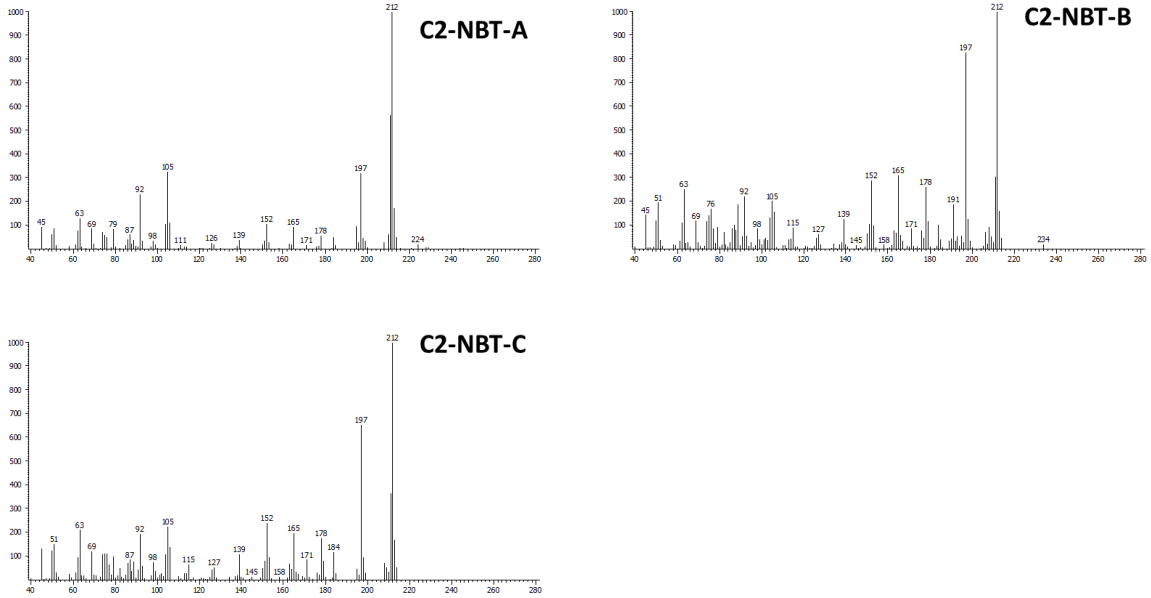

Figure 43 - 70 eV EI Mass Spectrum of C2-NBT-A to C2-NBT-C (m/z = 212).

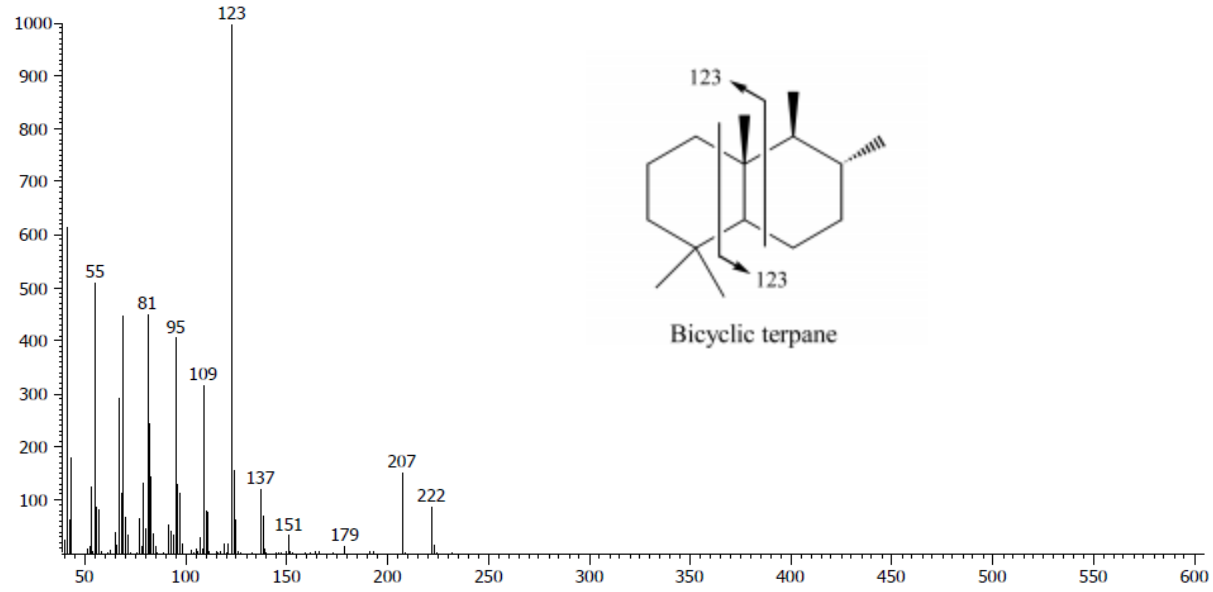

Figure 44 - 70 eV EI Mass Spectrum of drimane and fragmentation occurring at m/z = 212[30].

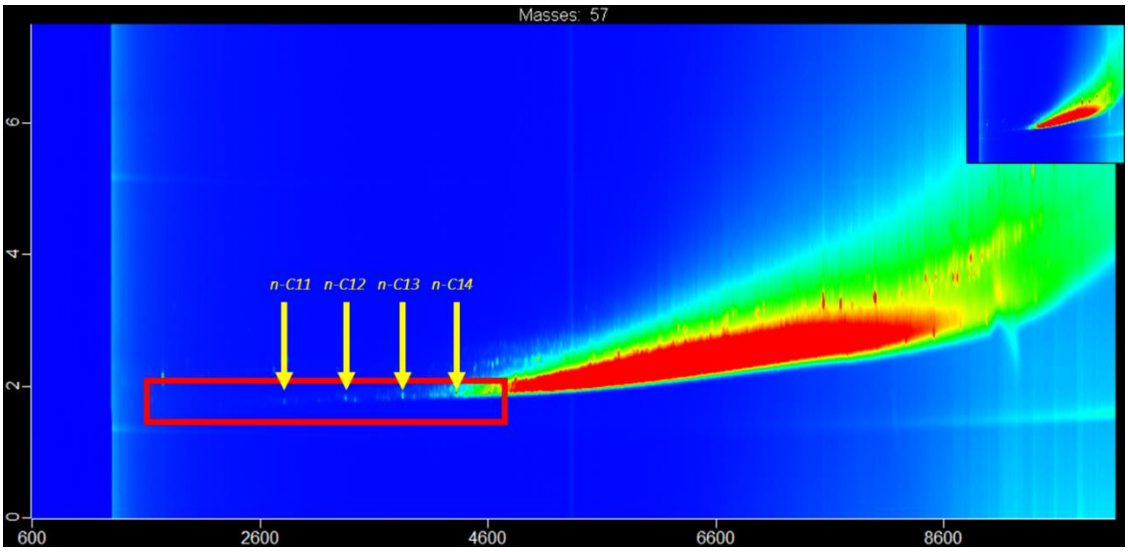

Figure 45 – C11:C14 *n*-alkane GCxGC/QTOF Chromatographic Separation in P1 2017 BML FFT TLE.

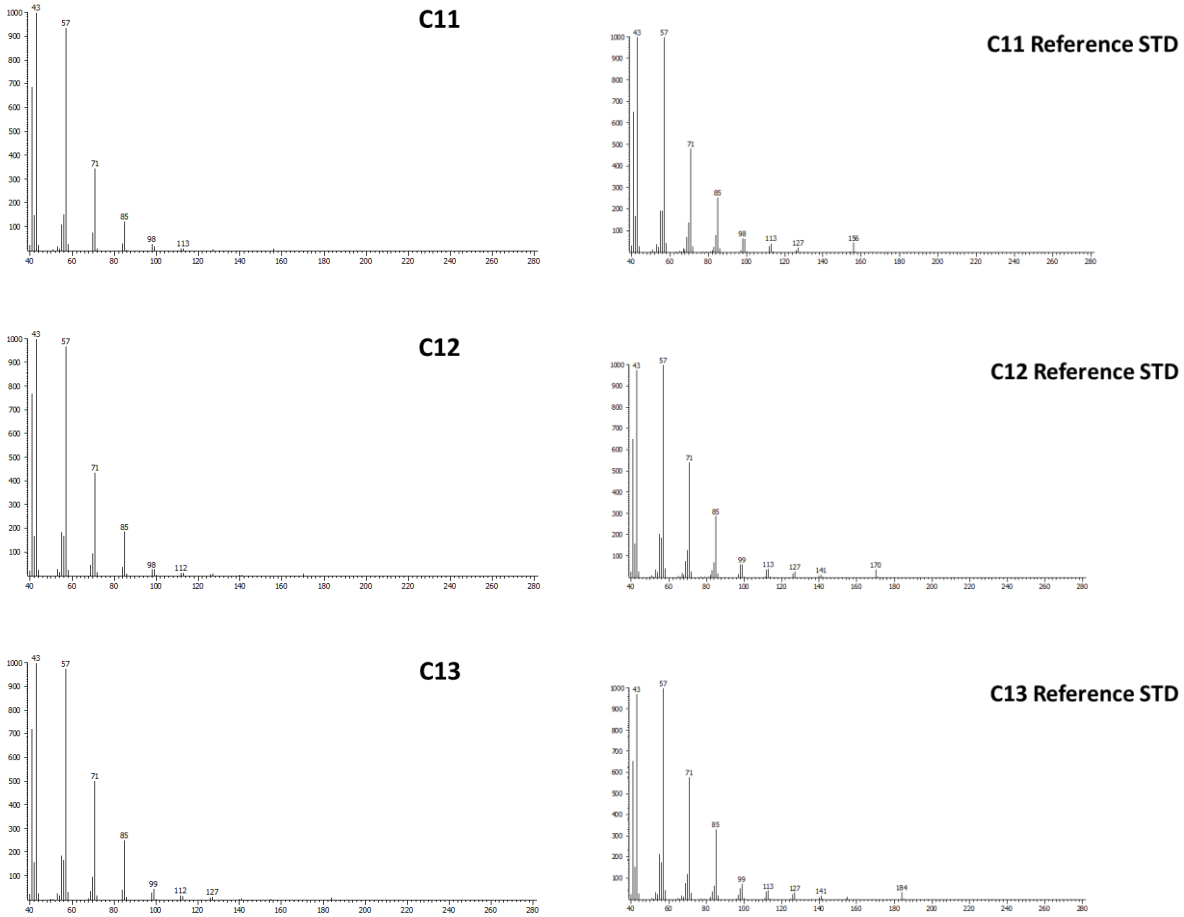

Figure 46 - 70 eV EI Mass Spectrum of C11 – C13 *n*-alkane with Authentic Standards.

Chapter Three: High-Resolution Spatial Distribution of Near Surface Solvent Extractable Petroleum Hydrocarbons in Base Mine Lake Fluid Fine Tailing

Mikhail Dereviankin[1], Gregory F. Slater[1], Lesley Warren[2]

Author Affiliation:

[1]School of Geography and Earth Sciences, McMaster University, Hamilton, Ontario, Canada

[2]Department of Civil Engineering, University of Toronto, Toronto, Ontario, Canada

Author Contribution:

MD, GFS, and LAW conceived and designed the study. MD performed the sample extraction, GC×GC/TOFMS instrumental analysis, data analysis, interpretation, and wrote the manuscript. GFS edited the manuscript.

Abstract

High-resolution spatial depth profiles of fluid fine tailings (FFT) collected near the fluid water interface (FWI) of Syncrude Ltd. Canada's Base Mine Lake (BML) were examined to characterize the near surface distribution of solvent extracted petroleum hydrocarbons (PHCs) potentially undergoing biogeochemical cycling and/or exchange with the water column. FFT depth profiles were collected from the near surface (0.2 to 1.9 m below the FWI) and at one reference point below these depths (3.8 to 5.0 m below FWI) at three sampling platforms (P1 – P3) in July 2017. Comprehensive two-dimensional gas chromatography time of flight mass spectrometry (GC×GC/TOFMS) was used to characterize the solvent extractable PHC isomers at each depth intervals. A subset of well resolved and identifiable isomers were quantified or semi-quantified with authenticated standards: 69 alkylated poly-cyclic aromatic hydrocarbons grouped by species, 1 petroleum biomarker (drimane) and 3 *n*-alkanes. The "fingerprint" constructed from the concentration of each isomer at a given depth shared a similar signature between platforms with the concentration of one isomer contributing the majority of the observed concentration of each species. The ability to monitor the dominant isomer for a species and construct fingerprints to affirm a singular source of PHCs highlights the advantage of using GC×GC. If the FFT samples had been analyzed via one-dimensional gas chromatograph (1-D GC), these source signature evaluations would not have been achieved as the summation of all isomers can only be resolved due to the overlaying unresolved complex matrix (UCM). The fingerprints also highlighted that the variabilities between isomers were pronounced for the low molecular weight *n*-alkanes (C11 – C13) and drimane between all platform depth intervals. As these low molecular weight compounds, with the exception of drimane, are components of the residual naphtha, the large variabilities in concentration for these species may be linked with fluctuating inputs and/or sorption of naphtha to the organic phase of the FFT. Equally possibly, these variations in concentration may also reflect differences in biogeochemical processing as these lower molecular weight compounds have been demonstrated *in-vivo* to readily undergo anaerobic biodegradation to

produce methane. The concentration range of isomers across the near surface FFT were the highest at P1 (range = 6.0×10^{1} – 1.6×10^{4} ng/g), followed by P2 (range = 5.0×10^{1} – 9.2×10^{3} ng/g) and were lowest at P3 (range = 5.0×10^{1} – 4.9×10^{3} ng/g). At P3, the site with the lowest abundance of solvent extractable PHCs, the fingerprints were the most consistent across the range of FFT depth intervals. At P1, the overall fingerprint was consistent with depth, although concentrations were variable with the samples collected nearest the FWI (0.2 m from FWI) being depleted for the isomers being investigated. At P2, both the fingerprint and concentrations of isomers were consistent across the depth intervals but were distinctly different for the deep reference sample. P1 and P2 preferentially retained the same higher molecular isomers between depth intervals (C3-NAP, C4-NAP and C1-DBT class isomers), while P1 contained relatively depleted concentrations for a subset of lower molecular weight isomers (C1-NAP-A, C2-NAP-B,D,E, C4-NAP-A, C2-PH-H, C1 and C2-FL). The decreased concentration of these lower molecular isomers relative to the heavier isomers may indicate a lower potential for ongoing biogeochemical cycling and/or exchange with the water column, either due to lower initial inputs of these isomers or to ongoing cycling reducing the abundances of the compounds originally present.

Introduction

Surface mining operations in the Athabasca Oil Sands Regions (AOSR) in Northern Alberta, create large open pits to access oil sands deposits where crude oil is present in the form of bitumen[1]. To extract bitumen from the sands, the cretaceous ore is combined with hot water and sodium hydroxide in a process referred to as the 'Clark Hot Water Extraction'[2]. Although only 20% of all bitumen reserves are extracted with this protocol[1], over 1.18 trillion liters of by product in the form of tailings containing solids, naphthenic acids (NA), dissolved salts, unextracted bitumen, oil sands process-affected water (OSPW) and trace amounts of residual low molecular weight paraffin diluent, referred to as naphtha, used in the extraction procedure are stored in tailings ponds[1,2]. Differential consolidation of tailing fractions occurs within tailing storage facilities and the fraction that remains suspended is referred to fluid fine tailings (FFT)[4]. The FFT matrix contains 25 to 35 % (w/w) solids in the form of clay, sorbed petroleum hydrocarbons (PHCs) (3 to 5 % (w/w) unextracted bitumen and <1% (w/w) unrecovered naphtha for tailings where naphtha was used during extraction), with the remaining matrix dominated by OSPW which generally contain concentrations of dissolved salts and naphthenic acids (NAs) above regulatory limits[3-5]. The Tailing Management Framework (TMF) issued by the Alberta Energy Regulators in 2015 has emboldened oil sands operators to continue their investigation into management strategies for the reduction of their FFT inventory[1]. One strategy being undertaken to manage these tailings is water capped tailings technology (WCTT), a reclamation strategy that involves the development of Pit Lakes (PLs) by sequestering FFT below a water cap. PLs are constructed by introducing FFT into open pit mines and capping with several meters of water allowing the FFT to steadily densify over time[6].

Regulatory specifications for PLs require that oxygen inputs from atmospheric diffusion, watershed, rain inputs and any *in-situ* photosynthetic production exceed oxygen consumption driven by biogeochemical cycling of the organic constituents within FFT[19]. The FFT underlying a PL is expected to be anoxic dominated by diverse microbial communities capable of anaerobic

methanotrophy, methanogenesis, and nitrate and sulfur reduction[5]. Fermentation of PHCs sorbed to FFT produces H_2 and acetate, which may be subsequently utilized by these anaerobic microbial communities[5]. As FFT settles and densifies porewater containing oxygen consuming constituents (OCC) derived from these anaerobic microbial degradation of labile PHCs, such as gases (e.g. H_2S, CH_4), dissolved organic carbon (DOC) and dissolved ions (e.g. NH_4^+, HS^-, and Fe^{2+}) have the potential to be mobilized into to the overlying water cap[8]. Oxidation of these components by either chemical or biological reactions within the water column has the potential to hinder the progression of these reclamation projects. Thus, a thorough understanding of the geochemistry of PHC biogeochemical cycling within the FFT and/or species exchange with the water column is crucial for anticipating the long-term evolution of water quality[7].

The focus of this study is Base Mine Lake (BML) (**Figure 47**), the first full scale PL in the Athabasca Oil Sands Region (AOSR) commissioned by Syncrude in 2012[9]. As of October 2012, the FFT deposit underlying BML had reached a maximum thickness of 48 m and was submerged under a 52 Million m^3 water cover, with a surface area of approximately 8 km^2 and average depth of 6.5 m. Densification of the FFT from 2012 to 2017 has resulted in the settlement of FFT up to 6m, which has increased the average water depth to 10.5 m. Yearly freshwater addition – ranging from 2 to 6 Million m^3 – to BML has been undertaken to simulate future water inflow from adjacent reclaimed landforms[4]. Water is currently pumped from the BML water cap for utilization in the oil sands extraction process such that the lake maintains a surface elevation of 308.7 ± 0.5 meters above sea level. Field studies beginning in 2015 have extensively characterized the temporal and spatial geochemistry of OCC mobilization from the fluid water interface (FWI) into the overlaying water column[19]. Specially, transport of methane and ammonia produced by *in-situ* anerobic microbial communities have been implicated in the drawdown of oxygen from the BML water cover[19]. There is a need to understand the spatial distribution of PHCs within BML FFT and their potential for driving *in-situ* anaerobic biogeochemical cycling releasing OCCs into the water column of BML. This study applies the increased peak capacity of comprehensive two-

dimensional gas chromatography coupled to time of flight mass spectrometry (GC×GC/TOFMS) to assess the high-resolution spatial variability of PHCs representative of residual inputs of naphtha and/or bitumen within near surface FFT (defined herein as the region extending 0.2 – 1.9 M from FWI from FWI) and a reference sample below these depths (range = 3.8 – 5.0 m from FWI) at BML in 2017. The objective was to monitor the concentrations for a subset of PHCs and characterize their isomer "fingerprint" at each site. Additionally, the correlation between the concentrations for labile PHCs and considerable less biogeochemically active isomers are expected to ascertain whether there is evidence of *in-situ* anaerobic biogeochemical processing on residual inputs of naphtha and/or bitumen that potentially mobilize OCCs into the overlaying water cap.

Experimental

Site Location & Sampling Method

BML site sampling of FFT was conducted in July 2017 where eighteen FFT samples were collected from platform 1 (6 samples), platform 2 (6 samples) and platform 3 (6 samples) using a non-commercial pneumatic piston sampling device deployed from a specialized sampling boat as per the protocol from *Dompierre et al.* (2016). Four samples from each platform were from the FFT-Water cap (FWI) interface in increments of 0.2 m, one sample was collected 0.5 m from the previous set of samples and the deepest samples were collected ~ 15 m from the water surface (~ 5 m from FWI). For platform 1 and 2, the first samples collected that had enough sediment for analysis were collected from 0.2 m while in platform 3 the first sample was collected at 0.4m from the FWI. The primary focus of sampling were the samples collected from the near surface FFT depth profile (0.2 – 1.9 m from FWI), which have been proposed by *Dompierre et al.* (2016) to undergo exchange with the water column. A sample was collected below these depths (range = 3.8 – 5.0 m from FWI) in each platform as a point of reference.

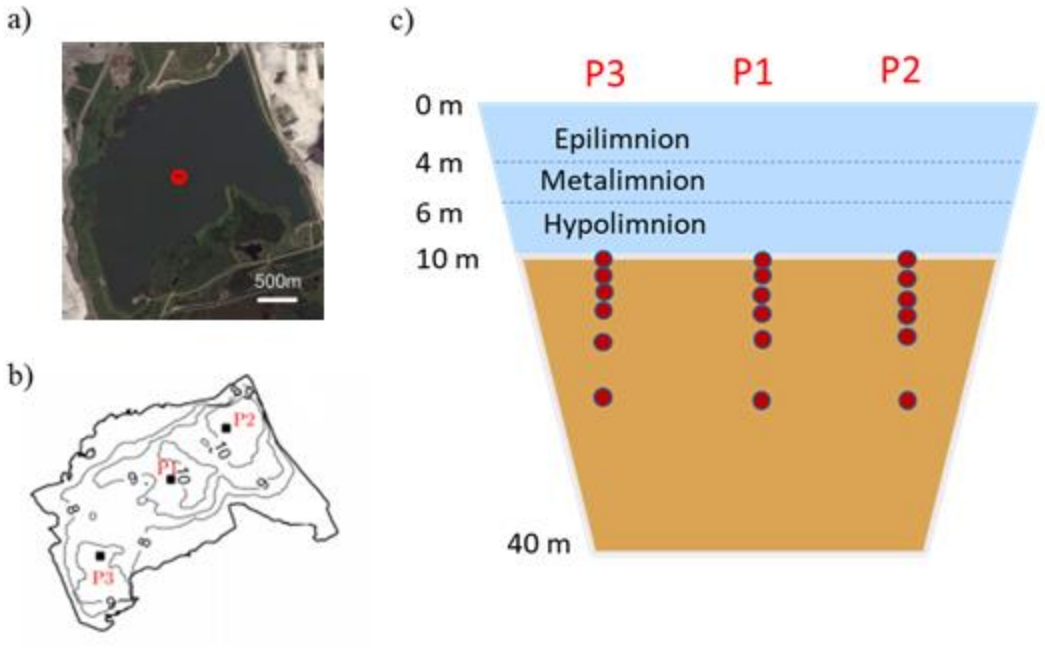

Figure 47 - map of BML and the locations of the 3 sampling platforms (Platform 1, or P1; Platform 2, or P2; Platform 3, or P3), a schematic diagram of the spatial section of FFT studied and stratification of water cap.

Chemicals & Reagents

Dichloromethane, methanol, hexane (distilled in glass) was purchased from EMO Millipore Corporation. The following compounds were purchased and used as recovery/internal standards in this study: m-terphenyl (96%, Sigma-Aldrich) and benzo[a]anthracene-d12 (98%, Sigma-Aldrich). The following standards were purchased for semi-quantification of target compounds: 1-methylnaphthalene (95%, Sigma-Aldrich), 2-ethylnaphthalene (98%, Sigma-Aldrich), 2,3,5-trimethylnaphthalene (98%, Sigma-Aldrich), 1,4,6,7-tetramethylnaphthalene (98%, Sigma-Aldrich), 1-methylfluorene (98%, Sigma-Aldrich), 1,8-dimethyl-9H-fluorene (98%, Sigma-Aldrich), 9-methylanthracene (98%, Sigma-Aldrich), 9,10-dimethylanthracene (98%, Sigma-Aldrich), 3-methylbenzothiophene (96%, Sigma-Aldrich), 4-methyldibenzothiophene (96%, Sigma-Aldrich), 4,6-dimethyldibenzothiophene (97%, Sigma-Aldrich), Supelco SS TCL Polynuclear Aromatic

Hydrocarbon Mix in methylene chloride : benzene (Sigma-Aldrich), Supelco C7-C40 Saturated Alkane Mixture in hexane (Sigma-Aldrich).

Extraction Procedure

The method for total lipid extraction (TLE) of the solvent extractable organics from FFT was modified from the method developed by Lopez-Avlla *et. al* (1994). Briefly, 500 mL Nalgene bottles containing FFT were thawed overnight and freeze dried for 72 hours to remove residual moisture. The freeze dried FFT sample was aliquoted in triplicate and spiked with recovery standard, *m* – terphenyl. A 1:1 hexane: acetone solution was introduced into the sample matrix to extract the organic constituents from the FFT. The mixture underwent microwave extraction with a MARS Microwave Extractor (Serial # MD7382) with the following parameters: Power 100%, Ramp to 115^{o}C hold for 10 mins. The microwaved extract was decanted and passed through a 1.5 µm VWR glass microfiber filter (product number: 691, 28333-125) and washed with hexane. Samples were diluted to their final volume with hexane and the extract was transferred into GCMS vials using a 0.45 µm PTEE filter syringe. Prior to analysis, all vials were spiked with benzo[a]anthracene-d12 as the internal standard.

Instrumental Analysis

GC×GC/QTOF

The FFT total lipid extracts were analyzed using a Pegasus 4D system (LECO Corp., St Joseph, MI, USA). The non-polar/polar (NP/P) column orientation utilized a DB1-MS column (60 m x 0.25mm x 0.25 µm film thickness) as the primary column and DB-17ms column (1.25 m x 0.10mm x 0.10 µm film thickness) as the secondary column. The primary oven was programmed to hold at 80 °C for fifteen minutes, ramp to 335 °C at a rate of 1.66 °C/min. The secondary oven offset was set to +5 °C relative to the primary oven. A modulation period of 7.5 s was used. The modulator temperature offset was +3 °C relative to the secondary oven. The ion source and transfer line temperatures were set to 240 °C and 280 °C, respectively. Helium was used as the

carrier gas at a flow rate of 1 mL/min. The time-of-flight mass spectrometer was scanned over a mass range of m/z 40 to 600 at a sample acquisition rate of 100 scans/s with a solvent delay set to 1300s. The detector voltage was offset by 100V with an acquisition voltage of 1678. Data processing of GC×GC/QTOFMS data was performed by ChromaTOF version 4.50.8.0 (LECO Corp), which included automatic peak finding with mass spectral deconvolution. Library searches were conducted with the NIST/EPA/NIH Mass Spectral Library 2008 (NIST 08, Gaithersburg, MC, USA) and a user library containing alkylated polyaromatic hydrocarbon reference standards.

Identification and Quantification of Solvent Extractable Organics Derived from 2017 BML Near Surface FFT Total Lipid Extracts

The structure of individual solvent extractable organics, defined herein as species, derived from residual inputs of bitumen and/or naphtha within the FFT TLE were elucidated through the interpretation of EI mass spectra, comparison to EI mass spectral database and, if available, confirmed with reference spectra from authenticated standards. In total 69 individual alkylated poly-cyclic aromatic hydrocarbons were semi-quantified: two isomers of C1-naphthalene, nine isomers of C2-naphthalene, eight isomers of C3-naphthalene, fourteen isomers of C4-naphthalene, four isomers of C1-fluorene, five isomers of C2-fluorene, four isomers of C1-phenanthrene, eight isomers of C2-phenanthrene, four isomers of C1-benzothiopehene, 3 isomers of dibenzothiophenes and six isomers of C2-dibenzothiophene. One petroleum biomarker was identified, drimane, and semi-quantified with the closest available standard. In total 3 *n*-alkanes (C11-C13) were quantified with authentic standards. The remaining low molecular weight paraffins present in the unresolved complex matrix (UCM) of BML FFT TLE were not quantified based on limitations of authenticated standards.

Statistical Analysis

Univariate, multivariant, parametric statistical analysis was performed using JMP Software Package (Version 15.1) and customized code in R Studio (Version 1.2.5033). Data was tested for

normality and homogeneity of variance using Shapiro-Wilk (α = 0.05). Data which did not meet the parametric assumptions of normality and homoscedasticity was log transformed. Principal component analysis (PCA) and Hierarchical Clustering Analysis (HCA) was performed using JMP Software Package (Version 15.1) and customized code in R Studio (Version 1.2.5033), following log transformation of the dataset. Isomers which were not present in more than 75% of the samples were removed from the dataset prior to incorporation into HCA and PCA.

Results & Discussion

Spatial Distribution of Solvent Extractable Petroleum Hydrocarbon Concentrations in Near Surface Fluid Fine Tailings

The well resolved species examined in this study demonstrated distinct variabilities between the three platforms depth intervals dependent on concentrations (**Figure 48**). The concentration range of species across the near surface FFT (0.2 to 1.9 m from FWI) were the highest at P1 (range = 6.0×10^{1} – 1.6×10^{4} ng/g), followed by P2 (range = 5.0×10^{1} – 9.2×10^{3} ng/g) and were lowest at P3 (range = 5.0×10^{1} – 4.9×10^{3} ng/g). Although there were variabilities between concentrations, the “fingerprint” constructed from the abundance of each isomer at a given depth were generally similar between platforms. The fingerprints in **Figure 48** categorize isomers within their respective chemical species class with the isomeric alkylated poly-cyclic aromatic hydrocarbon isomers ordered by increasing degree of alkylation, the lower molecular weight *n*-alkanes ordered by increasing carbon number and drimane separated as an individual chemical species class. The notable similarity between these platforms fingerprints was that the same individual isomers were markedly elevated (shaded species in **Figure 48**) for each species of alkylated poly-cyclic aromatic hydrocarbons: C1-DBT-C, C1-FL-C, C1-PH-C, C2-DBT-A, C2-FL-C, C2-NAP-E, C2-PH-C, C3-CAP-E and N4-NAP-K. The variability observed in the fingerprints was further assessed by plotting the concentrations of species, defined as the sum of all isomers for a species class, between depth intervals (**Figure 49**). These depth profiles highlight the same

variability as observed in **Figure 48** but are aimed at determining the concentration trend with depth and if a correlation exists between species.

At P3, the site with the lowest range of species concentration, the fingerprints were the most consistent across the range of FFT depth intervals (**Figure 48**). The largest variations existed in the concentration of lower molecular weight *n*-alkanes C12, C13 and drimane between depth intervals (range = 4.6×10^{2} – 4.9×10^{3} ng/g). The concentration of species were generally consistent from the samples collected nearest the FWI (0.4 m from FWI) and then gradually increased to a maximum concentration at 1.0 m from FWI apart from C13 *n*-alkane, which had the lowest concentration at 1.0 m (**Figure 49c**). After the maximum species concentrations at 1.0 m from FWI, the depth intervals were followed by a relatively minor decrease in concentration to the deep reference sample collected at 5.0 m from FWI. All species, except for the lower molecular weight *n*-alkanes and drimane, followed a correlated trend with depth. While the majority of species classes exhibited minor spatial variations in concentration (max < 1 fold change), C13 and drimane underwent larger spatial variations in concentration (max ~ 5 fold change).

At P1, the site with the highest range of species concentration, the fingerprints between the depth intervals were generally consistent throughout the near surface (**Figure 48**). The notable outlier depth interval corresponded to the sample collected nearest the FWI (0.2 m from FWI), which was depleted for the majority of species, except for of the *n*-alkanes, compared to the rest of the near surface depth profile (range = 6.0×10^{1} – 2.7×10^{3} ng/g and 9.3×10^{1} – 1.6×10^{4} ng/g respectively). Although the concentration of species were depleted for the sample collected nearest the FWI in P1, it was not innately apparent whether the isomer fingerprint was altered. The subsequent depth interval at 0.4m from FWI exhibited the largest abundance of species, which was followed by a decrease at 0.6 m and a subsequently increase at 0.8 m from the FWI (**Figure 49a**). After this fluctuation, the species concentrations generally remained consistent until the deep reference samples at 5.0 m from the FWI. The exception to this trend was for the

concentration of lower molecular weight *n*-alkanes C11, C13 and drimane, which demonstrated a decorrelation to the other species classes with depth. Additionally, while the majority of species exhibited minor spatial variations in concentration (max ~ 2 fold change), the lower molecular weight *n*-alkanes C11 and C13 and drimane underwent the largest spatial variations (max ~ 5 fold change) with concentrations ranging from 7.5×10^{2} – 1.6×10^{4} ng/g.

For P2, the species concentrations generally remained consistent across the near surface FFT depth intervals (range = 5.0×10^{1} – 5.0×10^{3} ng/g), with the notable exception of the deep reference sample which had a depleted species concentration and different isomer fingerprint comparable to all other samples (**Figure 48**). The deep reference sample fingerprint exhibited elevated concentrations of C2-NAP-H and C3-NAP-A to C3-NAP-E isomers relative to the other samples, while the remaining species concentration were comparable to those observed at. The fingerprint for the majority of P2 samples demonstrated elevated concentration of C2-FL and C2-NAP isomers compared to P1 and P3. Additionally, unlike P1 and P3, the near surface samples in P2 (range = 0.2 m from FWI) exhibited elevated concentrations for species comparably to the subsequent depth interval at 0.4 m from FWI (**Figure 49b**). Following the declined concentration at 0.4 m from the FWI, the majority of species exhibited a gradually increase to 1.0 m from the FWI. The subsequent samples collected at 1.4 m from the FWI exhibited declined concentrations of species followed by an increase at 1.9 m from the FWI and gradual decline to the deep reference sample collected at 3.8m from the FWI. All species, except for lower molecular weight n-alkanes C11 – C13, and drimane, followed this correlated trend with depth. As with P1 and P3, while the majority of species exhibited minor spatial variations in concentration (max ~ 2 fold change), the *n*-alkanes C11-C13, and drimane underwent large spatial variations (max ~ 3 fold change) with concentrations ranging from 6.2×10^{2} – 5.0×10^{3} ng/g.

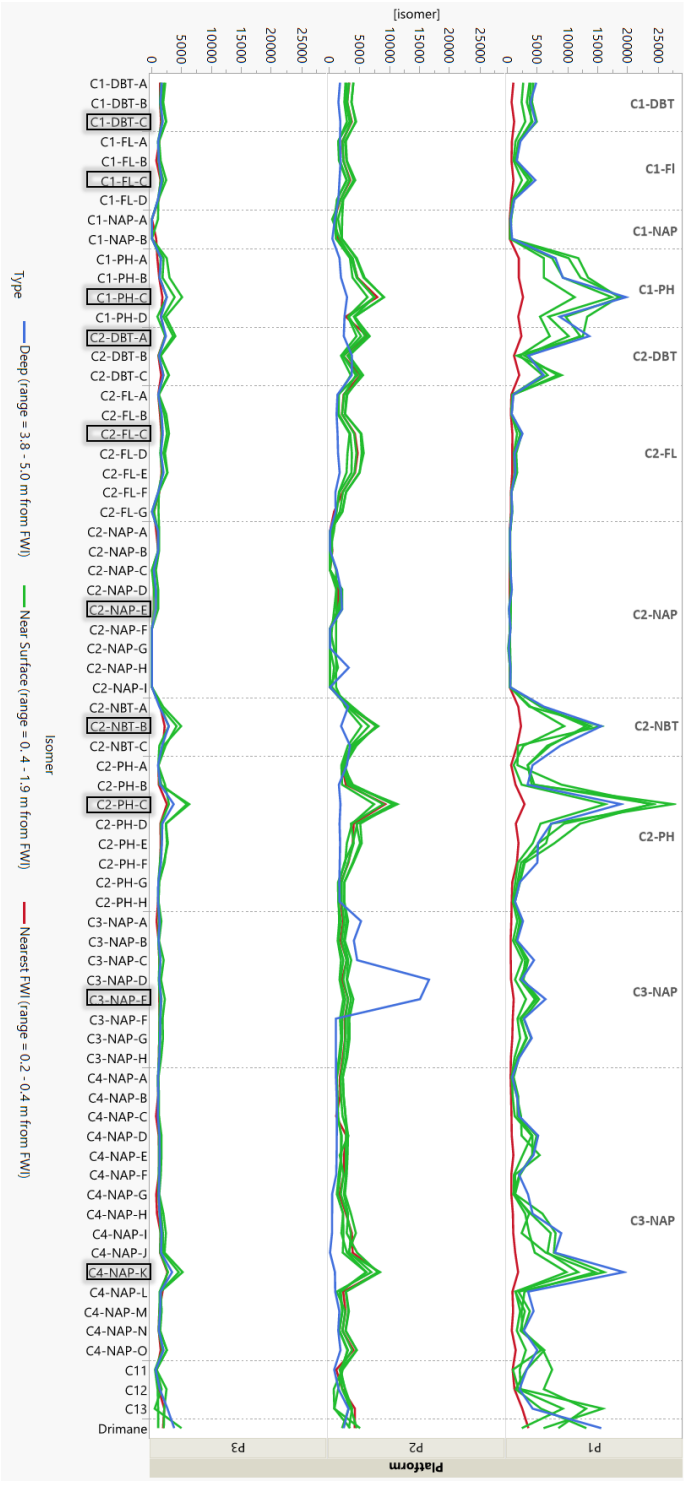

Figure 48 – Spatial variability in fingerprint for the solvent extractable PHC isomers examined between sampling platforms in 2017 BML near surface FFT. These fingerprints are generated using the concentrations of each isomer (y axis) of each isomer studied (indicated by horizontal

lines dividing species labelled on right hand side of figure). The subset of isomeric alkylated poly-cyclic aromatic hydrocarbons were ordered based on increasing degree of alkylation. The lower molecular weight *n*-alkanes are ordered based on increasing carbon number and are followed by drimane. As can be seen, the concentration of each chemical species was generally dominated by the same isomer of that class between platforms. The most elevated isomer of it's respective species class is highlighted with a shaded rectangle: C1-DBT-C, C1-FL-C, C1-PH-C, C2-DBT-A, C2-FL-C, C2-NAP-E, C2-PH-C, C3-CAP-E and N4-NAP-K. Samples collected nearest the FWI (0.2 or 0.4 m from FWI) are colored red, samples collected in the near surface (range = 0.4 m to 1.9 m from FWI) are colored green, while the deep reference samples (range = 3.8 to 5.0 m) are colored blue.

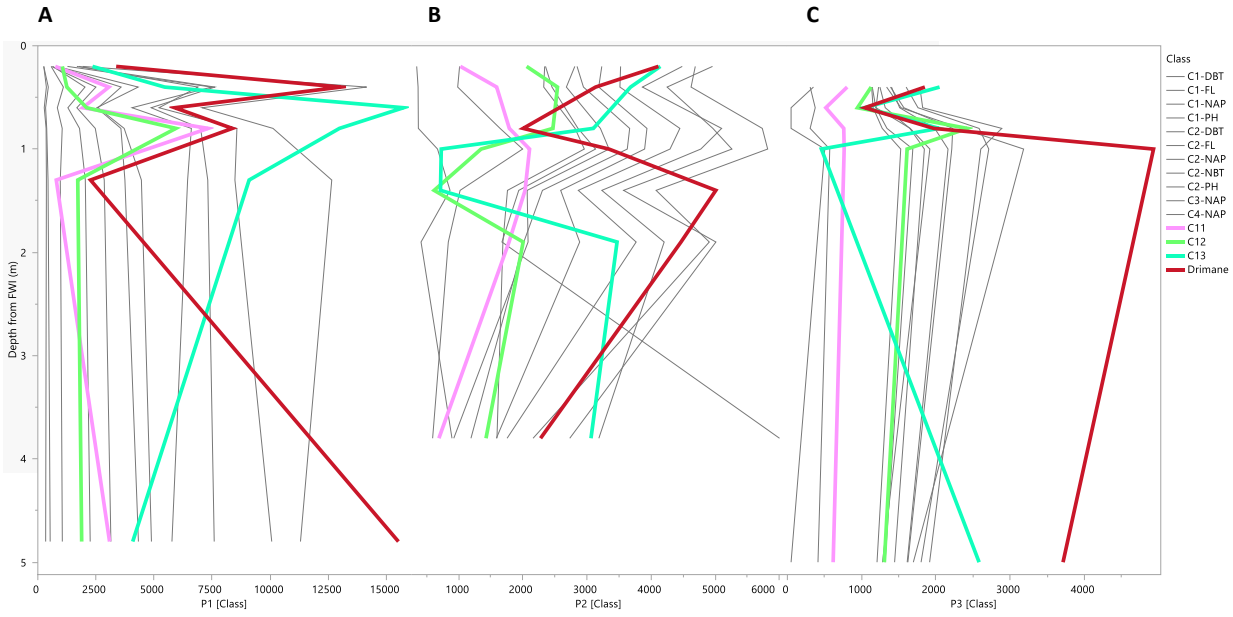

Figure 49 – High-resolution depth profile for the for chemical species in 2017 BML near surface FFT (A) Platform 1 (B) Platform 2 (C) Platform 3. The concentrations of alkylated poly-cyclic aromatic hydrocarbons which followed a consistent pattern are shown in grey while the species showing the greatest variability between depths (C11, C12, C13 and drimane) are shown in thicker lines with varied colors.

Chemometric Comparison of the Chemical Species Fingerprint Between Platforms in Base Mine Lake Fluid Fine Tailings

The high-resolution depth profiles (**Figure 48** – **49**) qualitatively demonstrate that a generally consistent isomer fingerprint persists between platforms with variability in the concentration of the lower molecular weight *n*-alkanes and drimane being most pronounced. To further assess the variation between platform isomer concentrations principal component analysis (PCA) was conducted (**Figure 50**). Two components, PC1 and PC2, explained 71% of the total variance in species concentration between the platforms.

P3 had a relatively smaller variance with it's platform clustering density ellipses being distinctly different from the majority of other samples, which affirm the spatial trends illustrated in **Figure 48** where P3 fingerprints were the most consistent across the range of FFT depth intervals (**Figure 50a**).The clustering associated with P1 and P2 depth intervals shared a similar variability in the first principal component, which explained the majority of the total variance (45.8%) for isomer concentrations. A distinct variability in P1 was associated with the samples collected nearest the FWI (range = 0.2 m from FWI) and in P2 the deep reference sample (range = 3.8 m from FWI). The similarity between the clustering for these samples is driven by depleted species concentrations as illustrated in **Figure 48**. The samples from P1 and P2 were effectively separated in the second principal component, which explained the lesser component of the total variance (24.9%). Integration of the loading plot (**Figure 50b**) with the score plot was used to determine which specific isomer variabilities in concentration were driving the separation of platform density ellipses. The variability in isomer concentrations driving the directionality of P3 samples in the score plot was strongly influenced by elevated variation in two specific isomers, C2-NAP-A and B. The isomer variability in concentration contributing to the separation between P1 and P2 were the elevated concentrations for a subset of lower molecular weight isomers (C2-FL and C2-NAP species class) in P2 and the elevated concentration for a subset of C1-BT isomers and drimane in P1. Effectively, the score plot of the PCA determined the relative variability

in concentrations between platform species concentrations, while the loading plot affirmed the differences in species variability across the platforms.

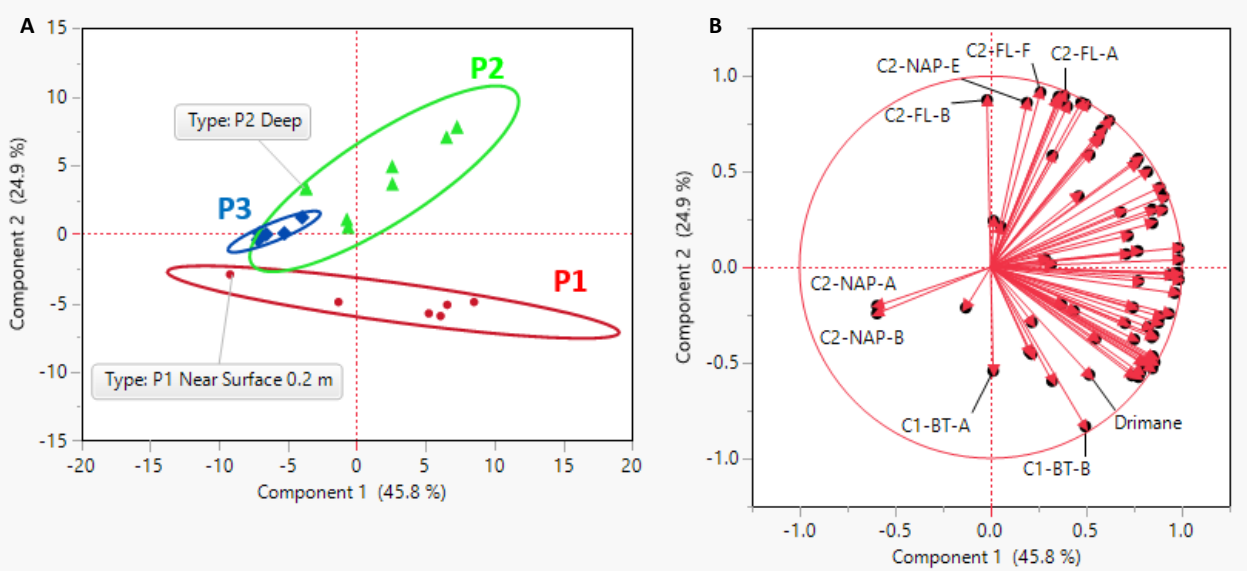

Figure 50 – (a) PCA score plot for FFT depth intervals constructed from isomers concentrations and categorized by their respective platforms with density ellipses representing the 95 % confidence interval between clustering groups. Near surface sample in P1 (range = 0.2 m from FWI) and deep reference sample in P2 (range = 3.8 m from FWI) are labelled to illustrate the large separation within their respective platform density ellipses. (b) PCA loading plot for isomers influence on principal component separation. C2-NAP-A to B, C2-FL-A, B, F and C2-NAP-E are labelled to illustrate their distinct characteristic from the rest of the isomers.

Although the PCA effectively captured the variability in isomer concentrations between the platforms, which were not innately apparent in **Figure 48**, a limitation of the methodology is that the isomers driving separation (C2-NAP, C2-FL species etc.) cannot be grouped and compared. To further asses if individual isomers contributing to distinct variabilities in concentration between platforms can be identified and grouped, two-way clustering Hierarchical Clustering Analysis (HCA) was conducted (**Figure 51**).

Four distinct clusters of depth interval exhibiting similarities between concentrations of isomers were revealed from the HCA (**Figure 51 Group 1 – 4**). The first cluster of depth intervals identified (**Figure 51 Group 1**) were the sample collected nearest the FWI in P1 and the depth intervals of P3, which were depleted for the majority of isomers relative to the other clusters. Within this cluster P3 depth intervals were separated from the samples collected nearest the FWI in P1 based on the relative elevated concentrations of two chemical isomers, C2-NAP-A, C2-NAP-B. The majority of depth intervals in P1 (**Figure 51 Group 3**) and P2 (**Figure 51 Group 4**) were grouped based on relative concentration of 3 distinct cluster of isomers (**Figure 51 Group A** – **B**). Near surface samples collected at 0.4 m, 0.8 m, 1.3 m from FWI and the deep reference sample in P1 clustered together with the lower molecular weight alkylated poly-cyclic aromatic hydrocarbon isomers C1-NAP-A, C2-NAP-B,D,E, C4-NAP-A, C2-PH-H, C1 and C2-FL species being depleted comparable to the other depth profiles between platforms (**Figure 51 Group A**). In contrast, the heavy molecular weight alkylated poly-cyclic aromatic hydrocarbons C3-NAP, C4-NAP and C1-DBT (**Figure 51 Group C**) and the remaining concentration of isomers (**Figure 51 Group B**) were relatively elevated. Near surface samples collected at 0.4 m, 0.8 m and 1.0 m from FWI in P2 clustered together with the lower molecular weight alkylated poly-cyclic hydrocarbon isomers that were depleted in the P1 cluster being comparably elevated (**Figure 51 Group A**), the majority of high molecular weight alkylated poly-cyclic aromatic hydrocarbons isomers and C11 – C13 *n*-alkanes remaining consistent with P1 concentrations (**Figure 51 Group C**) and the remaining isomers being relatively depleted comparably to the P1 (**Figure 51 Group B**). The cluster of depth intervals with the least consistent grouping of isomers (**Figure 51 Group 2**) included P1 near surface samples collected at 0.6 m from FWI, P2 near surface collected at 1.9 and 1.4 m from the FWI and the P2 deep reference sample.

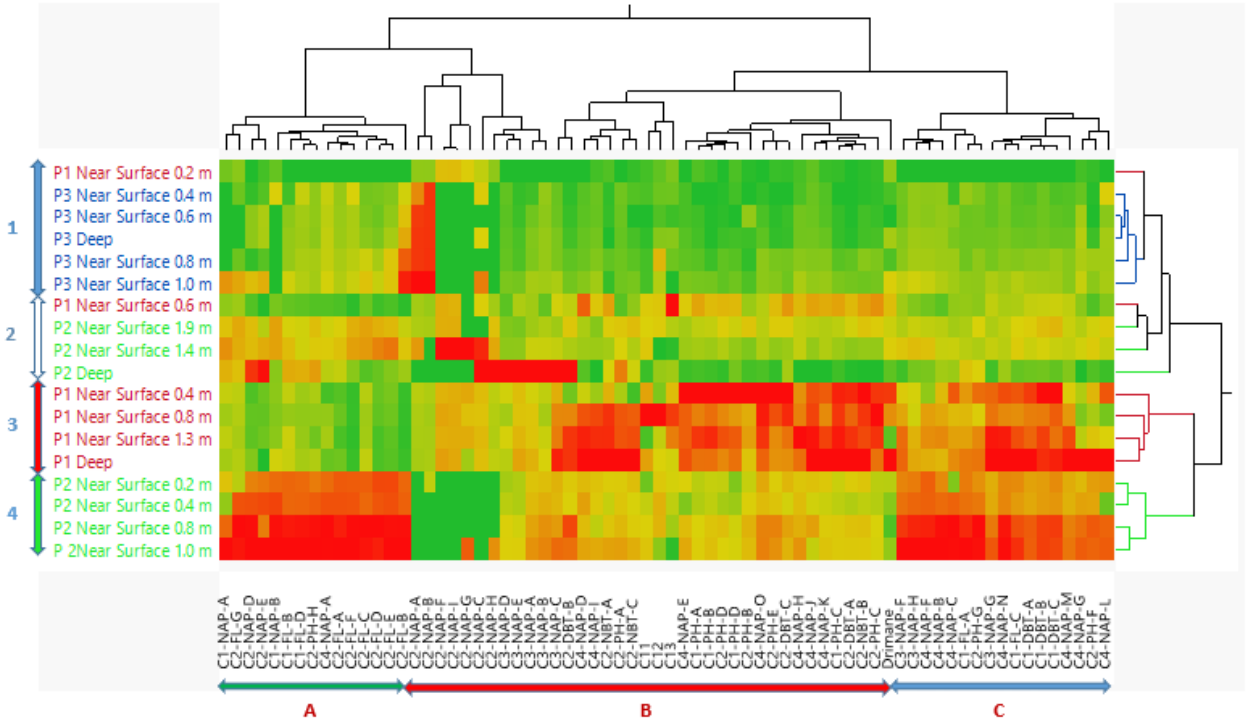

Figure 51 – Two-way Hierarchical Clustering Analysis (HCA) between the solvent extractable isomers and high-resolution depth profiles of 2017 BML FFT. The conditioning formula within the HCA color map utilizes a red-green color schematic where red indicates relatively elevated abundances between all platform depth intervals, while green inversely indicates depleted abundances. Three distinct clusters of isomer concentration were present (Group A – B), while the depth intervals clustered together to form four distinct clusters (Group 1 – 4).

Quantitative Comparison of the Species Fingerprint Between Platforms in Base Mine Lake Fluid Fine Tailings

In forensic applications, a cosine theta (cos-Θ) similarity metric (Johnson *et al.*, 2006) can be used to compare two histograms by treating each isomer distribution as a multi-dimensional vector, and to calculate the cosine of the angle (Θ) between the two vectors. As this metric is comparing the angle between two vectors, magnitude differences between samples does not affect the comparison between species fingerprints. For each multivariate sample, where the number of variables (isomers) is equal to *n*, the species fingerprint may be thought of as an *n*-dimensional

vector. The angle between two sample vectors is a function of the similarity in the two isomer fingerprints. If the two samples are identical, the vectors will be coincident, the angle between the vectors will be 0 degrees, and the cosine of that angle is 1.0. Similarity, if two samples share no common isomeric distributions, the angle defined between them is 90 degrees and the cosine of that angle is zero. Thus, cos-*Θ* is bonded between zero and one where zero is indicative of 0 percent vector similarity and 1 is indicative of 100 percent vector similarity. When comparing two samples (samples *i* and *j*) with reported concentrations of *n* chemicals measured in each sample, cos-Θ is calculated as follows:

$$\cos - \Theta = \frac{\sum_{k=1}^{n} x_{ik} x_{jk}}{\sqrt{\sum_{k=1}^{n} x_{ik}^2 \sum_{k=1}^{n} x_{jk}^2}}$$

Equation 11 – cos-*Θ* calculation[17].

A cos-*Θ* similarity metric (**Figure 52**) was applied to further quantify the similarity between the isomer fingerprint for platform depth intervals in **Figure 48**. The depth intervals were grouped by the qualitative evidence in **Figure 48** that illustrated a variation in concentration and/or isomer fingerprint between the samples collected nearest the FWI (range = 0.2 or 0.4 m from FWI), the remaining near surface depth intervals (range = 0.4 – 1.9 m from the FWI) and the deep reference sample (range = 3.8 – 5.0 m from FWI). Although there was qualitative data indicating that certain groupings of depth intervals exhibited a variability, it was not affirmed if these variations were dependent on the concentration between depth intervals or an alteration in the isomer fingerprint. A high degree of similarity (cos-*Θ* close to 1.0) between depth intervals is indicative that the variability in **Figure 48** is driven by differences in concentration and not changes in isomer fingerprint. At P1, the fingerprint between all depth intervals exhibited relatively high cos-*Θ* similarity with the near surface depth intervals having a 92% similarity to the samples collected nearest the FWI and a 95% to the deep reference sample. For P2, the fingerprint between the

sample collected nearest the FWI and the remaining near surface depth intervals exhibited high cos-θ similarity, 99%, while the deep reference sample had a markedly lower cos-θ similarity, 54%. Comparable to P2, the fingerprint between the samples collected nearest the FWI and near surface depth intervals in P3 exhibited high cos-θ similarity, 96%. Although the deep reference sample had a lower cos-θ similarity relative to the other depth intervals, 87%, this was a markedly higher degree of similarity in comparison to what was observed in P2. These similarities highlight that the variability within platform depth interval for samples collected nearest the FWI and the remaining near surface samples in **Figure 48** are associated with differences in concentration and not changes in isomer fingerprint. Additionally, these metrics provide insight into the distinctions driving the separation between platforms within the PCA and HCA. Although the C2-FL and C2-NAP isomers demonstrate a markedly increased variability between platform depth intervals for both the PCA and HCA (**Figure 50** – **51**), these cos-θ similarity metrics affirm that these variations are related to variability between concentration and not changes in the fingerprint. The only exception to the consistent fingerprint was confirmed to be present for the deep sample in P2, which exhibit a unique fingerprint comparable to the rest of the samples (range = 45 – 59% cos-θ similarity).

	P1 Nearest FWI	P1 Near Surface	P1 Deep	P2 Nearest FWI	P2 Near Surface	P2 Deep	P3 Nearest FWI	P3 Near Surface	P3 Deep
P1 Nearest FWI	1								
P1 Near Surface	0.92	1							
P1 Deep	0.92	0.95	1						
P2 Nearest FWI	0.93	0.92	0.92	1					
P2 Near Surface	0.93	0.91	0.91	0.99	1				
P2 Deep	0.53	0.45	0.46	0.54	0.56	1			
P3 Nearest FWI	0.91	0.82	0.84	0.95	0.95	0.59	1		
P3 Near Surface	0.93	0.89	0.91	0.98	0.98	0.55	0.96	1	
P3 Deep	0.78	0.7	0.73	0.86	0.83	0.5	0.9	0.87	1

Figure 52 - Cos-Θ similarity matrix for the isomer fingerprint of FFT between sampling platforms grouped into three regions where nearest FWI represents the samples collected nearest the FWI (range = 0.2 – 0.4 m from FWI), near surface represent the mean remaining depth intervals (range = 0.4 – 1.9 m from FWI) and deep represents the reference sample below the near surface (range = 3.8 – 5.0 m from FWI). It is evident from the cos-Θ similarity matrix that the deep reference sample in P2 exhibits a unique fingerprint comparable to the rest of depth intervals (range = 45 – 59 %).

Evaluating Variability in Petroleum Hydrocarbon Inputs and Potential Biogeochemical Cycling Within Near Surface Fluid Fine Tailings

The various approaches of comparing the fingerprints across the near surface FFT (0.1 to 1.9m from FWI) demonstrated a similar signature representative of a related source of PHCs containing a subset of isomers being elevated within their respective chemical class (C1-DBT-C, C1-FL-C, C1-PH-C, C2-DBT-A, C2-FL-C, C2-NAP-E, C2-PH-C, C3-CAP-E and N4-NAP-K). The consistency between samples in the dominant isomer provides a more comprehensive indication of a consistent source comparatively to evaluation of the alkylated poly-cyclic hydrocarbon

species, which further highlights the importance of monitoring PHC isomers. The indication of a similar source is not unexpected as the FFT in BML was filled from the same tailing storage facility. Nevertheless, these approaches of affirming a consistent fingerprint provide a novel approach that can be further utilized to source apportionment PHCs in other regions of BML, such as the overlaying water cap. Although a singular source contributes to the PHC deposition within FFT, distinctions in isomer concentration between platform depth interval are persisting either due to variable inputs, biogeochemical cycling and/or species exchange with the water column. Notable, the variability in concentrations were pronounced for the low molecular weight *n*-alkanes (C11 – C13) and drimane between platform depth intervals. The variabilities between platform isomer concentrations were more pronounced in P1 and P2 relative to P3. For P3, the variability between isomer concentrations were markedly decreased throughout the depth profile in comparison to P1 and P2 (**Figure 49** – **51**) which may be attributed to decreased inputs, historic biogeochemical activity, and/or increased species exchange with the water column. Although multiple mechanisms may be contributing to reduced isomer concentrations in P3, a variable PHC input comparable to P1 and P2 is a more probable source as there is no preferential depletion of more labile isomers supportive of increased biogeochemical and/or species exchange with the water column. The contribution of PHC inputs and/or biogeochemically cycling within P1 and P2 were distinguished through the comparison between the relative species concentration of the variable labile low molecular weight isomers to the heavier molecular weight isomers (**Figure 50** & **51**). The two-way HCA clustering highlighted both platforms preferentially retained the same higher molecular weight poly-cyclic aromatic hydrocarbon isomers between depth intervals (C3-NAP, C4-NAP and C1-DBT species), while P1 contained isomer concentration depleted for a subset of lower molecular weight alkylated poly-cyclic aromatic hydrocarbons (C1-NAP-A, C2-NAP-B,D,E, C4-NAP-A, C2-PH-H, C1 and C2-FL) relative to P2. The reduced concentration of lower molecular weight isomers relative to the less labile heavier molecular weight isomers in P1 may be attributed to increased historic biogeochemical cycling, either directly through anaerobic microbial

degradation and/or via species exchange with the water column. Alternatively, the PHC inputs within P1 were originally depleted for these lower molecular weight isomers comparable to the heavier molecular weight isomers. As the lower molecular weight species are expected to be preferentially biodegraded and have higher water solubilities, increased concentration of the lower molecular weight species relative to the heavier molecular weight species in P2 may be indicative of increased potential for biogeochemical cycling and/or species exchange with the water column.

Conclusion

The isomer fingerprint in BML near surface FFT confirmed that a spatial variation exists across sampling platforms with P2 exhibiting increased concentrations in the samples collected nearest the FWI, but P1 exhibiting overall larger concentrations and P3 exhibiting the lowest concentrations of isomers across the near surface. The concentration of isomers with depth generally remained consistent in the near surface FFT until the deep reference samples with the exception of the lower molecular weight *n*-alkanes and drimane, which exhibited large variabilities in concentration. As these low molecular weight compounds, with the exception of drimane, are components of the residual naphtha, the variable concentrations of these species may be linked to either increased rates of biogeochemical cycling, fluctuating inputs and/or sorption of naphtha to the organic phase of the FFT. The variability in overall isomer concentrations were elevated in both P1 and P2, while comparably depleted in P3 suggestive of a decreased PHC input. While P1 and P2 preferentially retained the same higher molecular isomers between depth intervals (C3-NAP, C4-NAP and C1-DBT class isomers), P1 contained relatively depleted concentrations for a subset of lower molecular weight isomers (C1-NAP-A, C2-NAP-B,D,E, C4-NAP-A, C2-PH-H, C1 and C2-FL). The decreased concentration of these lower molecular species relative to the heavier species in P2 may indicate a lower potential for biogeochemical cycling and/or exchange with the water column, either due to lower initial inputs of these species or to ongoing cycling reducing the abundances of the compounds originally present. Although the concentration of

species exhibited a distinct spatial variability, the various approaches of comparing the species fingerprints across the near surface FFT demonstrated a similar signature representative of a related source of PHCs with one isomer contributing to the majority the species class (C1-DBT-C, C1-FL-C, C1-PH-C, C2-DBT-A, C2-FL-C, C2-NAP-E, C2-PH-C, C3-CAP-E and N4-NAP-K). The ability to evaluate the PHCs source signature via the dominant isomer within each species highlights the advantage of using GC×GC for monitoring of individual isomers. If the FFT samples had been analyzed via one-dimensional gas chromatograph (1-D GC), these source signature evaluations would not have been achieved as isomers can only be resolved as a summation of all isomers within a species due to the overlaying unresolved complex matrix (UCM).

References

1. Government of Alberta (**2015**). Lower Athabasca Region: Tailings Management Framework for the Mineable Athabasca Oil Sands. https://open.alberta.ca/dataset/962bc8f4-3924-46ce-baf8 d6b7a26467ae/resource/7c49eb63-751b-49fd-b746-87d5edee3131/download/2015-larp-tailingsmgtathabascaoilsands.pdf.
2. Natural Resources Canada (**2016**). Oil Sands Extraction Processing. https://www.nrcan.gc.ca/energy/energy-sources-distribution/crude-oil/oil-sands-extraction-and-processing/18094.
3. Siddique, T., Fedorak, P.M., MacKinnon, M.D., Foght, J.M. (**2007)**. Metabolism of BTEX and naphtha compounds to methane in oil sands tailings. *Environ. Sci. Technol*. 41, 2350–2356.
4. Dompierre, K. A., Lindsay, M. B. J., Cruz-Hernández, P., & Halferdahl, G. M. (**2016**). Initial geochemical characteristics of fluid fine tailings in an oil sands end pit lake. *Science of the Total Environment*, 556, 196–206.
5. Siddique, T., Fedorak, P.M., Foght, J.M. (**2006**). Biodegradation of short-chain n-alkanes in oil sands tailings under methanogenic conditions. *Environ. Sci. Technol*. 40, 5459–5464.
6. Allen, E.W. (**2008**). Process Water Treatment in Canada's Oil Sands Industry I. Target Pollutants and Treatment Objectives. *J. Environ. Eng. Sci*. 7, 123-138.
7. Arriaga, D., Colenbrander, T., Risacher, F. F., Morris, P. K., Goad, C., Slater, G. F., & Warren, L. A. (**2019**). Applied Geochemistry The co-importance of physical mixing and biogeochemical consumption in controlling water cap oxygen levels in Base Mine Lake. *Applied Geochemistry*, 111, 104442.
8. Siddique, T., Stasik, S., Mohamad Shahimin, M. F., & Wendt-Potthoff, K. (**2018**). Microbial Communities in Oil Sands Tailings: Their Implications in Biogeochemical Processes and Tailings Management. In Microbial Communities Utilizing Hydrocarbons and Lipids: Members, Metagenomics and Ecophysiology. *Handbook of Hydrocarbon and Lipid Microbiology*. 1-33.
9. Rowland, S. J., West, C. E., Scarlett, A. G., Ho, C., Jones, D. (**2012**). Differentiation of two industrial oil sands process-affected waters by two-dimensional gas chromatography/mass spectrometry of diamondoid acid profiles. *Rapid Commun. Mass Spectrom*. 26 (5), 572– 576.

10. Llamas, A., Al-Lal, A.M., García-Martínez, M.J., Ortega, M.F., Llamas, J.F., Lapuerta, M., Canoira, L. (**2017**). Polycyclic Aromatic Hydrocarbons (PAHs) produced in the combustion of fatty acid alkyl esters from different feedstocks: quantification, statistical analysis and mechanisms of formation. *Sci. Tot. Environ*. 586, 446–456.
11. Ravindra, K., Sokhi, R., Van Grieken, R. (**2008**). Atmospheric polycyclic aromatic hydrocarbons: source attribution, emission factors and regulation. *Atmos Environ*. 42, 2895–2921.
12. Shukla, B.M., Koshi, M. (**2012**). Importance of fundamental sp, sp2, sp3 hydrocarbon radicals in the growth of polycyclic aromatic hydrocarbons. *Anal Chem*. 84, 5007–5016.
13. Hurley, D. L. (**2017**). Wind waves and internal waves in Base Mine Lake. T*hesis*.
14. Holowenko, F. M., MacKinnon, M. D., Fedorak, P. M. (**2000**). Methanogens and sulfate-reducing bacteria in oil sands fine tailings waste. *Can. J. Microbiol*. 46, 927-937.
15. Nzila, A. (**2018**). Biodegradation of high-molecular-weight polycyclic aromatic hydrocarbons under anaerobic conditions: Overview of studies, proposed pathways and future perspectives. *Environ. Pollut*. 239, 788-802.
16. White, W.M. (**2013**). *Geochemistry*. Wiley-Blackwell. 608-609.
17. Johnson, G.W., Quensen III, J.F., Chiarenzelli, J., Hamilton, C. (**2006**). Chapter 10: Polychlorinated Biphenyls. In: Morrison, R., Murphy, B. (Eds.), Environmental Forensics: A Contaminant Specific Guide. Elsevier, Amsterdam, pp. 187-225.
18. Rahimi, P.M., Gentzis, T. (**2006**) The Chemistry of Bitumen and Heavy Oil Processing. In: Hsu C.S., Robinson P.R. (eds) Practical Advances in Petroleum Processing. Springer, New York, NY.
19. Risacher, F. F., Morris, P. K., Arriaga, D., Goad, C., Nelson, T. C., Slater, G. F., & Warren, L. A. (**2018**). The interplay of methane and ammonia as key oxygen consuming constituents in early stage development of Base Mine Lake, the first demonstration oil sands pit lake. *Applied Geochemistry*, 93, 49–59.
20. Fingas, Merv. (**2015**). Review of The Properties and Behaviour of Diluted Bitumens. Proceedings of the 38th AMOP Technical Seminar on Environmental Contamination and Response.

Chapter Four: Summary for Monitoring Spatial Distribution of Solvent Extractable Petroleum Hydrocarbon in Pit Lake Fluid Fine Tailings

Project Summary

This project is focused on developing an optimized comprehensive two-dimensional gas chromatography time-of-flight mass spectrometry (GC×GC/TOFMS) methodology for analyzing the spatial distribution of solvent extractable petroleum hydrocarbon (PHC) species in oil sands tailings within Base Mine Lake (BML) the first full-scale demonstration of Pit Lake (PL) technology by Syncrude Canada Ltd. BML is expected to produce a viable solution for the long-term management of oil sands tailings in the form of Fluid Fine Tailings (FFT), through facilitating the densification and de-watering of FFT, while also meeting the regulatory oxygen requirements to be considered a functioning boreal ecosystem. The biogeochemical cycling and/or species exchange of labile PHC in the FFT are suspected to be contributing to the mobilization of oxygen consuming constituents (OCCs) into the overlaying water column increasing the chemical oxygen demand (COD) within BML. In order to assess the PHC inputs, source attribution and potential biogeochemical cycling and/or species exchange with the water column contributing to the draw down of oxygen, the concentration for a subset of solvent extractable organics were extensive monitoring in high-resolution depth intervals collected between different spatial regions of BML. The spatial depth intervals were focused within the near surface FFT (0.2 – 1.9 m from Fluid Water Interface (FWI)), which have been proposed by *Dompierre et al.* (2016) to undergo the largest extent of FFT species exchange with the water column.

Firstly, the focus of the project was accomplished through the identification of a subset of alkylated poly-cyclic aromatic hydrocarbon isomers, petroleum biomarker and *n*-alkanes within FFT samples representative of residual inputs of PHC derived from either naphtha and/or bitumen. The identification of individual isomers was achieved through the enhanced peak capacity of GC×GC, which can separate isomers from the unresolved complex matrix in the second dimension dissimilar to the conventional one-dimensional gas chromatograph (1-D GC).

Secondly, the spatial variability of these isomers was used to evaluate PHC inputs, source apportionment, biogeochemical cycling and/or species exchange with the water column potentially contributing to the release of OCCs. Concentration of individual isomers and the relative concentration trends between depth intervals beginning nearest the FWI were used to assess the relative spatial PHC inputs throughout the FFT. The isomer "fingerprint" constructed from the abundance of each isomer at a given depth and cosine theta (cos-θ) similarity metric were the primary criterion for evaluating the spatial PHC source signatures within the FFT. The potential biogeochemical cycling and/or species exchange with the water column was evaluated through a chemometric approach using Principal Component Analysis (PCA) and Hierarchical Cluster Analysis (HCA) that compared the spatial concentration between the suspected more labile lower molecular weight isomers to heavier molecular weight isomers.

Development and Optimization of a Comprehensive Two-Dimensional Gas Chromatography Methodology for Monitoring Solvent Extractable Petroleum Hydrocarbons in Fluid Fine Tailings

The direct comparison of the molecular weight range and peak capacity between the aromatic and aliphatic components of the 2017 BML FFT UCM of samples, demonstrated a novel approach for comparing between the conventional GC×GC column orientation, non-polar/polar (NP/P) and polar/non-polar (P/NP) column orientation, alternatively referred to as "reverse phase". The peak capacity associated with the NP/P column orientation strongly supported the use of this GC×GC column parameter for the identification of individual solvent extractable petroleum hydrocarbon isomers from highly biogeochemically degraded oil sands tailings. Although the alternative P/NP column orientation resolved a relatively similar number of alkylated poly-cyclic aromatic hydrocarbon (74 - 81%), the NP/P column orientation was advantageous for this study as it can resolved these isomers in the total ion chromatograph (TIC) without the need for nominal mass extraction. The NP/P column orientation also provided more contextual information about the

species present as it resolved low molecular weight (C7 – C12) paraffins associated with potential labile organic carbon inputs.

High-Resolution Spatial Distribution of Near Surface Solvent Extractable Petroleum Hydrocarbon in Base Mine Lake Fluid Fine Tailing

The spatial distribution of the subset of solvent extractable PHC isomers identified are supportive that a variability in concentration existed across the near surface FFT (range = 0.2 – 1.9 m from FWI) with the highest abundance at P1 (range = 6.0×10^{1} – 1.6×10^{4} ng/g), followed by P2 (range = 5.0×10^{1} – 9.2×10^{3} ng/g) and were lowest at P3 (range = 5.0×10^{1} – 4.9×10^{3} ng/g). The concentration of isomers with depth generally remained consistent in the near surface FFT until the deep reference samples with the exception of the lower molecular weight *n*-alkanes and drimane, which exhibited large variabilities in concentration and a dissimilar trend with depth comparable to the majority of other isomers.

The PCA evidently demonstrated that the variabilities in species concentration between P1 and P2 were similar but were effectively separated by difference in the concentration for a subset of lower molecular weight alkylated poly-cyclic aromatic hydrocarbons. Evaluation of species clusters exhibiting similar concentrations within the HCA illustrated that the majority of depth intervals for P1 were depleted for the lower molecular weight alkylated poly-cyclic aromatic hydrocarbon isomers C1-NAP-A, C2-NAP-B,D,E, C2-PH-H, C1 and C2-FL class comparable to P2. While these lower molecular weight alkylated poly-cyclic aromatic hydrocarbon isomers exhibited a variability between the concentrations in P1 and P2, the concentration heavy molecular weight alkylated poly-cyclic aromatic hydrocarbons C3-NAP, C4-NAP and C1-DBT remained consistent between both platforms. As the lower molecular weight isomers are expected to be preferentially biodegraded and have higher water solubilities, increased concentration of these lower molecular weight species relative to the heavier molecular weight isomers in P2 may

be indicative of increased potential for biogeochemical cycling and/or species exchange with the water column.

Project Conclusion

The persistence of a similar species fingerprint throughout the FFT depth intervals studied suggest the contribution of a singular source of PHCs within BML. Within the depth profiles, the species concentrations remained consistent between samples for the majority of alkylated poly-cyclic aromatic hydrocarbons, while conversely a large variation in concentration occurred for the labile low molecular weight *n*-alkanes (C11 – C13) and drimane. In addition, these components exhibit a distinctly different trend in concentration with depth dissimilar to the majority of heavier molecular weight alkylated poly-cyclic aromatic hydrocarbons, which are uniquely sourced from bitumen. As these low molecular weight compounds, with the exception of drimane, are suspected components of residual naphtha, the large variabilities in concentration and decorrelation with bitumen compounds are suggestive that these species may be linked with either increased rates of biogeochemical cycling, fluctuating inputs and/or sorption of naphtha to the organic phase of the FFT. The large variability in drimane concentration between samples contradicts the study design which incorporated drimane as a postulated inert biomarker and as a proxy for total organic carbon. Although a similar source fingerprint persisted throughout the study site, the spatial distribution for the subset of solvent extractable PHC isomers identified are supportive that a differences in concentration existed across sampling platforms with P2 exhibiting increased concentrations in the samples collected nearest the FWI, but P1 exhibiting overall larger concentrations and P3 exhibiting the lowest concentrations of species across the near surface. Further assessment of the variability in isomer concentration with PCA determined that the variabilities in P3 species concentration were the most consistent across the range of FFT depth intervals while P1 and P2 shared a similar variability in isomer concentration. The majority of depth intervals in P1 were distinguished from P2 due to a relatively depleted concentration for a

subset of lower molecular weight alkylated poly-cyclic aromatic hydrocarbons in P1 (primarily C1 and C2-FL class species). In contrast, the concentration for the heavy molecular weight alkylated poly-cyclic aromatic hydrocarbons C3-NAP, C4-NAP and C1-DBT remained consistent between P1 and P2. As the lower molecular weight isomers are expected to be preferentially biodegraded and have higher water solubilities, increased concentration of the lower molecular weight species relative to the heavier molecular weight isomers may be indicative of increased potential for biogeochemical cycling and/or species exchange with the water column in P2.

Future Work

As this dissertation only focused on the spatial resolution of a subset of solvent extractable PHC isomers in BML collected at one sampling time, it is recommended that the methodology be repeated for several different sampling dates to understand the temporal variabilities in isomer concentration. If the potential for biogeochemical cycling and/or species exchange with the water column is higher in P2 based on the relative increase in concentration for the lower molecular C1 and C2-FL isomers, temporal studies should demonstrate a progressive decrease in these isomers. To further evaluate whether biogeochemical cycling and/or species exchange with the water column is correlated to the relative depleted concentration of lower molecular weight isomers in P2, the variability in abundance of OCCs derived from anaerobic microbial degradation of PHCs, such as gases (e.g. H_2S, CH_4), dissolved organic carbon (DOC) and dissolved ions (e.g. NH_4^+, HS^-, and Fe^{2+}) should be compared to the solvent extractable isomers within this study. The positive correlation between increases in these OCC constituents to increased concentrations of lower molecular weight isomer would be suggestive that preferential biogeochemical cycling and/or species exchange is occurring. If the native microbial communities in BML FFT continue to cycle these lower molecular weight isomers, the mobilization of OCCs into the overlaying water column may be reduced and/or completely concluded once the input of the lower molecular weight isomers is consumed.

All illustrated in chapter 2, the optimized GC×GC methodology is able to not only separate alkylated poly-cyclic aromatic hydrocarbons from the unresolved complex matrix (UCM), but can also resolve individual aliphatic components suspected to be associated with inputs of sorbed naphtha to the organic phase of the FFT. Due to the limitation of authenticated standards, only 3 identifiable compounds within this region (C11 – C13 *n*-alkane) were quantified. However, the resolved aliphatic components can be further categorized based on their carbon number and semi-quantified based on the *n*-alkane standard used within this study. The structure of individual aliphatic components can be interpreted through their EI mass spectra, comparison to EI mass spectral database and, if available, confirmed with reference spectra from authenticated standards. It has been shown *in-vivo* by Siddique *et al.* 2006 that native hydrogenotrophic and acetoclastic methanogens present in FFT biodegraded *n*-alkanes in the sequence C > C8 > C7 > C6 with degradation of 100% C10, 97% C8, 74% C7, and 44% C6. The resulting trend of preferential microbial degradation is expected to be associated with the acclimatization of microcosms to naphtha components dominated by relatively high molecular weight aliphatic compounds (>C10). The relative spatial variation in concentration between the relatively shorter aliphatic compounds (<C10) compared to longer chain compounds (>C10), may provide a complementary *in-situ* metric for determining the potential for biodegradation of naphtha components by methanogens present in BML FFT. The potential for these native microbial communities to biodegrade naphtha components is suspected to be lessened if the aliphatic components are dominated by relatively shorter compounds, while elevated abundances of the longer chain aliphatic compounds may indicate a greater potential for biodegradation.